9-2012

Parity Violation in Neutron Deuteron Scattering in Pionless Effective Field Theory

Jared James Vanasse
University of Massachusetts Amherst

PARITY VIOLATION IN NEUTRON DEUTERON SCATTERING IN PIONLESS EFFECTIVE FIELD THEORY

A Dissertation Presented

by

JARED J. VANASSE

Submitted to the Graduate School of the
University of Massachusetts Amherst in partial fulfillment
of the requirements for the degree of

DOCTOR OF PHILOSOPHY

September 2012

Physics Department

PARITY VIOLATION IN NEUTRON DEUTERON SCATTERING IN PIONLESS EFFECTIVE FIELD THEORY

A Dissertation Presented

by

JARED J. VANASSE

Approved as to style and content by:

Barry Holstein, Chair

John Donoghue, Member

Krishna Kumar, Member

Murugappan Muthukumar, Member

Donald Candela, Department Chair
Physics Department

To my parents
because without them I literally would not be here.

ACKNOWLEDGMENTS

I would like to aknowledge Barry Holstein for useful guidance during this project. Also I would like to thank Harald Griesshammer and Matthias Schindler for useful consversations during the course of this work.

ABSTRACT

PARITY VIOLATION IN NEUTRON DEUTERON SCATTERING IN PIONLESS EFFECTIVE FIELD THEORY

SEPTEMBER 2012

JARED J. VANASSE

B.Sc., UNIVERSITY OF RHODE ISLAND

M.Sc., UNIVERSITY OF MASSACHUSETTS AMHERST

Ph.D., UNIVERSITY OF MASSACHUSETTS AMHERST

Directed by: Professor Barry Holstein

In this dissertation the parity violating neutron deuteron scattering amplitudes are calculated using pionless effective field theory to leading order. The five low energy parity violating constants present in pionless effective field theory are estimated by matching onto the "best" values for the parameters of the model by Desplanques, Donoghue, and Holstein (DDH). Using these estimates and the calculated amplitudes, predictions for the spin rotation of a neutron through a deuteron target are given with a value of 1.8×10^{-8} rad cm^{-1}. Also given are the longitudinal analyzing power in neutron deuteron scattering with a polarized neutron yielding 2.2×10^{-8}, and a polarized deuteron giving 4.0×10^{-8}. These observables are discussed in the broader context of hadronic parity violation and as possible future experiments to determine the values of the five low energy parity violating constant present in pionless effective theory.

TABLE OF CONTENTS

APPENDICES

LIST OF TABLES

Table **Page**

LIST OF FIGURES

Figure **Page**

CHAPTER 1

HADRONIC PARITY VIOLATION

1.1 Experiment

Before Lee and Yang suggested looking for parity violation [80], and its discovery by Wu et al. in ^{60}Co beta decay [26] most physicists assumed that parity was conserved. After this discovery it was soon realized that parity violating (PV) effects should be observed in the nucleon-nucleon interaction, and the first experimental attempt to observe PV effects in nucleon-nucleon interactions were carried out by Tanner in 1958 in the reaction $^{19}F(p,\alpha)^{16}O$. However he was unable to observe a signal as his experiment was not sensitive enough [102]. Such experiments had to be performed in one part of 10^8, as the scale for PV experiments is roughly set by $G_F m_\pi^2 \sim 10^{-7}$. Fortunately it was soon realized that for certain nuclei the nuclear structure amplifies the PV signal. The typical spacing between nuclear levels is of the order of MeV, but for certain nuclei there exists spacings between $J^+ - J^-$ levels that are much smaller. For example in the case of ^{18}F one finds the levels 0^+ and 0^- at 1081 keV separated by an energy of 39 keV. The amplification of the PV signal can be seen quite trivially by the use of first order non-degenerate perturbation theory. (Note perturbation theory calls for a sum over all intermediate states, however only one state is shown as it is the dominant contribution of this sum)

$$|\psi_{J^+}\rangle \simeq |J^+\rangle + |J^-\rangle \frac{\langle J^-|\mathcal{H}_{weak}|J^+\rangle}{E_{J^+} - E_{J^-}} \tag{1.1}$$

$$|\psi_{J^-}\rangle \simeq |J^-\rangle - |J^+\rangle \frac{\langle J^+|\mathcal{H}_{weak}|J^-\rangle}{E_{J^+} - E_{J^-}} \tag{1.2}$$

Typically the mixing parameter $\langle J^{\pm}|\mathcal{H}_{weak}|J^{\mp}\rangle/(E_{J^{\pm}} - E_{J^{\mp}})$ is of order 10^{-6} for energy differences on the order of an MeV. However the energy differences between states for the example ^{18}F is on the order of keV. Thus the denominator of our mixing parameter is larger than the typical case by a factor of 100 and the mixing parameter is of the order of 10^{-4}, thus enhancing the PV signal. The 1081 keV 0^- state in ^{18}F decays to the 1^+ ground state as in Fig. 1.1b. Normally only an electric dipole ($E1$) decay is allowed from the 0^- state to the 1^+ ground state and magnetic dipole ($M1$) decay is forbidden by parity. However, since there is a mixture of the 0^+ state in the 0^- state the $M1$ decay is allowed. In the decay of the 1081 keV state of unpolarized ^{18}F the $E1$ and $M1$ decay interfere creating an asymmetry in the circular polarization of outgoing photons. This asymmetry is given approximately by Eq. (1.3) in the two level mixing approximation [61] where we only go to first order in parity violation, include the lowest order multipoles, and ignore radiative corrections.

$$P_{\gamma}(^{18}F, 1081\text{keV}) \approx 2\text{Re}\left[\frac{\langle 0^+, 1|\mathcal{H}_{weak}|0^-0\rangle}{(E_{0^+} - E_{0^-})}\frac{\langle 1^+||M1||0^+\rangle}{\langle 1^+||E1||0^-\rangle}\right] \tag{1.3}$$

The ratio $|\langle M_1\rangle/\langle E_1\rangle| = 112$ is found from experiment as the ratio of the $0^+ \to 1^+$ and $0^- \to 1^+$ lifetimes [73, 74, 107]. However, this does not give the sign of the ratio which must be calculated and the weak transition matrix element must also be calculated. The photon circular polarization P_{γ} in ^{18}F has been measured by five different groups all giving bounds

$$P_{\gamma}(^{18}F, 1.018\text{MeV}) = \begin{cases} (-7 \pm 20) \times 10^{-4} & \text{Caltech/Florence} & [7] \\ (3 \pm 6) \times 10^{-4} & \text{Florence} & [17] \\ (-10 \pm 18) \times 10^{-4} & \text{Mainz} & [49] \\ (2 \pm 6) \times 10^{-4} & \text{Queens} & [47] \\ (-4 \pm 30) \times 10^{-4} & \text{Florence} & [18] \end{cases} \tag{1.4}$$

Two other important measurements of this type are the photon asymmetry, A_γ, of polarized ^{19}F and the photon circular polarization asymmetry, P_γ of unpolarized ^{21}Ne. In the case of ^{19}F the $\frac{1}{2}^-$ state is separated from the $\frac{1}{2}^+$ ground state by 110 keV and the next nearest state is at 5337 keV as seen from Fig. 1.1a. Using the two level approximation the photon asymmetry A_γ is given by the interference of the $M1$ and $E1$ transitions in Eq. (1.5). This equation is slightly more complicated than the ^{18}F case because the state to which the nucleus decays to is one of the states in the parity admixture and therefore both the excited state and the ground state have an $M1$ transition associated with them

$$A_\gamma(^{19}F, 110\text{keV}) \approx 2\text{Re}\left[\frac{\langle \frac{1}{2}^+, \frac{1}{2}|\mathcal{H}_{weak}|\frac{1}{2}^-, \frac{1}{2}\rangle}{(E_{\frac{1}{2}^+} - E_{\frac{1}{2}^-})} \times \frac{\langle \frac{1}{2}^+||M1||\frac{1}{2}^+\rangle - \langle \frac{1}{2}^-||M1||\frac{1}{2}^-\rangle}{\langle \frac{1}{2}^+||E1||\frac{1}{2}^-\rangle}\right] \tag{1.5}$$

The matrix element $\langle \frac{1}{2}^+||M1||\frac{1}{2}^+\rangle = i8.69\times10^{-5}$ and is determined from the magnetic moment of 2.6289 [44,45] of the ^{19}F ground state. The matrix element $|\langle \frac{1}{2}^+||E1||\frac{1}{2}^-\rangle| = 0.88\times10^{-5}$ is determined by the 853 ± 10 psec lifetime of the $\frac{1}{2}^-$ level. Finally the sign of the $E1$ matrix element, the weak transition matrix element, and the $\langle \frac{1}{2}^-||M1||\frac{1}{2}^-\rangle$ matrix element must all be calculated. The photon asymmetry of polarized ^{19}F has been measured by a group at Seattle achieving $(-8.5 \pm 2.6) \times 10^{-5}$ [2] and a group at Mainz [42, 43] achieving $(-6.8 \pm 1.8) \times 10^{-5}$.

In the case of ^{21}Ne there is a 2795 keV $\frac{1}{2}^+$ state which is above the $1/2^-$ state by 5.7 keV, and the next nearest excited state is the 3662 keV $\frac{3}{2}^-$ state as seen in Fig 1.1c. Again using the two level approximation the photon circular polarization of ^{21}Ne is given by the interference of the $M1$ and $E1$ transitions in Eq. (1.6)

$$P_\gamma(^{21}Ne, 2789\text{keV}) \approx 2\frac{\langle \frac{1}{2}^+, \frac{1}{2}|\mathcal{H}_{weak}|\frac{1}{2}^-\frac{1}{2}\rangle}{(E_{\frac{1}{2}^+} - E_{\frac{1}{2}^-})}\frac{1+\delta_-^*\delta_+}{1+|\delta_-|^2}\text{Re}\left[\frac{\langle \frac{3}{2}^+||M1||\frac{1}{2}^+\rangle}{\langle \frac{3}{2}^+||E1||\frac{1}{2}^-\rangle}\right] \tag{1.6}$$

where in addition to the $M1$ and $E1$ moments there is also corrections from the electric (magnetic) quadrupole terms $E2$ ($M2$) which are given by the δ_+ and δ_- terms from Eqs. (1.7) and (1.8) respectively.

$$\delta_- = \langle \tfrac{3}{2}^+||M2||\tfrac{1}{2}^-\rangle/\langle \tfrac{3}{2}^+||E1||\tfrac{1}{2}^-\rangle \tag{1.7}$$

$$\delta_+ = \langle \tfrac{3}{2}^+||E2||\tfrac{1}{2}^+\rangle/\langle \tfrac{3}{2}^+||M1||\tfrac{1}{2}^+\rangle \tag{1.8}$$

The lifetimes for the $\frac{1}{2}^+ \to \frac{3}{2}^+$ and $\frac{1}{2}^- \to \frac{3}{2}^+$ decays in ^{21}Ne are respectively $\tau_+ = 7.6\pm$ .8 fsec [105–107] and $\tau_- = 696\pm51$psec [44,45]. The $\frac{1}{2}^+ \to \frac{3}{2}^+$ decay is determined by a combination of the $M1$ and $E2$ moment. Under the extreme assumption $B(E2) = 30$ W.u., one can obtain the bound $|\delta^+| < .39$, while using a measurement of pair emission from the $\frac{1}{2}^- \to \frac{3}{2}^+$ transition one obtains the bound $|\delta_-| < .6$ [83]. However, one must again calculate the sign of these quantities as well as the weak transition matrix element. The photon circular polarization asymmetry for unpolarized ^{21}Ne has been measured by a group at Seattle and Chalk River giving bounds of $(24\pm24)\times10^{-4}$ [99] and $(3 \pm 16) \times 10^{-4}$ [38].

An extreme example of the amplification effect is given by the photon asymmetry in the 501 keV γ decay of an excited state of ^{180}Hf in which the measured result is $-(1.66 \pm .18) \times 10^{-2}$ [77, 78]. In this decay the nearby opposite parity 8^- and 8^+ states are separated 57 keV, and the 8^- state decays to the 6^+ state giving off a 501 keV photon as seen in Fig. 1.2. The PV signal in ^{180m}Hf is further enhanced since the parity conserving decay mode is sixfold K-forbidden leading to the large observed asymmetry in polarized ^{180m}Hf. These nuclei with adjacent energy levels of opposite parity were the only source of nuclear PV measurements until the 1980's, during which a solid PV measurement for proton proton (pp) scattering of $-(0.93 \pm$

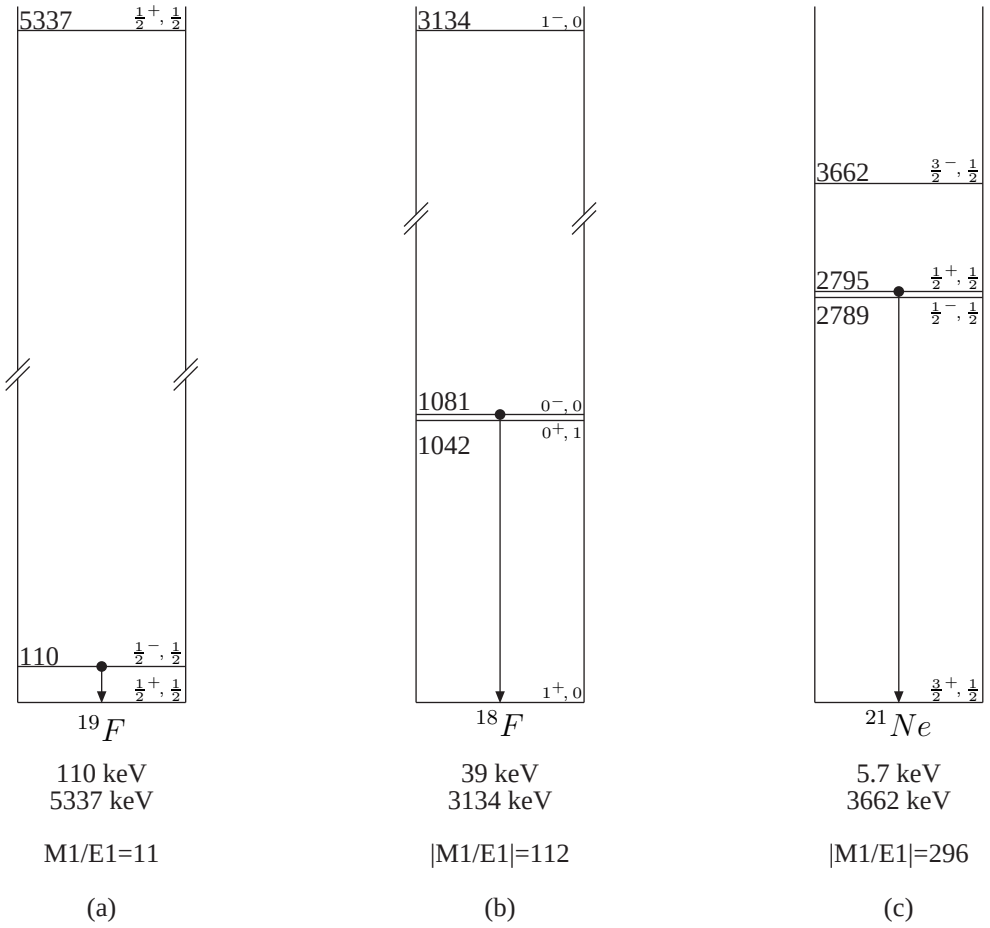

Figure 1.1: (a)Lowest lying energy levels of ^{19}F with opposite parity states $\frac{1}{2}^-$- $\frac{1}{2}^+$ separated by 110 keV.(b)Lowest lying energy levels of ^{18}F with opposite parity states 0^-- 0^+ separated by 39 keV.(c)Lowest lying energy levels of ^{21}Ne with opposite parity states $\frac{1}{2}^+$- $\frac{1}{2}^-$ separated by 5.7 keV.

$0.20 \pm 0.05) \times 10^{-7}$ was given by the Bonn experiment at 13.6 MeV [46], as well as a PSI measurement of $-(1.57 \pm 0.23) \times 10^{-7}$ at 45.0 MeV [89, 92]. A measurement for proton alpha particle ($p\alpha$) scattering of $-(3.34 \pm 0.93) \times 10^{-7}$ was also carried out at 46.0 MeV [69].

In the mid 1990's new PV measurements were carried out on the nuclear anapole moments of ^{133}Cs and ^{205}Tl [103, 108]. The anapole moment was proposed by Vaks and Zeldovich soon after the discovery of parity violation as a PV extension of normal

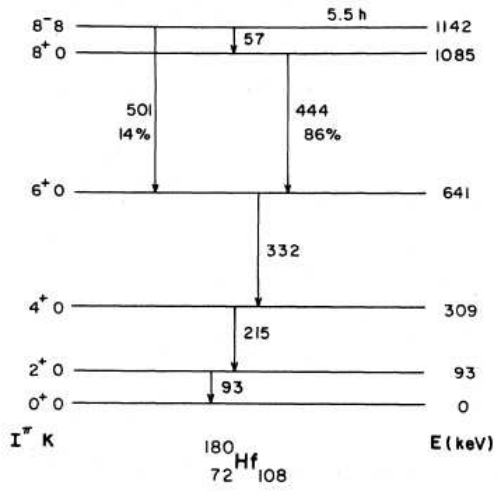

Figure 1.2: Decay scheme of ^{180m}Hf

electromagnetic multipole moments [109]. The form of the anapole moment as given in Eq. (1.9) is zero for on shell photons.

$$\frac{a(q^2)}{M_N^2}\left(\not{q}q^\mu - q^2\gamma^\mu\right)\gamma_5 \tag{1.9}$$

Therefore the anapole moment cannot be probed by electromagnetic fields but rather is probed by off shell photons via interactions with electrons. In the case of the ^{133}Cs nucleus the electrons of the ^{133}Cs atom interact with the anapole moment of ^{133}Cs. The $7S_{1/2} \rightarrow 6S1/2$ atomic transition is suppressed and only allowed by M1 decay. However, due to an interaction with the anapole moment the $7S_{1/2}$ state mixes with the $6P_{3/2}$ state and due to this small mixing decay from the modified $7S_{1/2}$ to the $6S_{1/2}$ state can decay via the E1 channel. In the actual experiment an electric field is applied which gives an observable E1 decay from the $7S_{1/2}$ to $6S_{1/2}$ state. The nuclear spin is then effectively flipped back and forth which causes a modulation in this E1 decay because of the PV $7S_{1/2} \rightarrow 6S_{1/2}$ nuclear spin dependent transition which is predominantly dependent on the nuclear anapole moment. After

subtracting out other subdominant nuclear PV effects from the ^{133}Cs measurement a value of $(.090 \pm .016)$ is found for the ^{133}Cs anapole moment [63].

In the case of ^{205}Tl the allowed M1 decay of the atomic levels $6P_{1/2} \leftrightarrow 6P_{3/2}$ interferes with the E1 decay that occurs due to parity mixing between S and P atomic states, because of PV interactions with the nucleus. This interference results in the rotation of polarized light sent through a Thallium vapor target. In order to measure the spin dependent part of the PV interaction the hyperfine $F = 0$ and $F = 1$ transitions were compared, where $F = I + J$, I being the nuclear spin and J the spin plus orbital angular momentum of the valence electron. The measurement of ^{205}Tl was carried out by two groups one at Oxford [40] and the other at Seattle [103] both only achieving bounds. From the measurements of the Seattle group a value of $(.376 \pm .400)$ was obtained for the anapole moment after subtracting other subdominant nuclear PV effects [63]. (Note the Seattle result was used because its central value was more restrictive to the weak meson-nucleon coupling parameter space of the PV experiments shown in Fig. 1.4).

Finally for the photon asymmetry in $np \rightarrow d\gamma$ the NPDGamma experiment formerly at LANSCE (Los Alamos Neutron Science Center) is being reassembled at the new fundamental neutron physics beamline at SNS (Spallation Neutron Source at Oak Ridge National Laboratory) [52]. Due to the increased luminosity at SNS this experiment should have the requisite sensitivity to measure the expected PV signal of roughly 5×10^{-8} at an expected level of 1×10^{-8}.

1.2 Theory

Nuclear parity-violation has typically been viewed in the context of the model by Desplanques, Donoghue, and Holstein (DDH) [31], which is a one meson exchange model where the degrees of freedom exchanged are the lightest possible such that $\Delta S = 0$, namely the charged pions, omega, and rho. All light neutral pseudoscalar

mesons π_0, η, and η' are excluded from the DDH model by Barton's theorem [8]. The model contains a total of seven phenomenological weak couplings, whose form and the resultant DDH potential are given later on in this thesis in Chapter 4 Section 2. DDH determined the value of these coupling by use of $SU(6)_W$ and quark model techniques. In the quark model (non-leptonic weak sector) parity violation is mediated by the exchange of $W^{\pm}$ and Z bosons and in the standard model is given by the Lagrangian in Eq. (1.10) (Note $|g| = 2M_W\sqrt{|G_F|\sqrt{2}}$ and M_W is the mass of the $W^{\pm}$ boson.)

$$\mathcal{L}_{weak} = \frac{g}{\sqrt{2}}(W^+ J_\mu^- + W^- J_\mu^+ + Z J_\mu^Z) \tag{1.10}$$

where the $W^{\pm}$ and Z boson couple to quark currents of u,d, and s quarks which are defined in Eqs. (1.11). (Note that $\left(J_\mu^+\right)^\dagger = J_\mu^-$ and all heavy quarks have been integrated out)

$$J_\mu^+ = \cos\theta_C \bar{u}\gamma_\mu(1+\gamma_5)d + \sin\theta_C \bar{u}\gamma_\mu(1+\gamma_5)s \tag{1.11a}$$

$$J_\mu^Z = \bar{u}\gamma_\mu(1+\gamma_5)u - \bar{d}\gamma_\mu(1+\gamma_5)d - \bar{s}\gamma_\mu(1+\gamma_5)s - 4\sin^2\theta_W J_\mu^{em} \tag{1.11b}$$

$$J_\mu^{em} = \frac{2}{3}\bar{u}\gamma_\mu u - \frac{1}{3}\bar{d}\gamma_\mu d - \frac{1}{3}\bar{s}\gamma_\mu s \tag{1.11c}$$

These currents can further be broken up into their isospin and strangeness dependence yielding

$$J_{\mu\ (\Delta I=1)}^{+(\Delta S=0)} = \cos\theta_C \bar{u}\gamma_\mu(1+\gamma_5)d \tag{1.12}$$

$$J_{\mu\ (\Delta I=1/2)}^{+(\Delta S=-1/2)} = \sin\theta_C \bar{u}\gamma_\mu(1+\gamma_5)s \tag{1.13}$$

$$J^{Z\,(\Delta S=0)}_{\mu\ (\Delta I=0)} = \bar{u}\gamma_\mu(1+\gamma_5)\bar{\mu} - \bar{d}\gamma_\mu(1+\gamma_5)d - \bar{s}\gamma_\mu(1+\gamma_5)s - \frac{2}{3}\sin^2\theta_W\left(\bar{u}\gamma_\mu u - \bar{d}\gamma_\mu d - 2\bar{s}\gamma_\mu s\right) \tag{1.14}$$

$$J^{Z\,(\Delta S=0)}_{\mu\ (\Delta I=1)} = -2\sin^2\theta_W\left(\bar{u}\gamma_\mu u + \bar{d}\gamma_\mu d\right) \tag{1.15}$$

The masses of the $W^\pm$ and Z bosons are roughly 100 GeV. The nuclear energies we consider range from an MeV to a GeV and therefore at the scales we are considering the $W^\pm$ and Z bosons are heavy degrees of freedom and can be integrated out leaving one with an effective weak Hamiltonian between quarks. Keeping only the $\Delta S = 0$ part of the weak Hamiltonian we find Eq (1.16)

$$\begin{aligned}\mathcal{H}_{weak}(\Delta S=0) = \frac{G_F}{\sqrt{2}}\Big[&J^{-\,(\Delta S=0)}_{\mu\ (\Delta I=1)}J^{+\,(\Delta S=0)}_{\mu\ (\Delta I=1)} + J^{-\,(\Delta S=-1/2)}_{\mu\ (\Delta I=1/2)}J^{+\,(\Delta S=-1/2)}_{\mu\ (\Delta I=1/2)} \\ &+J^{Z\,(\Delta S=0)}_{\mu\ (\Delta I=0)}\left(J^{Z\,(\Delta S=0)}_{\mu\ (\Delta I=0)}\right)^\dagger + J^{Z\,(\Delta S=0)}_{\mu\ (\Delta I=1)}\left(J^{Z\,(\Delta S=0)}_{\mu\ (\Delta I=1)}\right)^\dagger \\ &+J^{Z\,(\Delta S=0)}_{\mu\ (\Delta I=0)}\left(J^{Z\,(\Delta S=0)}_{\mu\ (\Delta I=1)}\right)^\dagger + J^{Z\,(\Delta S=0)}_{\mu\ (\Delta I=1)}\left(J^{Z\,(\Delta S=0)}_{\mu\ (\Delta I=0)}\right)^\dagger\Big] + h.c.\end{aligned} \tag{1.16}$$

With the weak Hamiltonian known the primary task at hand is to calculate the vertices $\langle B'M|\mathcal{H}_{weak}|B\rangle$ and $\langle B'V|\mathcal{H}_{weak}|B\rangle$ where B and B' are baryons, M pseudoscalar mesons, and V vector mesons. The first attempt to calculate these vertices was in the factorization approximation carried out by Michel [86]. In this procedure one inserts a sum of intermediate states but only keeps the ground state as in Eq. (1.17)

$$\langle \rho^- p|H_{weak}|n\rangle = \frac{G_F}{\sqrt{2}}\cos^2\theta_C \langle \rho^- p|A_+^\mu(0)V_\mu^-|n\rangle \tag{1.17}$$
$$\approx \frac{G_F}{\sqrt{2}}\cos^2\theta_C \langle \rho|V_\mu^-(0)|0\rangle\langle p|A_+^\mu(0)|n\rangle$$

Going beyond the factorization approximation DDH calculated further contributions to these amplitudes by using the quark model and $SU(6)_W$ symmetry whose use was advocated by McKellar and Pick in this context [84, 85]. ($SU(6)_W$ symmetry is the combination of $SU(3)$ flavor symmetry and $SU(2)$ symmetry that is invariant to Lorentz boosts along the z direction. This symmetry is useful in the context of two-body decay because the products decay along a line where the $SU(2)$ is valid) The important contributions are shown in Fig. 1.3, where diagram (a) corresponds to the factorization approximation used by Michel, diagram (b) involves baryons as intermediate states and is calculated by using the quark model. Finally diagram (c) is zero in the quark model and is calculated by using sum rules from $SU(3)$ symmetry and PCAC relations so that diagram (c) can be related to known hyperon $\Delta S = 1$ decay amplitudes.

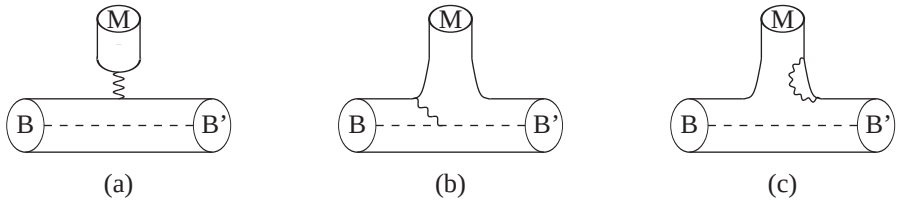

Figure 1.3: Important diagrams for $\langle B'M|\mathcal{H}_{weak}|B\rangle$ in quark model. (a)Diagram corresponding to factorization approximation.(b)Diagram corresponding to intermediate baryon states.(c)Diagram is calculated by using sum rules with $\Delta S = 1$ hyperon decay (This diagram is zero in the quark model).

In $SU(6)_W$ the pseudoscalar and vector mesons fall into the same 35-dimensional representation while the baryon octet and decuplet in $SU(3)$ are put into a 56-dimensional representation. Using a generalized Wigner-Eckart theorem and quark

model wavefunctions one can calculate all the non-zero diagrams as a geometrical factor (depending on $SU(6)_W$ Clebsch-Gordan coefficients) times a complicated radial integral coming from quark model wavefunctions. The quark model wavefunction used by DDH were those of the MIT bag model [24, 25]. In addition to this DDH also took into account the renormalization of the weak quark operators by hard gluon corrections [3, 4, 51]. However, due to $SU(6)_W$ symmetry breaking, uncertainty in the quark model wavefunctions, and hard gluon corrections DDH were only able to obtain reasonable ranges and "best" values for these vertices and in turn the DDH parameters.(An important thing to note is that one of the couplings $h_\rho^{1'}$ is shown to be small by quark model calculations and is thus ignored [66].)

1.3 DDH and experiment

In the few body sector is is straightforward to calculate PV observables. For example in the longitudinal analyzing power of pp scattering one uses the Distorted Wave Born Approximation (DWBA) to calculate the scattering amplitudes. In DWBA one calculates the wavefunctions from the strong and coulomb potential by any desired method while ignoring the PV potential. Then the PV potential is sandwiched between these wavefunctions to give the scattering amplitudes. The longitudinal analyzing power has been calculated by many groups [22, 34–36, 54, 68] The results for pp scattering at 13.6 MeV and 45.0 MeV as well as for $p\alpha$ scattering at 46.0 MeV are given in terms of the DDH parameters by Eqs. (1.18),(1.19), and (1.20) respectively [30, 32]

$$A_L(\vec{p}p, 13.6\text{MeV}) = .043(h_\rho^0 + h_\rho^1) + .017h_\rho^2 + .039(h_\omega^0 + h_\omega^1) \tag{1.18}$$

$$A_L(\vec{p}p, 45.0\text{MeV}) = .079(h_\rho^0 + h_\rho^1) + .032h_\rho^2 + .073(h_\omega^0 + h_\omega^1) \tag{1.19}$$

$$A_L(\vec{p}\alpha, 46.0\text{MeV}) = -.034 f_\pi + .014 h_\rho^0 + .047 h_\rho^1 + .059(h_\omega^0 + h_\omega^1) \tag{1.20}$$

In the many body sector the primary method for calculating PV observables is by the use of shell model wavefunctions as in the anapole moments of ^{133}Cs and ^{205}Tl [62]. Shell model calculations can also be used for ^{18}F and ^{19}F [2,16]. However, one can remove most of the nuclear structure uncertainty of the matrix elements of PV observables in ^{18}F (^{19}F) by matching it to the axial-charge β decay of ^{18}Ne (^{19}Ne) [2]. Doing this one finds good agreement with the shell model calculations. The shell model predictions for these observables in terms of the DDH coefficients are [63]. (Note we exclude a shell model prediction of ^{21}Ne as it contains five nucleons above the closed ^{16}O shell and thus is not believed to particularly reliable.)

$$P_\gamma(^{18}F, 1.081\text{MeV}) = 4330 f_\pi - 490 h_\rho^1 - 820 h_\omega^1 \tag{1.21}$$

$$A_\gamma(^{19}F, .110\text{MeV}) = -96 f_\pi + 35 h_\rho^0 + 10 h_\rho^1 + 20 h_\omega^0 + 17 h_\omega^1 \tag{1.22}$$

$$\kappa_{Anapole}(^{133}Cs) = 60.7 f_\pi - 25.8 h_\rho^0 - 3.9 h_\rho^1 + .4 h_\rho^2 - 10.1 h_\omega^0 - 4.9 h_\omega^1 \tag{1.23}$$

$$\kappa_{Anapole}(^{205}Tl) = -18.0 f_\pi + 3.8 h_\rho^0 - .3 h_\rho^1 - .3 h_\rho^2 + 2.8 h_\omega^0 + 1.3 h_\omega^1 \tag{1.24}$$

For most experiments it turns out the important contributions from the DDH model come from the isoscalar contribution $h_\rho^0 + .7 h_\omega^0$ and the isovector contribution

$f_\pi - .1h^1_\rho - .18h^1_\omega$. Plotting the PV observables using these combinations of coefficients and matching them to their measured values one obtains Fig. 1.4.

It is very clear from Fig. 1.4 that with the exception of the ^{133}Cs and ^{205}Tl anapole moment measurements that the other measurements overlap in a small region. In this overlap region the isoscalar DDH coefficients seem to be slightly larger than the DDH "best" values and the isovector combination of DDH coefficients (which is mostly determined by f_π) is much smaller than the DDH "best" value. The anapole moments do not overlap with these predictions. In particular the ^{133}Cs anapole moment [108] predicts a much larger value for the isovector combination $f_\pi - .1h^1_\rho - .18h^1_\omega$ than the ^{18}F bound. However, the ^{18}F bound is thought to be fairly reliable since it has been measured by five different groups and its theoretical determination by matching onto the beta decay of ^{19}Ne is mostly model independent. The theoretical determination of the ^{133}Cs anapole moment relies on the use of shell model wave functions whose theoretical uncertainties could be the source of the discrepancy. As for the ^{205}Tl anapole moment its band is about an order of magnitude larger that that of ^{133}Cs. Therefore most of the ^{205}Tl band lays to the lower left of the plot and within the bound does not overlap with all the other non-anapole measurements in the same region.

This discrepancy could be a result of either the modeling required to predict the anapole moment of ^{133}Cs, or the model dependence of the DDH potential. In order to overcome this model dependence it is incumbent to adopt a model independent tack. Such an approach at low energies is offered by pionless effective field theory ($\text{EFT}_{\not\pi}$), which requires only five low energy constants (LEC's)up to and including next-to-leading-order (NLO) in the two and three-body sector. Thus in order to understand parity-violation at low energies there must be at least five experiments and theoretical predictions for each. From the theoretical point of view few body interactions are the cleanest probes of hadronic parity-violation, since they are in

principle exactly calculable. However, the associated experiments are difficult as they require high precision.

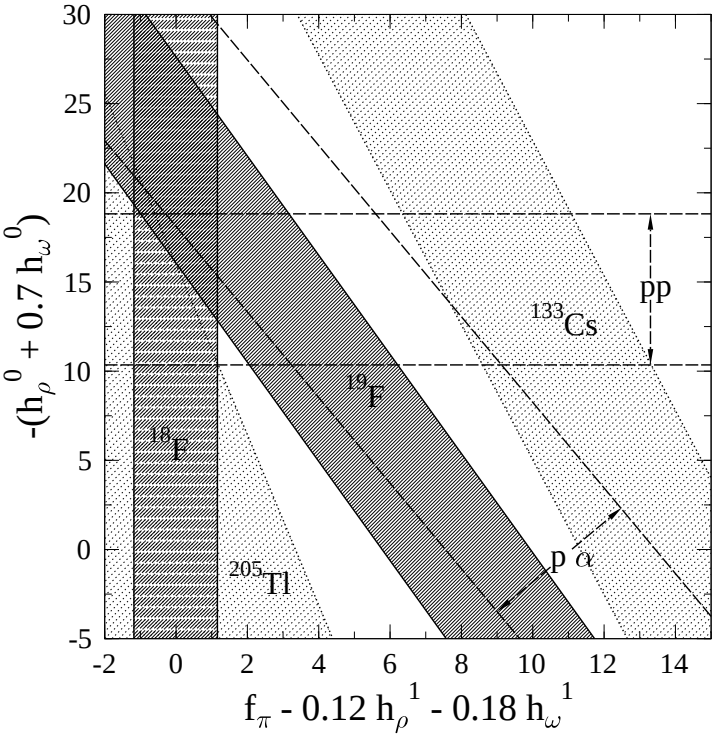

Figure 1.4: Experimental determination of DDH coefficients which are in units of 10^{-7} [63]. The error bands represent one standard deviation

1.4 EFT$_{\not\pi}$ to the rescue?

Many predictions for PV observables have been made in the two-body sector using EFT$_{\not\pi}$. The longitudinal analyzing power in neutron-neutron (nn), neutron-proton (np), and pp scattering has been calculated by Phillips, Schindler, and Springer [88] yielding

$$A_L^{pp} = -8\sqrt{2}p\,[g_3 + g_4 + g_5] \tag{1.25}$$

$$A_L^{nn} = -8\sqrt{2}p\,[g_3 - g_4 + g_5] \tag{1.26}$$

$$A_L^{np} = -8\sqrt{2}p\left[\frac{1}{1+3\gamma a^{(^1S_0)}}(g_3 - 2g_5) + \frac{\gamma_t a^{(^1S_0)}}{1+3\gamma_t a^{(^1S_0)}}(g_1 - 2g_2)\right] \tag{1.27}$$

where the asymmetries are taken at energies such that $p << \sqrt{2/|a|r}$ (here p is the external momentum, a the scattering length, and r the effective range) and the g_i are the PV LECs defined in Chapter 4. The advantage of using the notation g_i is that all results are the same in either the effective range expansion parametrization or Z-parametrization defined in the next chapter. Plugging in our estimates for the g_i based on DDH "best" values we find the predictions given below for the longitudinal asymmetries at $p = 1$ MeV. (Note for all predictions with two values the first prediction comes from dividing our estimate of g_2 by two and the other from using our prediction of g_2 as it is suspected that the estimate in this thesis for g_2 is a factor of two to large.)

$$A_L^{pp}(1\text{MeV}) = -2.4 \times 10^{-9} \tag{1.28}$$

$$A_L^{nn}(1\text{MeV}) = -2.0 \times 10^{-9} \tag{1.29}$$

$$A_L^{np}(1\text{MeV}) = -3.2 \times 10^{-9}, -5.7 \times 10^{-9} \tag{1.30}$$

These longitudinal asymmetries depend on all five PV LECs of EFT$_{\not\pi}$. In principle these longitudinal asymmetries allow one to perform four measurements that could determine four of the five PV LECs. The np asymmetry contains two different pieces that contain different energy dependence. (Note in our low energy limit this dependence goes away) Thus in principle measuring the np longitudinal asymmetry at two different energies where EFT$_{\not\pi}$ is valid will give two independent constraints on the PV LECs. The other two independent constraints on the PV LECs come from the

nn and *pp* longitudinal asymmetries. However, the longitudinal *nn* asymmetry is not a realistic experiment and therefore nucleon-nucleon longitudinal asymmetry measurements in practice could allow for three independent constraints on the PV LECs. As of now the only measurement of these asymmetries in the range of $\text{EFT}_{\not\pi}$ is the *pp* longitudinal asymmetry at 13.6 MeV. The 45.0 MeV *pp* longitudinal asymmetry would require the use of a pionful EFT.

In principle there is a whole other suite of polarization experiments that one could perform in the two-body sector that include spin correlation coefficients and spin transfer coefficients. In the case of spin correlation coefficients one must polarize both the target and the beam or collide two polarized beams. For spin transfer coefficients one polarizes either the beam or target initially and then measures the polarization of one of the nucleons after scattering. These experiments albeit much more difficult experimentally could provide further independent constraints on the PV LECs allowing them to be completely determined from just two body physics.

A different type of two-body experiment is the spin rotation of a neutron through a hydrogen target. Such an experiment must be performed at low energies such that the Compton wavelength of the neutron is sufficiently larger than the interatomic spacing of the hydrogen in order to interact coherently with the target. This condition is achieved with ultracold neutrons and liquid hydrogen where the Compton wavelength is of order 100 nm and the interatomic spacing of order 1 nm. One particular difficulty of this experiment is that the neutron will also rotate due to stray magnetic fields because of the Faraday effect. The earth's magnetic field alone is enough to potentially swamp any PV signal and care must be taken to take this into account. Neutron spin rotation in *np* scattering was calculated by Liu [81]. However strictly speaking Liu's calculation is not a pure effective field theory (EFT) calculation as he uses the potential determined by $\text{EFT}_{\not\pi}$ together with conventional nuclear

wavefunctions to make predictions. Using pure EFT$_{\not\pi}$ Griesshammer, Schindler, and Springer calculated the spin rotation to NLO obtaining

$$\frac{d\phi^{np}}{dz} = -[4.5 \pm .5](2g_2 + g_1) + [18.5 \pm 1.9](g_3 - 2g_5) \tag{1.31}$$

where the uncertainty is a conservative estimate of 10% due to the power counting estimates of NNLO effects and the units of the numbers are rad cm^{-1} MeV. Again plugging in estimates for g_i based on the DDH "best" values we obtain a prediction for the spin rotation of

$$\frac{d\phi^{np}}{dz} = 3.2 \times 10^{-9}\text{rad cm}^{-1}, 6.1 \times 10^{-9}\text{rad cm}^{-1} \tag{1.32}$$

The combination $(g_3 - 2g_5)$ of PV LECs in the np spin rotation is the same as in the longitudinal asymmetry in np scattering. However, the combination of the g_2 and g_1 coefficients are different. Thus these two observables could be used to isolate the values for g_1 and g_2 . (We assumed liquid hydrogen has a number density of $.22 \times 10^{23}$ atoms cm^{-3}.)

If one wishes to include interactions with photons then there is a whole other set of two-body observables with the radiative capture process $np \to d\gamma$. Two observables of particular interest in $np \to d\gamma$ are the photon asymmetry A_γ and the photon circular polarization P_γ. In the case of the photon asymmetry the neutron is transversely polarized and one measures the asymmetry of photons going in the lower and upper part of the detector. Measurement of the photon circular polarization is achieved by sending in an unpolarized neutron and measuring the asymmetry between left and right circularly polarized photons. The photon asymmetry and photon circular polarization in $np \to d\gamma$ has been calculated at zero energy by Schindler and Springer [97] as well as Ando and Hyun using EFT$_{\not\pi}$ giving results of

$$A_\gamma = 4\sqrt{2}M_N \frac{1 - \frac{\gamma_t a^{(^3S_1)}}{3}}{\kappa_1(1 - \gamma_t a^{(^1S_0)})} g_2 \tag{1.33}$$

$$P_\gamma = -4\sqrt{2}\frac{M_N}{\kappa_1(1-\gamma_t a^{(^1S_0)})}\left[\left(1-\frac{2}{3}\gamma_t a^{(^1S_0)}\right)g_2 + \frac{\gamma_t a^{(^1S_0)}}{3}\left(g_3 - 2g_5\right)\right] \tag{1.34}$$

where κ_1 is the nucleon isovector dipole moment, γ_t the deuteron binding momentum described in the next chapter, and $a^{(^1S_0)}$ ($a^{(^3S_1)}$) the scattering length in the $^1S_0$ ($^3S_1$) channel again described in the next chapter. Plugging in our estimates for the g_i based on DDH "best" values we find values for A_γ and P_γ of

$$A_\gamma = 3.2 \times 10^{-8}, 6.4 \times 10^{-8} \tag{1.35}$$

$$P_\gamma = 1.2 \times 10^{-7} \tag{1.36}$$

The photon asymmetry A_γ, in leading-order (LO) EFT$_{\not\pi}$ is solely determined by the $g^{^3S_1 - ^3P_1}$ coefficient of the auxiliary field formalism. This is important because it gives a value for the f_π coefficient in the DDH potential. This means the measurement of the photon asymmetry could explain the source of the discrepancy between ^{18}F and ^{133}Cs by giving an unambiguous prediction for the value of f_π. The measurement of P_γ will be difficult because the efficiency of the polarimeters used to measure the photon polarization is only about 8% whereas the polarization of the neutron beam at SNS used to measure A_γ is nearly 100%. One possible way around this is use to use the time reversed reaction $\gamma d \to np$ which is being proposed to run at the HIγS (High Intensity Gamma Source) facility. Again we see the same combination $(g_3 - 2g_5)$ for P_γ as for np spin rotation and A_L^{np}. This is simply due the fact that these observables project out the same isospin channels and the terms for g_3 through g_5 in the PV Lagrangian all have the same spin dependence.

There have also been predictions in the three-body sector for neutron spin rotation and the longitudinal beam asymmetry at a lab energy of 15 keV in nd scattering by

Song et al [100]. Again these calculations are not performed in pure EFT but use a PV potential determined by EFT with Faddeev type integral equations. Neutron spin rotation in nd scattering has also been predicted by Schiavilla et al. by using EFT potentials with wavefunctions determined by hyperspherical techniques [95, 96]. Both predictions for neutron spin rotation are comparable. Neutron spin rotation in nd scattering is carried out to LO in EFT$_{\not\pi}$ in this thesis and it has been carried out to NLO by Griesshammer, Schindler, and Springer. Below we show the results for the spin rotation, and beam and target asymmetry at 15 keV lab energy given in this thesis to LO

$$\frac{d\phi^{nd}}{dz} = -[19.0 \pm .3]g_1 - [37.1 \pm .9]g_2 - [13.5 \pm 3.3]g_3 + [8.96 \pm 2.15]g_4 \qquad (1.37)$$

$$A_L(\vec{n}d) = -[14.5 \pm .1]g_1 - [39.8 \pm .2]g_2 - [2.27 \pm .44]g_3 + [1.52 \pm .30]g_4 \qquad (1.38)$$

$$A_L(n\vec{d}) = [9.04 \pm .12]g_1 - [59.8 \pm .1]g_2 + [2.06 \pm .41]g_3 - [1.38 \pm .28]g_4 \qquad (1.39)$$

where the uncertainty is due to cutoff variation in the numerical integration. The units of the numbers in the spin rotation are rad cm^{-1} MeV and those of the target and beam asymmetry are MeV. Again plugging in values for the g_i based on DDH "best" values we find predictions for the nd spin rotation and target and beam asymmetries of

$$\frac{d\phi^{nd}}{dz} = 6.5 \times 10^{-9}\text{rad cm}^{-1}, 1.8 \times 10^{-8}\text{rad cm}^{-1} \tag{1.40}$$

$$A_L(\vec{n}d) = 9.8 \times 10^{-9}, 2.2 \times 10^{-8} \tag{1.41}$$

$$A_L(n\vec{d}) = 2.1 \times 10^{-8}, 4.0 \times 10^{-8} \tag{1.42}$$

The EFT$_{\not\pi}$ predictions are in rough agreement with those of the hybrid techniques except for a as of yet mysterious factor of two which is due to the g_2 coefficient. Assuming DDH "best" values the dominant contribution to the spin rotation comes from the $g^{^3S_1-^3P_1}$ coefficient. Thus measurement of the photon asymmetry in $np \to d\gamma$ could give us a rough idea for the order of magnitude of the nd spin rotation. The spin rotation prediction is determined by all of the PV LECs with the exception of the $g^{^1S_0-^3P_0}_{(\Delta I=2)}$ term. This fact follows trivially since nd scattering has total isospin $1/2$ and isospin $1/2$ cannot be connected to another isospin $1/2$ with an isotensor. Despite the spin rotation being determined by four PV LECs it will only give the value of the dominant contribution from the $g^{^3S_1-^3P_1}$ term under the assumption that the coefficients are roughly determined by the DDH "best" values. The EFT$_{\not\pi}$ prediction for beam asymmetry agrees with the hybrid calculation of Song et al. up to a factor of two, and the beam asymmetry value has not yet been independently verified.

In the three-body sector another possible experiment is the longitudinal analyzing power in pd scattering which has not been calculated in EFT$_{\not\pi}$. However, a rough estimate at 15 MeV in terms of the Danilov parameters described in Chapter 4 has been carried out by Desplanques and Missimer using the Bethe Goldstone equation giving [32].

$$A_L(\vec{p}d)(15\text{MeV}) = -[.21\rho_t + .07\lambda_s^{pp} - .13\lambda_t - .04\lambda_s^{pn}]M_N \tag{1.43}$$

and plugging in values for the Danilov parameters based on DDH "best" values one finds

$$A_L(\vec{p}d)(15\text{MeV}) = -1.3 \times 10^{-7} \tag{1.44}$$

There is also many other PV observables in elastic nd and pd scattering such as spin correlation coefficients and spin transfer coefficients. Again these experiments are complicated as they require either a polarized target or two polarized beams in the correlation coefficient measurement or measuring the final polarization in the spin transfer coefficient case. Including interactions with external photons there is many other possible observables in the threebody sector. In particular there is the photon asymmetry A_γ, for capture of polarized neutrons (protons) on a deuteron target resulting in the process $\vec{n}d \to t\gamma$ ($\vec{p}d \to {}^3He\gamma$). There is also the circular polarization asymmetry, P_γ, for an unpolarized neutron (proton) on a deuteron target resulting in $nd \to t\gamma^{\circlearrowleft}$ ($pd \to {}^3He\gamma^{\circlearrowleft}$). One could also perform the time reversed version of these reactions and measure parity violation in the photodisintegration of ${}^3He$ or tritium and these are possible future experiments at HIγS. However, an experiment with a tritium target is not likely because of safety issues. As of now none of these observables have been calculated using EFT$_{\not\pi}$.

There are also predictions for $A > 3$. Viviani et al. have calculated parity violation in the longitudinal asymmetry of the charge-exchange reaction ${}^3He(n,p)^3H$ by using EFT potentials with wavefunctions determined from hyperspherical techniques [104]. Calculating this observable at zero incident neutron energy they found the expression Eq. (1.45) for the longitudinal asymmetry in terms of the DDH parameters.

$$A_L({}^3He(\vec{n},p)^3H) = -.18f_\pi - .14h_\rho^0 + .27h_\rho^1 + .0012h_\rho^2 - .13h_\omega^0 + .05h_\omega^1 \tag{1.45}$$

Plugging in the "best" values for the DDH parameters one finds the prediction below for the longitudinal asymmetry.

$$A_L(^3He(\vec{n},p)^3H) = 1 \times 10^{-7} \tag{1.46}$$

Gudkov has also done the same calculation by using the resonance approach and obtained good agreement with the calculation of Viviani et al. [58]. However, no EFT calculation has been done for these many body interactions.

There are a plethora of possible PV observables for $A > 3$ reactions. However, these reactions fall into three basic categories that one might like to consider namely polarization experiments in nN or pN scattering where N is a nucleus with $A > 2$ (e.g. longitudinal asymmetries, spin transfer coefficients, and spin correlation coefficients), n or p capture on N, and neutron spin rotation through an N target. In principle there are many other possible reactions that one could consider because of various different breakup or exchange channels. Measurements involving higher body interactions may be easier to perform, and there is an existing 46.0 MeV measurement for the longitudinal asymmetry in $\vec{p}\alpha$ scattering. Thus it is important that we predict these measurements using EFT, and nd scattering in an EFT$_{\not\pi}$ formalism is an important first step in understanding how to perform PV calculations for $A > 3$ nuclei. However as one adds more and more nucleons, EFT$_{\not\pi}$ methods become more and more cumbersome, but more importantly they start to lose their validity as the binding energy of nuclei becomes comparable to the cutoff of the theory. As one goes to heavier and heavier nuclei it will be necessary to use a pionful EFT. In fact already at $A = 4$ the binding energy of ^4He is $E_B = 28.3$ MeV, which is considerably higher than the cutoff energy of EFT$_{\not\pi}$, at roughly $m_\pi^2/M_N \sim 20$ MeV. Despite this we can still extend EFT to the four-body sector by including pions which will take considerable work and which requires an understanding of the three-body sector that

is described in nd scattering by either pionful or pionless EFT. However, this will be deferred to future work.

CHAPTER 2

PIONLESS EFT

2.1 Introduction

EFT$_{\not\pi}$ offers a model independent scheme by which low energy observables involving nucleons and couplings to external currents (photons, electrons, neutrinos and etc.) can be systematically calculated via an expansion of the momentum scale over the cutoff scale. The name EFT$_{\not\pi}$ obviously implies that pions are not degrees of freedom and are therefore integrated out. Thus the pion mass sets a rough scale for the momentum cutoff of the theory at about 100 MeV. Since the energy scale of this theory is well below the average nucleon mass of 938.918 MeV, nucleons can be treated non-relativistically with relativistic corrections. Indeed at these low energies our only degrees of freedom are nucleon fields and possible couplings to external currents. Focusing solely on nucleon-nucleon interactions one finds that the Lagrangian can be written as contact interactions between nucleon fields. For example in the $^3S_1$ channel for two-body nucleon interactions one finds the following interaction Lagrangian.

$$\begin{aligned}\mathcal{L}_2 = &- C_0^{(^3S_1)}(N^T P_i N)^\dagger (N^T P_i N) \\ &+ C_2^{(^3S_1)}\frac{1}{8}\left[(N^T P_i N)^\dagger (N^T P_i \overset{\leftrightarrow}{\nabla}^2 N) + h.c.\right] \\ &- \frac{1}{16}C_4^{(^3S_1)}\left(N^T P_i \overset{\leftrightarrow}{\nabla}^2 N\right)^\dagger \left(N^T P_i \overset{\leftrightarrow}{\nabla}^2 N\right) + \cdots\end{aligned} \tag{2.1}$$

where $P_i = \frac{1}{\sqrt{8}}\sigma_2\sigma_i\tau_2$ projects out the (spin) (vector) isoscalar part of the nucleon-nucleon interaction. We see right away that this is a non-renormalizable field theory.

However, this is not a problem as there exists an infinite number of terms in this Lagrangian into which all divergences can be absorbed. The symmetries of EFT$_{\not\pi}$ are also clear, rotational symmetry, and isospin symmetry. However, in reality isospin symmetry is broken by the small mass difference between neutron and proton, about 1.293 MeV, about .2% of the average nucleon mass. Thus isospin breaking terms will only become necessary if we desire precision beyond 1% and will therefore be ignored for our purposes. The important point here is that this theory contains all the symmetries of QCD in terms of nucleon fields, and it is this feature which makes the theory model independent. The last important feature of EFT$_{\not\pi}$ is its power counting scheme which allows one to to order the terms by the importance of their contributions. It turns out that naive dimensional analysis is too simple and does not lead to a consistent power counting scheme for energies above $|1/a_t|$ or $|1/a_s|$ where a_t is the scattering length in the ${}^3S_1$ channel and a_s the scattering length in the ${}^1S_0$ channel. It also turns out that a generic feature of nucleon-nucleon interactions is low energy bound states. These bound states are necessarily non-perturbative and thus require one to sum an infinite number of diagrams to reproduce the corresponding poles in the S matrix. A consistent power counting scheme for EFT$_{\not\pi}$ is given by KSW (Kaplan,Savage, and Wise) power counting [71, 72], wherein the term $C_0^{({}^3S_1)}$ is combined with an infinite series of bubble diagrams, which can then be summed via a geometric series. The power counting scheme is made consistent by calculating the loop diagrams using dimensional regularization with the power divergence subtraction (PDS) subtraction scheme in which the poles occurring in 4 and 3-dimensions are subtracted by counterterms, in which case all higher order terms in the EFT$_{\not\pi}$ can be treated perturbatively. This scheme has been used successfully in the two-body sector to calculate many observables including couplings to external currents [9, 23, 90].

In the ${}^3S_1$ channel, using the KSW power counting scheme, the coefficients are matched onto the effective range expansion for the ${}^3S_1$ channel amplitude. It is most

convenient to expand the effective range expansion about the deuteron pole that corresponds to the deuteron bound state in the ${}^3S_1$ channel

$$k\cot(\delta_0) = -\gamma_t + \frac{1}{2}\rho_t(\vec{\mathbf{k}}^2 + \gamma_t^2) + \cdots \tag{2.2}$$

Here $\gamma_t = 45.7025$ MeV is the deuteron binding momentum and $\rho_t = 1.764$ fm is the effective range about the deuteron pole. When matching the coefficients of the Lagrangian above onto this effective range expansion one finds that the coefficients need to be refitted at each order. In order to avoid this we will use an alternate approach [23]. If we were expanding the effective range expansion about zero momentum this would be unnecessary.

$$C_0^{^3S_1} = C_{0,-1}^{^3S_1} + C_{0,0}^{^3S_1} + C_{0,1}^{^3S_1} + \cdots \tag{2.3}$$

In this expansion of the coefficient $C_0^{^3S_1}$ above, the second part of the subscript refers to scaling of the coefficient with respect to powers of Q, where Q is the external momentum of our process in units of the cutoff scale Λ. Setting the scale μ introduced by the KSW power counting to $\mu \sim Q$ and noting that our effective range scales as $\rho_t \sim 1/\Lambda$ one can show the following scaling properties for the coefficients of the Lagrangian in the expansion described above.

$$C_{0,-1}^{^3S_1} \sim \frac{1}{MQ}, \quad C_{0,0}^{^3S_1} \sim \frac{1}{M\Lambda}, \quad C_{2,-2}^{^3S_1} \sim \frac{1}{M\Lambda Q^2}, \quad C_{4,-3}^{^3S_1} \sim \frac{1}{M\Lambda^2 Q^3} \tag{2.4}$$

One can see right away that the dominant contribution comes from the term $C_{0,-1}^{^3S_1}$. The other terms, although containing larger powers of momentum in their denominator, will be multiplied by additional powers of momentum due to the Lagrangian, thus making these terms higher order. These scaling properties determine the power counting of our theory. The term $C_{0,-1}^{^3S_1}$ will be summed up in an infinite series of

diagrams at LO and all of the other terms will be included perturbatively at higher orders. With this knowledge in hand we can now determine the scaling properties and ultimately the power counting in the auxillary field formalism which will be useful for our three-body calculations.

2.2 Auxiliary Field Formalism

In three-body calculations it is advantageous to use an interaction Lagrangian in terms of auxiliary fields [50, 70]

$$\begin{aligned}\mathcal{L}^d_{PC} =& N^\dagger \left(i\partial_0 + \frac{\vec{\nabla}^2}{2M_N} \right) N \\ & - t_i^\dagger \left(i\partial_0 + \frac{\vec{\nabla}^2}{4M_N} - \Delta^{(^3S_1)}_{(-1)} - \Delta^{(^3S_1)}_{(0)} \right) t_i + y_t \left[t_i^\dagger N^T P_i N + h.c. \right] \\ & - s_a^\dagger \left(i\partial_0 + \frac{\vec{\nabla}^2}{4M_N} - \Delta^{(^1S_0)}_{(-1)} - \Delta^{(^1S_0)}_{(0)} \right) s_a + y_s \left[s_a^\dagger N^T \bar{P}_a N + h.c. \right]\end{aligned} \tag{2.5}$$

where P_i is as described before, and $\bar{P}_a = \frac{1}{\sqrt{8}} \tau_2 \tau_a \sigma_2$ projects out the (spin) (scalar) isovector component of the nucleon-nucleon interaction. The field t_i is the deuteron auxiliary field and will henceforth be called the deuteron (strictly speaking this is not true as the deuteron contains a small D wave component). The field s_a is the singlet auxiliary field and refers to a pair of nucleons in the $^1S_0$ channel. (Since there is only a virtual bound state in this channel this auxiliary field does not correspond to any real particle.) This auxiliary field formalism can be shown to be equivalent to the standard paradigm for EFT$_{\not\pi}$ in which only nucleon fields occur by performing Gaussian integration over the auxiliary fields together with a field redefinition [11]. After this is done the field t_i is essentially replaced by $N^T P_i N$ and the field s_a by $N^T \bar{P}_a N$. The auxiliary field formalism will be used for the rest of this presentation as it makes calculations simpler. (Note in the Lagrangian $\Delta^{(^3S_1)}$ is split up into two

Figure 2.1: LO diagram contributions to dressed deuteron propagator

parts $\Delta_{(-1)}^{({}^3S_1)}$ a LO piece, and $\Delta_{(0)}^{({}^3S_1)}$ a NLO piece so that $\Delta^{({}^3S_1)}$ does not necessitate refitting at each order)

Performing Gaussian integration and the field redefinition one can match the coefficients of the auxiliary field formalism to that of the standard EFT$_{\not\pi}$. Then using the scaling properties of the coefficients of the standard EFT$_{\not\pi}$ we can find the scaling properties of our coefficients in the auxiliary field formalism. Doing so we find that our coefficients scale as follows in the ${}^3S_1$ channel [50].

$$\Delta_{(-1)}^{{}^3S_1} \sim \frac{Q\Lambda}{M_N}, \quad \Delta_{(0)}^{{}^3S_1} \sim \frac{Q^2}{M_N}, \quad y_d^2 \sim \frac{\Lambda}{M_N^2} \tag{2.6}$$

With the scaling properties in hand we can calculate the LO deuteron propagator. At LO the deuteron propagator is dressed by an infinite sum of nucleon bubbles as in Fig 2.1, and the bare deuteron propagator is given by $i/\Delta_{(-1)}^{{}^3S_1}$. (The solid line in Fig. 2.1 represents the bare deuteron propagator and the thin lines nucleon propagators.) All these diagrams contribute at LO and scale as $M_N/Q\Lambda$ with respect to the external momentum, as can be easily shown by power counting. For each nucleon bubble we get two nucleon propagators which each scale as M_N/Q^2, an integral over three momentum and energy which scales as Q^5/M_N, the coupling constant y_t^2 which scales as Λ/M_N^2, and an extra bare deuteron propagator which scales as $M_N/Q\Lambda$. Using these power counting rules we find that for any number of nucleon bubbles the diagram will scale as $M_N/Q\Lambda$.

The single nucleon bubble contribution can be straightforwardly calculated using dimensional regularization and the PDS subtraction scheme,

$$i\Sigma(p) \;=\; \text{ 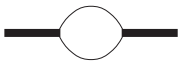 } \;=\; -i\tfrac{y_t^2 M_N}{4\pi}\left(\mu - \sqrt{\tfrac{1}{4}\vec{\mathbf{p}}^2 - M_N p_0 - i\epsilon}\right)$$

and summing this nucleon bubble to all orders we find the following simple expression for the deuteron propagator at LO

$$i\Delta_t^{LO}(p_0,\vec{\mathbf{p}}) = -\frac{4\pi i}{M y_t^2}\frac{1}{\frac{4\pi\Delta_{(-1)}^{(^3S_1)}}{M_N y_t^2} - \mu + \sqrt{\frac{\vec{\mathbf{p}}^2}{4} - M_N p_0 - i\epsilon}} \tag{2.7}$$

At NLO the deuteron propagator gets a correction from the deuteron kinetic energy term and the $\Delta_{(0)}^{^3S_1}$ term. These corrections are treated as perturbations and therefore are not resummed into a NLO propagator. At NNLO there are simply two such corrections added perturbatively to the LO deuteron propagator [50]. Thus we find that the NNLO deuteron propagator is given by (Note at NNLO there is in addition two other corrections. There is the relativistic correction, $\frac{\partial_0^2}{2M_N} \sim \frac{Q^4}{M_N^3}$, that is suppressed by two extra powers of the nucleon mass and thus ignored. There is also a correction term involving a self interaction of the deuteron with two derivatives. However, by renormalization group equations it can be shown that the first independent contribution of this term occurs at N3LO and is thus dropped at NNLO [23, 50]).

$$\begin{aligned} i\Delta_t^{NNLO}(p_0,\vec{\mathbf{p}}) = i\Delta_t^{LO}(p_0,\vec{\mathbf{p}})\Bigg(1 &+ \Delta_t^{LO}(p_0,\vec{\mathbf{p}})(\Delta_{(0)}^{(^3S_1)} + p_0 - \frac{\vec{\mathbf{p}}^2}{4M_N}) \\ &+ (\Delta_t^{LO}(p_0,\vec{\mathbf{p}}))^2(\Delta_{(0)}^{(^3S_1)} + p_0 - \frac{\vec{\mathbf{p}}^2}{4M_N})^2\Bigg) \end{aligned} \tag{2.8}$$

With the NNLO deuteron propagator in hand there exist two approaches to fit these coefficients to physical observables. One is to fit the NNLO propagator onto

the effective range expansion in the ${}^3S_1$ channel, and the second is coined the Z parametrization [55, 87]. In the Z parametrization the deuteron pole is fit at LO. Then at NLO and higher orders the coefficients are chosen such that the deuteron pole does not move and has the correct residue. We will first start with the effective range expansion. Since there is a pole in the ${}^3S_1$ channel which corresponds to the physical bound state of the deuteron we will expand the effective range expansion about this pole as given in (2.2). Now since $\rho_t << \gamma_t$ we can expand our scattering amplitude T, with ρ_t treated perturbatively.

$$\begin{aligned} T =& \frac{4\pi}{M_N} \frac{1}{-\gamma_t + \frac{1}{2}\rho_t(\vec{\mathbf{k}}^2 + \gamma_t^2) + \cdots - i|\vec{\mathbf{k}}|} \\ =& -\frac{4\pi}{M_N} \frac{1}{\gamma_t + i|\vec{\mathbf{k}}|} \left(1 + \frac{1}{2}\rho_t \frac{(\gamma_t^2 + \vec{\mathbf{k}}^2)}{\gamma_t + i|\vec{\mathbf{k}}|} + \frac{1}{4}\rho_t^2 \frac{(\gamma_t^2 + \vec{\mathbf{k}}^2)^2}{(\gamma_t + i|\vec{\mathbf{k}}|)^2} + \cdots \right) \end{aligned} \tag{2.9}$$

It is this expression that we wish to match to the deuteron propagator in order to obtain values for our coefficients. The quantity $-y_t^2 \Delta_t(\frac{\vec{\mathbf{k}}^2}{M_N}, 0)$ is equivalent to the scattering amplitude. Matching this quantity onto Eq. (2.9) we find the following values for our coefficients and the NNLO propagator.

$$\begin{aligned} i\Delta_t^{NNLO}(p_0, \vec{\mathbf{p}}) = \frac{4\pi i}{M_N y_t^2} \Bigg[& \frac{1}{\gamma_t - \sqrt{\frac{\vec{\mathbf{p}}^2}{4} - M_N p_0 - i\epsilon}} + \frac{\rho_t}{2} \frac{\gamma_t^2 + M_N p_0 - \frac{\vec{\mathbf{p}}^2}{4}}{\left(\gamma_t - \sqrt{\frac{\vec{\mathbf{p}}^2}{4} - M_N p_0 - i\epsilon}\right)^2} \\ & + \left(\frac{\rho_t}{2}\right)^2 \frac{\left(\gamma_t^2 + M_N p_0 - \frac{\vec{\mathbf{p}}^2}{4}\right)^2}{\left(\gamma_t - \sqrt{\frac{\vec{\mathbf{p}}^2}{4} - M_N p_0 - i\epsilon}\right)^3} \Bigg] \end{aligned} \tag{2.10}$$

$$\Delta_{(-1)}^{({}^3S_1)} = \frac{2}{M_N} \frac{\mu - \gamma_t}{\rho_d}, \quad \Delta_{(0)}^{({}^3S_1)} = \frac{\gamma_t^2}{M_N}, \quad y_t^2 = \frac{8\pi}{M_N^2} \frac{1}{\rho_t} \tag{2.11}$$

The last bit of information we need from the deuteron propagator is the deuteron wave function renormalization Z_D, which is needed when calculating the amplitudes for nd scattering. Z_D is simply given by the residue of the deuteron propagator about the deuteron pole which is located at $\vec{\mathbf{p}} = 0$ and $p_0 = -\gamma_t/M_N^2$ [50].

$$Z_D = \left[\frac{\partial}{\partial p_0} \left. \frac{1}{\Delta_t^{NNLO}(p_0, 0)} \right|_{p_0 = -\frac{\gamma_t^2}{M_N}} \right]^{-1} \tag{2.12}$$

Using this formula we obtain a form which contains the LO, NLO, and NNLO contributions. Note that such contributions perturbatively approach the deuteron pole residue in the ${}^3S_1$ scattering amplitude which is $Z_t = 1/(1 - \rho_t \gamma_t)$.

$$Z_D = \frac{8\pi\gamma_t}{M_N^2 y_t^2} \left[\underbrace{1}_{\text{LO}} + \underbrace{\rho_t \gamma_t}_{\text{NLO}} + \underbrace{(\rho_t \gamma_t)^2}_{\text{NNLO}} \right] \tag{2.13}$$

We next address the deuteron propagator in the Z parametrization. First we must rewrite the scattering amplitude in the ${}^3S_1$ channel in terms of the deuteron's pole residue Z_t. In order to do this we factor out the pole from the first line of the expression (2.9), then multiply and divide by Z_t, and finally we use that fact that $Z_t - 1 = \gamma_t \rho_t Z_t$ to find [55]

$$\begin{aligned} T =& -\frac{4\pi}{M_N} \frac{1 + (Z_t - 1)}{\gamma_t + i|\vec{\mathbf{k}}|} \frac{1}{1 + \frac{1}{2}(Z_t - 1)\left(1 + \frac{i|\vec{\mathbf{k}}|}{\gamma_t}\right) + \cdots} \\ =& -\frac{4\pi}{M_N} \frac{1 + (Z_t - 1)}{\gamma_t + i|\vec{\mathbf{k}}|} \left(1 - \frac{1}{2}(Z_t - 1)\left(1 + \frac{i|\vec{\mathbf{k}}|}{\gamma_t}\right) + \frac{1}{4}(Z_t - 1)^2 \left(1 + \frac{i|\vec{\mathbf{k}}|}{\gamma_t}\right)^2 + \cdots \right) \end{aligned} \tag{2.14}$$

Now we match this expression to the quantity $-y_t^2 \Delta_t^{\text{NNLO}}(\frac{\vec{\mathbf{k}}^2}{M_N}, 0)$ to obtain the values of our coefficients and the resulting NNLO deuteron propagator. However, in order to match these expressions $1/y_t^2$ has to be treated as a perturbation expansion in

$(Z_t - 1)$. Noting that $\rho_t = (Z_t - 1)/\gamma_t Z_t$, and using our effective range expansion expression (2.11) for y_t^2, we find the following perturbative expansion for $1/y_t^2$

$$\frac{1}{y_t^2} = \frac{M_N^2}{8\pi\gamma_t}\frac{Z_t - 1}{1 + (Z_t - 1)} = \frac{M_N^2}{8\pi\gamma_d}(Z_t - 1)\left[1 + (Z_t - 1) + \cdots\right] \tag{2.15}$$

For the expression $-y_t^2\Delta_t^{\rm NNLO}(\frac{\vec{\mathbf{k}}^2}{M_N}, 0)$ in Eq. (2.8) we will expand $1/y_t^2$ in a series in terms of $(Z_t - 1)$ (Note the expansion above is justified since $Z_t - 1 = .690(3)$) and rewrite the terms in our expansion via $\gamma_t - i|\vec{\mathbf{k}}| = \gamma_t(2 - (1 + i|\vec{\mathbf{k}}|/\gamma_t))$. Finally, we expand in powers of $(Z_t - 1)$ and $(1 + i|\vec{\mathbf{k}}|/\gamma_t)$ and keep all terms up to order $(Z_t - 1)^3$ and $(1 + i|\vec{\mathbf{k}}|/\gamma_t)^2$. Doing so we will reproduce the Z parametrization expression (2.14) for the ${}^3S_1$ channel amplitude. Our coefficients acquire the values

$$\Delta_{(-1)}^{({}^3S_1)} = \frac{M_N y_t^2}{4\pi}\frac{\mu - \gamma_t}{Z_t - 1}, \quad \Delta_{(0)}^{({}^3S_1)} = \frac{\gamma_t^2}{M_N} \tag{2.16}$$

and we obtain the NNLO Z parametrization deuteron propagator

$$\begin{aligned} i\Delta_{tZ}^{NNLO}(p_0, \vec{\mathbf{p}}) = \frac{4\pi i}{M_N y_t^2}\frac{1}{\gamma_t - \sqrt{\frac{\vec{\mathbf{p}}^2}{4} - M_N p_0 - i\epsilon}}\times \\ \times\left[1 + \frac{Z_t - 1}{2\gamma_t}\left(\gamma_t + \sqrt{\frac{\vec{\mathbf{p}}^2}{4} - M_N p_0 - i\epsilon}\right)\right. \\ \left. + \left(\frac{Z_t - 1}{2\gamma_t}\right)^2\left(\frac{\vec{\mathbf{p}}^2}{4} - M_N p_0 - \gamma_t^2\right) + \cdots\right] \end{aligned} \tag{2.17}$$

(Note $\Delta_{(-1)}^{({}^3S_1)}$ is written in terms of y_t^2 since this expression will change depending on which order we calculate to.)

In the Z parametrization method the deuteron wave function renormalization is given by Eq (2.18). We can see that the deuteron wave function renormalization is exact at NLO and produces the correct deuteron pole residue, instead of being approached perturbatively in terms of the not so small parameter $\rho_t\gamma_t = .409$ as in

the effective range expansion . This is one of the advantages of Z parametrization over matching onto the effective range expansion.

$$Z_D = \frac{8\pi\gamma_t}{M_N^2 y_t^2}\left[\underbrace{1}_{\text{LO}} + \underbrace{(Z_t - 1)}_{\text{NLO}} + \underbrace{0}_{\text{NNLO}}\right] \tag{2.18}$$

Thus the deuteron propagator has been calculated to NNLO in both the effective range and Z parametrization formalisms. We must now do the same for the singlet propagator at NNLO. Fortunately the steps are basically the same and we will not show all the work. The ${}^1S_0$ channel does not have any real bound state poles which must be fitted. Therefore the effective range expansion is about zero momentum giving the following expression.

$$k\cot(\delta_0) = -\frac{1}{a_s} + \frac{1}{2}r_{0s}\vec{\mathbf{k}}^2 + \cdots \tag{2.19}$$

where $a_s = -23.714$ fm is the scattering length in the ${}^1S_0$ channel and $r_{0s} = 2.73$ fm is the effective range in the ${}^1S_0$ channel. Using Eq. (2.19) one finds the following NNLO propagator and values for coefficients in the singlet channel.

$$\begin{aligned} i\Delta_s^{NNLO}(p_0,\vec{\mathbf{p}}) = -\frac{4\pi i}{M_N y_s^2}\Bigg[&\frac{1}{\frac{1}{a_s} - \sqrt{\frac{\vec{\mathbf{p}}^2}{4} - M_N p_0 - i\epsilon}} + \frac{r_{0s}}{2}\frac{M_N p_0 - \frac{\vec{\mathbf{p}}^2}{4}}{\left(\frac{1}{a_s} - \sqrt{\frac{\vec{\mathbf{p}}^2}{4} - M_N p_0 - i\epsilon}\right)^2} \\ &+ \left(\frac{r_{0s}}{2}\right)^2 \frac{\left(M_N p_0 - \frac{\vec{\mathbf{p}}^2}{4}\right)^2}{\left(\frac{1}{a_s} - \sqrt{\frac{\vec{\mathbf{p}}^2}{4} - M_N p_0 - i\epsilon}\right)^3}\Bigg] \end{aligned} \tag{2.20}$$

$$\Delta_{(-1)}^{({}^1S_0)} = \frac{2}{M_N}\frac{\mu - \frac{1}{a_s}}{r_{0s}}, \quad \Delta_{(0)}^{({}^1S_0)} = 0, \quad y_t^2 = \frac{8\pi}{M_N^2}\frac{1}{r_{0s}} \tag{2.21}$$

All that is left to do is to determine the singlet propagator in the Z parametrization. It turns out that in the ${}^1S_0$ channel there is a pole in the S matrix on the negative imaginary axis where the S matrix is a function of momentum. This pole is referred to as a virtual bound state. The amplitude can be expanded about this pole just as in the ${}^3S_1$ channel we expanded about the deuteron pole. We then find the effective range expansion

$$k\cot(\delta_0) = -\gamma_s + \frac{1}{2}\rho_s(\vec{\mathbf{k}}^2 + \gamma_s^2) + \cdots \tag{2.22}$$

Unfortunately γ_s and ρ_s are not determined experimentally, since the virtual bound state is not accessible experimentally. Thus in order to determine the values for γ_s and ρ_s we match our new effective range expansion onto the old effective range expansion about zero momentum by matching the coefficients of the powers of $\vec{\mathbf{k}}$. Doing this and ignoring terms higher order in both effective range expansions we find [55].

$$\begin{aligned} \rho_s &= r_{0s} \\ \gamma_s &= \frac{1}{a_s} + \frac{1}{2}\rho_s\gamma_s^2 \end{aligned} \tag{2.23}$$

Solving these equations we get the values $\gamma_s = -7.8904$ MeV and $\rho_s = 2.730$ fm. Inclusion of the shape parameter in the effective range expansion changes these values slightly to $\gamma_s = -7.8902$ MeV and $\rho_s = 2.733$ fm. From these results we determine the singlet residue to be $Z_s = 1/(1-\gamma_s\rho_s) = .9016$. Inclusion of the shape parameter changes this value slightly to $Z_s = .9015$. Now with knowledge of these parameters the singlet propagator in the Z parametrization is simply a carbon copy of the deuteron propagator in the Z parametrization, and we can make the following substitutions $\gamma_t \to \gamma_s$ and $Z_t \to Z_s$. Carrying this out we find the following constraints on our coefficients and NNLO singlet propagator.

$$\frac{1}{y_s^2} = \frac{M_N^2}{8\pi\gamma_s}\frac{Z_s-1}{1+(Z_s-1)} = \frac{M_N^2}{8\pi\gamma_s}(Z_s-1)\left[1+(Z_s-1)+\cdots\right] \tag{2.24}$$

$$\Delta^{(^1S_0)}_{(-1)} = \frac{M_N y_s^2}{4\pi}\frac{\mu-\gamma_s}{Z_s-1}, \quad \Delta^{(^1S_0)}_{(0)} = \frac{\gamma_s^2}{M_N} \tag{2.25}$$

$$\begin{aligned} i\Delta^{NNLO}_{sZ}(p_0,\vec{\mathbf{p}}) = -\frac{4\pi i}{M_N y_s^2}\frac{1}{\gamma_s - \sqrt{\frac{\vec{\mathbf{p}}^2}{4} - M_N p_0 - i\epsilon}}\times \\ \times\left[1+\frac{Z_s-1}{2\gamma_s}\left(\gamma_t + \sqrt{\frac{\vec{\mathbf{p}}^2}{4} - M_N p_0 - i\epsilon}\right)\right. \\ \left. + \left(\frac{Z_s-1}{2\gamma_s}\right)^2\left(\frac{\vec{\mathbf{p}}^2}{4} - M_N p_0 - \gamma_s^2\right) + \cdots\right] \end{aligned} \tag{2.26}$$

One should note that we did not calculate the singlet wave function renormalization. This calculation is unnecessary, as the singlet propagator is not our physical state of interest. Channels that contain the singlet propagator as an asymptotic state can be given an arbitrary renormalization. This ability will be useful when performing numerical computations. With the singlet and deuteron propagator forms up to NNLO known, we can proceed to use them to calculate parity-conserving (PC) and PV amplitudes in nd scattering.

CHAPTER 3

PARITY CONSERVING ND SCATTERING

3.1 Quartet Channel LO

Before including parity violation we first examine PC nd scattering. In this case there exist two different channels, quartet and doublet, which refer to the two different possible combinations of neutron and deuteron spin, spin 3/2 and spin 1/2 respectively. We will first address the quartet channel, as it is the simpler of the two. In the quartet channel there are no diagrams with singlet propagators, since singlet propagators have spin zero and can never combine with a spin one half neutron to yield spin 3/2. Thus at LO we find we need to solve the following infinite sum of diagrams [50].

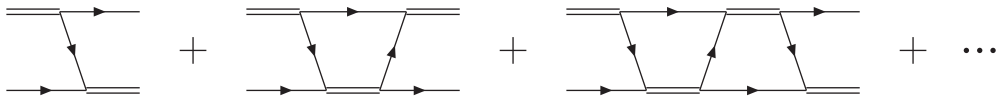

Figure 3.1: infinite sum of diagrams required at LO in Quartet channel

In the two-body case we found that we could sum the infinite sum of diagrams via a geometric series. Unfortunately in the three-body case we are not so lucky; the diagrams do not factorize since there are overlapping divergences. In order to solve this infinite sum of diagrams we are forced to solve an integral equation, Eq. (3.1) via numerical methods. This integral equation approach is equivalent to the Faddeev equations for three-body scattering and was first done by Skornyakov and Ter-Martirosian [60]. The integral equations can be represented diagramatically as

in Fig 3.2. (Note the red oval is often referred to as a pinball and the corresponding diagram a pinball diagram)

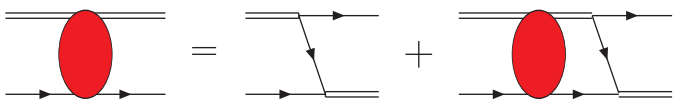

Figure 3.2: Integral equation for Quartet channel at LO

We will calculate this integral equation half off shell. The incoming momentum $\vec{\mathbf{k}}$ and energy $E = \frac{3}{4}\frac{\vec{\mathbf{k}}^2}{M_N} - \frac{\gamma_t^2}{M_N}$ in the center of mass system (c.m.) will be treated as on shell while the outgoing momentum $\vec{\mathbf{p}}$ and energy will be off shell. We will define the quantity $h = \frac{\vec{\mathbf{k}}^2}{2M_N} - \frac{\vec{\mathbf{p}}^2}{2M_N}$ which vanishes if our integral equation is full on shell as then we would have $|\vec{\mathbf{p}}| = |\vec{\mathbf{k}}|$. Therefore h is a measure of the amount that we are off shell. Finally we write out the expression for the scattering amplitude where i (j) refer to the initial (final) deuteron polarizations, α (β) the initial (final) nucleon spin, and a (b) the initial (final) nucleon isospin.

$$
\begin{aligned}
\left(it^{ji}\right)^{\beta b}_{\alpha a}(\vec{\mathbf{k}},\vec{\mathbf{p}},h) =& \frac{y_t^2}{2}(\sigma^i\sigma^j)^\beta_\alpha\delta^b_a \frac{i}{-\frac{\vec{\mathbf{k}}^2}{4M_N} - \frac{\gamma_t^2}{M_N} + h - \frac{(\vec{\mathbf{k}}+\vec{\mathbf{p}})^2}{2M_N} + i\epsilon} + \\
&+ \frac{y_t^2}{2}(\sigma^i\sigma^k)^\beta_\gamma\delta^b_c \int \frac{d^4q}{(2\pi)^4}(it^{jk})^{\gamma c}_{\alpha a}(\vec{\mathbf{k}},\vec{\mathbf{q}},h+q_0)\times \\
&\times i\Delta_t^{LO}\left(\frac{\vec{\mathbf{k}}^2}{4M_N} - \frac{\gamma_t^2}{M_N} + h + q_0, \vec{\mathbf{q}}\right)\frac{i}{\frac{\vec{\mathbf{k}}^2}{2M_N} - h - q_0 - \frac{\vec{\mathbf{q}}^2}{2M_N} + i\epsilon}\times \\
&\times \frac{i}{-\frac{\vec{\mathbf{k}}^2}{4M_N} - \frac{\gamma_t^2}{M_N} + 2h + q_0 - \frac{(\vec{\mathbf{q}}+\vec{\mathbf{p}})^2}{2M_N} + i\epsilon}
\end{aligned}
\tag{3.1}
$$

We now integrate over the energy q_0, which can be done by choosing a contour in the lower half plane, whereby our integral is simply the residue of the pole at $q_0 = \frac{\vec{\mathbf{q}}^2}{2M_N} - \frac{\vec{\mathbf{k}}^2}{2M_N} + h - i\epsilon$ due to one of the nucleon propagators. Then we pick out the

quartet channel and project onto an angular momentum basis by using the Legendre polynomials. Doing this we find the simple one dimensional integral equations Eq. (3.2) expressing the partial wave basis of our amplitude.

$$t^l(k,p) = -\frac{y_t^2 M_N}{pk} Q_l\left(\frac{p^2+k^2-M_N E-i\epsilon}{pk}\right) - \tag{3.2}$$
$$+\frac{2}{\pi}\int_0^\Lambda dq q^2 t^l(k,q)\frac{1}{\gamma_t-\sqrt{\frac{3\vec{q}^2}{4}-M_N E-i\epsilon}}\frac{1}{qp}Q_l\left(\frac{p^2+q^2-M_N E-i\epsilon}{pq}\right)$$

where

$$Q_l(a) = \frac{1}{2}\int_{-1}^{1} dx \frac{P_l(x)}{x+a} \tag{3.3}$$

is equivalent to the Legendre polynomials of the second kind up to a factor of $(-1)^l$. We note that in Eq. (3.2) the integral ranges from 0 to Λ instead of 0 to infinity. The use of a cutoff for the integral serves two purposes. Firstly, it gives a cutoff regularization for potential divergences. Secondly, since we will have to solve this integral equation numerically we have to impose some cutoff anyway since we cannot integrate to infinity. One may be concerned that we are using two different regularization schemes here. We are using dimensional regularization for the deuteron propagator and a cutoff regularization for the integral equation. However any effects from choosing different regularization schemes are of higher order [14].

3.2 Doublet Channel LO

Now we move to the doublet channel. There are two extra complications that arise in this case. One comes from the fact that we now need to include the singlet propagator since it can combine with the spin one half nucleon to give a total spin of one half. This feature leads to having to solve two sets of coupled integral equations.

The second complication arises from three-body forces. The three-body force only arises in the doublet S wave channel at LO because there is no centrifugal barrier and the Pauli exclusion principle does not exclude a bound state in this channel. Since the resulting kernel of the integral equation in the doublet S wave channel is non-compact, the equation does not possess a unique solution (in the limit $\Lambda \to \infty$). At finite cutoff this results in the solution varying greatly with the choice of cutoff. This can be remedied by the insertion of a three-body force with an appropriate scale dependence on Λ. The basic form of the three-body force up to NNLO is given by [13–15]

$$\mathcal{H}(E,\Lambda) = \frac{2H_0^{LO}(\Lambda)}{\Lambda^2} + \frac{2H_0^{NLO}(\Lambda)}{\Lambda^2} + \frac{2H_0^{NNLO}(\Lambda)}{\Lambda^2} + \frac{2H_2^{NNLO}(\Lambda)}{\Lambda^4}(M_N E + \gamma_t^2) \quad (3.4)$$

The term H_0 is chosen at each order so that we get the correct scattering length of $a_{\frac{1}{2}} = .65$ fm at zero energy in the doublet S wave channel. This parameter is split up into pieces depending on the order at which we are working so that H_0 doesn't have to be refit at each order. The value of H_2 is chosen such that we get the correct triton binding energy of $B_d = -8.48$ MeV. Now with all these complications in mind we must solve a set of coupled integral equations which is represented by the diagrams in Fig. 3.3. The diagrams with three-body forces will only contribute to the Doublet S wave channel. In the diagrams of Fig. 3.3 the double dashed line represents the LO singlet propagator and the thick solid blue line represents a sum of two diagrams, one containing a deuteron propagator and the other having a singlet propagator in place of the solid blue line.

Now similarly to the quartet channel we integrate over the energy, project out the doublet channel, and project into an angular momentum basis. We then get the coupled Eqs. (3.5) and (3.6), where $t^l_{Nt\to Nt}(k,p)$ is the amplitude for neutron and deuteron going to a neutron and deuteron, while $t^l_{Nt\to Ns}(k,p)$ is the amplitude for

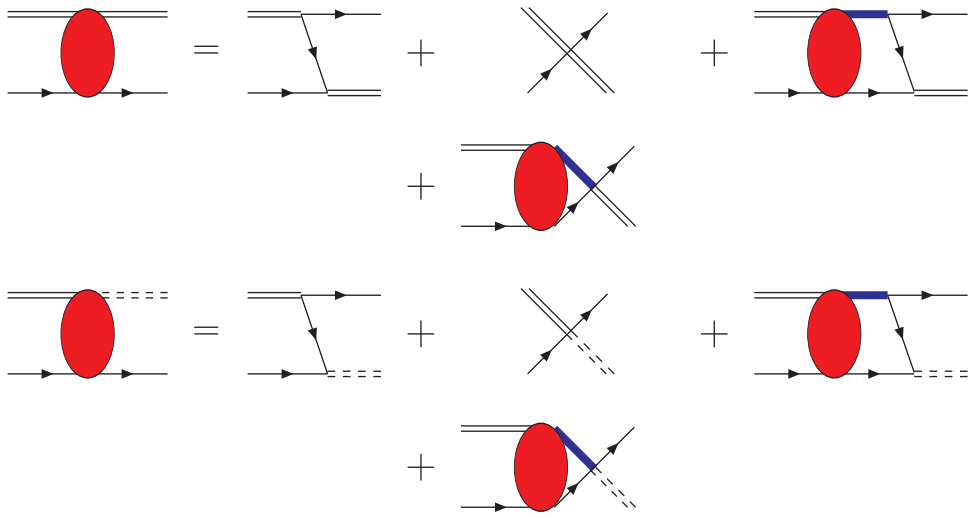

Figure 3.3: Integral Equations for doublet channel at LO

neutron and deuteron going to neutron and singlet combination of nucleons. In these expressions we note the δ_{l0} associated with the three-body force. This simply states that the three-body force only enters in the S wave. Finally it should be noted that $\mathcal{H}(E,\Lambda)$ only contains the leading order contribution from Eq. (3.4).

$$
\begin{aligned}
t^l_{Nt\to Nt}(k,p) =& \frac{4y_t^2 M_N}{pk} Q_l\left(\frac{p^2+k^2-M_N E-i\epsilon}{pk}\right) + \delta_{l0}\mathcal{H}(E,\Lambda) \\
&- \frac{1}{\pi}\int_0^\Lambda dq q^2 t^l_{Nt\to Nt}(k,q)\frac{1}{\gamma_t - \sqrt{\frac{3\vec{\mathbf{q}}^2}{4} - M_N E - i\epsilon}}\times \\
&\times\left[\frac{1}{qp}Q_l\left(\frac{p^2+q^2-M_N E-i\epsilon}{pq}\right) + \delta_{l0}\mathcal{H}(E,\Lambda)\right] \\
&+ \frac{3}{\pi}\frac{y_t}{y_s}\int_0^\Lambda dq q^2 t^l_{Nt\to Ns}(k,q)\frac{1}{\gamma_s - \sqrt{\frac{3\vec{\mathbf{q}}^2}{4} - M_N E - i\epsilon}}\times \\
&\times\left[\frac{1}{qp}Q_l\left(\frac{p^2+q^2-M_N E-i\epsilon}{pq}\right) + \delta_{l0}\mathcal{H}(E,\Lambda)\right]
\end{aligned}
\tag{3.5}
$$

$$
\begin{aligned}
t^l_{Nt\to Ns}(k,p) = &-\frac{12 y_d y_s M_N}{pk} Q_l\left(\frac{p^2+k^2-M_N E-i\epsilon}{pk}\right)+\delta_{l0}\mathcal{H}(E,\Lambda) \\
&-\frac{1}{\pi}\int_\Lambda^\infty dq q^2 t^l_{Nt\to Nt}(k,q)\frac{1}{\gamma_t-\sqrt{\frac{3\vec{\mathbf{q}}^2}{4}-M_N E-i\epsilon}}\times \\
&\times\left[\frac{1}{qp}Q_l\left(\frac{p^2+q^2-M_N E-i\epsilon}{pq}\right)+\delta_{l0}\mathcal{H}(E,\Lambda)\right] \\
&+\frac{3}{\pi}\frac{y_t}{y_s}\int_0^\Lambda dq q^2 t^l_{Nt\to Ns}(k,q)\frac{1}{\gamma_s-\sqrt{\frac{3\vec{\mathbf{q}}^2}{4}-M_N E-i\epsilon}}\times \\
&\times\left[\frac{1}{qp}Q_l\left(\frac{p^2+q^2-M_N E-i\epsilon}{pq}\right)+\delta_{l0}\mathcal{H}(E,\Lambda)\right]
\end{aligned}
\tag{3.6}
$$

Note that all these amplitudes are unrenormalized. In order to find the renormalized amplitude we must multiply $t^l_{Nt\to Nt}(k,p)$ by the LO deuteron wavefunction renormalization Z_D. Lastly since the channel $t^l_{Nt\to Ns}(k,p)$ is of no direct physical interest to us we can renormalize it in any manner we wish. At higher orders one must renormalize the amplitude $t^l_{Nt\to Nt}(k,p)$ with the corresponding order in deuteron wavefunction renormalization Z_D.

3.3 Higher orders

With the integral equations for these amplitudes solved at LO two natural questions arise. Firstly how do we solve these integral equations and secondly how do we continue this to higher orders. The issue of how these equations are solved will be saved for the next section so instead we will now focus on the issue of higher orders. Once the LO amplitudes are calculated we can evaluate the NLO amplitude by simply solving the diagrams in Fig. 3.4 where the cross denotes an insertion of the deuteron (singlet) kinetic energy term and the $\Delta^{^3S_1}_{(0)}$ ($\Delta^{^1S_0}_{(0)}$) term. We note that the deuteron (singlet) propagator with a cross is simply our deuteron (singlet) propagator at NLO. In order to solve these diagrams one can numerically integrate them with the

half off shell LO amplitudes. Finally it should be noted that only the first diagram contributes in the quartet channel and the other two will contribute to the doublet channel. Also we have ignored NLO diagrams with three-body forces as they only occur in the Doublet S wave channel

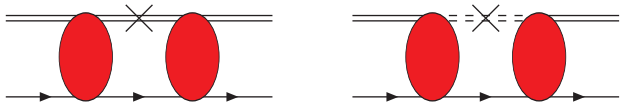

Figure 3.4: Diagrams at NLO (Three-Body Forces are ignored)

At NNLO one has to solve the set of diagrams in Fig. 3.5. The first two diagrams can be solved as before by using numerical integration with our half off shell LO amplitudes. However the the next four diagrams represent an issue, as they require knowledge of the full off shell LO amplitude. So we are either forced to solve the full off shell LO amplitude which is numerically expensive or we must adopt another approach.

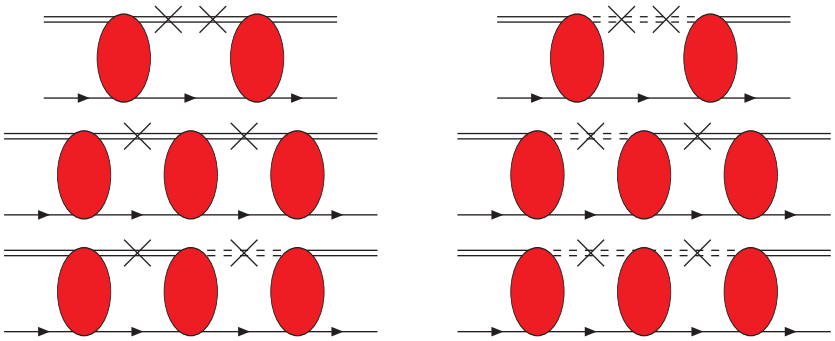

Figure 3.5: Diagrams at NNLO (Again Three-Body Forces are ignored)

It turns out that there is a relatively simple way to calculate to higher orders without calculating the full off shell LO amplitude [15]. At NLO we simply replace the LO deuteron and singlet propagators in our integral equation by the NLO propagators. Likewise for NNLO we replace the LO propagators with their NNLO counterparts.

In the doublet S wave channel we must also replace the LO three-body force with its NLO and NNLO counterparts. Doing this we can get the amplitudes correct up to NNLO. However, the amplitudes will contain an infinite number of certain higher order terms. For example in this method one will get the higher order terms at NLO in Fig. 3.6 and NNLO in Fig. 3.7. Despite these higher order terms our calculation is still correct up to NNLO and does not necessitate the calculation of the full off shell LO amplitude.

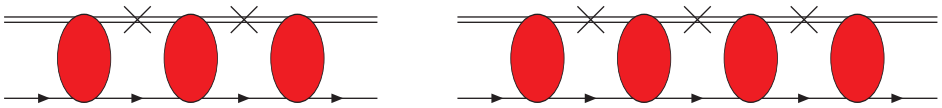

Figure 3.6: Certain Higher order contributions present at NLO in Quartet channel

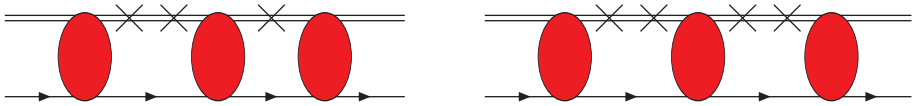

Figure 3.7: Certain Higher order contributions present at NNLO in Quartet channel

Also at NNLO their are contributions from a two-body SD mixing operator which is given by the Lagrangian in Eq. (3.7) for the auxiliary field formalism

$$\mathcal{L}^{SD} = y_{SD} d^{i\dagger} \left[N \left((\overrightarrow{\partial} - \overleftarrow{\partial})^i (\overrightarrow{\partial} - \overleftarrow{\partial})^j - \frac{1}{3} (\overrightarrow{\partial} - \overleftarrow{\partial})^2 \right) P_j N \right] + h.c \tag{3.7}$$

As of now the contributions of this term to the nd scattering amplitude at NNLO have not been calculated. It can be shown that if averaged over $\vec{\mathbf{J}}$ (total angular momentum $\vec{\mathbf{J}} = \vec{\mathbf{L}} + \vec{\mathbf{S}}$) that these terms cancel out, which is explicitly shown in the appendix. A calculation of the NNLO phase shifts has been calculated in [50] where the $\vec{\mathbf{J}}$ values have been averaged over rendering this SD mixing term needless.

However these terms will be necessary to give an accurate description of polarization phenomena in nd scattering, therefore these terms have been projected out in angular momentum in the appendix for possible future use in nd polarization phenomena

3.4 Numerical Methods

We will now address the method by which we will solve the integral equations. For simplicity we will only focus on the quartet channel as the method used in the Doublet channel is identical but only slightly more complicated due to the presence of two coupled integral equations and the three-body force. In order to simplify our notation we will rewrite the integral equation in the quartet channel as(Note we are calculating the renormalized amplitude at LO.)

$$t^l(k,p) = B(k,p) + \int_0^\Lambda dq K(k,p,q) t(k,q) \tag{3.8}$$

where

$$B(k,p) = -\frac{8\pi\gamma_t}{M_N}\frac{1}{pk}Q_l\left(\frac{p^2+k^2-M_N E - i\epsilon}{pk}\right) \tag{3.9}$$

and

$$K(k,p,q) = \frac{2}{\pi}\frac{1}{\gamma_t - \sqrt{\frac{3q^2}{4} - M_N E - i\epsilon}}\frac{1}{qp}Q_l\left(\frac{p^2+q^2-M_N E - i\epsilon}{qp}\right) \tag{3.10}$$

The integral equation we are faced with is a simple first order linear Fredholm type integral equation of the second kind, and can in general be simply solved by use of the Nystrom method [29]. In this procedure one discretizes the integral equation by use of a quadrature where in our case q_j are the quadrature points and w_j are the corresponding quadrature weights. Discretizing our integral equation we can rewrite it as

$$t_i = B_i + \sum_j w_j K_{ij} t_j \tag{3.11}$$

where

$$t_i = t(k, p_i), \quad B_i = B(k, p_i), \quad K(k, p_i, q_j) = K_{ij} \tag{3.12}$$

Our integral equation has now been turned into a system of linear equations. This system can be simply solved by inverting a matrix, yielding

$$t_i = \left(\delta_{ij} - \sum_j w_j K_{ij} \right)^{-1} B_j \tag{3.13}$$

This method of solution would be fine except that our kernel $K(k, p, q)$ has singularities along the real axis. Thus in order to have our solution converge we would need to choose and inordinately large number of mesh points. The first singularity comes from the deuteron propagator and is located at two positions

$$q = k + i\epsilon, -k - i\epsilon \tag{3.14}$$

We see the singularity $k + i\epsilon$ is located in the first and fourth quadrants and in the limit $\epsilon \to 0$ will lay on the real axis. For certain values of momentum the function $Q_l(a)$, where $a = (p^2 + q^2 - M_N E - i\epsilon)/qp$, gives branch point singularities. Below threshold, namely $E < 0$ it is easy to see that these singularities do not come close to the real axis. However, when $E \geq 0$ the branch point singularities will be a distance ϵ away from the real axis. The singularity due to the deuteron propagator is fixed and can be dealt with numerically by several different methods [29]. However the branch point singularities are not fixed, and occur when the argument in $Q_l(a)$ approaches 1 or -1, i.e. when

$$q = \pm\frac{1}{2}p \pm \sqrt{M_N E - \frac{3}{4}p^2 + i\epsilon} \tag{3.15}$$

In order to deal with such singularities we will use the method invented by Hetherington and Schick [64]. We first analytically continue the amplitude $t(k,p)$ into the complex plane by letting p be defined along the path $C'B$ in the complex plane as shown below. However the Nystron method demands that we use the same values for p and q. Thus we change the integral to be along the path $C'B$ in the complex plane.

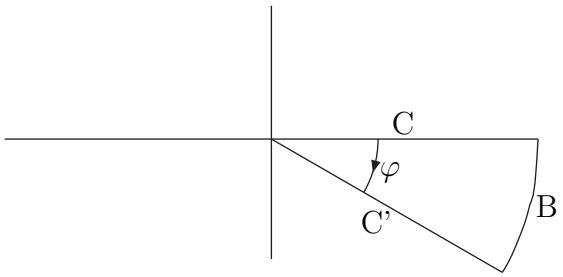

Figure 3.8: Contour used for integral equation

The integral along the path $C'B$ will be equivalent to the integral along the real axis as long as there are no singularities inside the contour $C'BC$. It has been shown by Brayshaw that there are no singularities from the solution $t(k,p)$ for $\varphi < \tan^{-1}(2k/\gamma_t)$ [19]. The singularities from the deuteron propagator are clearly not an issue as they are only in the first and third quadrants. Finally it can also be shown that there are no branch point singularities inside the contour [1, 21]. Thus we can solve the half off shell amplitude along the path $C'B$. Now setting $p = k$ and again integrating q along the path $C'B$ we can solve the full on shell amplitude along the real axis by integrating the solution from the path $C'B$. This is allowed as long as there are no new singularities introduced into the contour by setting $p = k$. By changing the value of p the only singularities that move are the branch points. However, it can be easily shown that since p is on shell there are no branch point singularities in the

contour. Thus integrating along the path $C'B$ is again equivalent to integrating along the real axis. In order to stay as far away from the singularities as possible we choose the angle $\varphi = \frac{1}{2}\tan^{-1}(2k/\gamma_t)$. Finally note we never solve the amplitude along the real axis. We simply use the amplitude along the path $C'B$ to solve all of our PV amplitudes.

CHAPTER 4

THREE-BODY PARITY-VIOLATION

4.1 Three-Body Parity-Violation LO

In the auxiliary field formulation the two-body PV Lagrangian is given by a form including five low energy constants [97].

$$\begin{aligned}\mathcal{L}^d_{PV} = -\Big[& g^{({}^3S_1-{}^1P_1)} t_i^\dagger \left(N^t \sigma_2 \tau_2 i \overset{\leftrightarrow}{\nabla}_i N \right) \\ & + g^{({}^1S_0-{}^3P_0)}_{(\Delta I=0)} s_a^\dagger \left(N^T \sigma_2 \vec{\boldsymbol{\sigma}} \cdot \tau_2 \tau_a i \overset{\leftrightarrow}{\nabla} N \right) \\ & + g^{({}^1S_0-{}^3P_0)}_{(\Delta I=1)} \epsilon^{3ab} (s^a)^\dagger \left(N^T \sigma_2 \vec{\boldsymbol{\sigma}} \cdot \tau_2 \tau^b \overset{\leftrightarrow}{\nabla} N \right) \\ & + g^{({}^1S_0-{}^3P_0)}_{(\Delta I=2)} \mathcal{I}^{ab} (s^a)^\dagger \left(N^T \sigma_2 \vec{\boldsymbol{\sigma}} \cdot \tau_2 \tau^b i \overset{\leftrightarrow}{\nabla} N \right) \\ & + g^{({}^3S_1-{}^3P_1)} \epsilon^{ijk} (t_i)^\dagger \left(N^T \sigma_2 \sigma^k \tau_2 \tau_3 \overset{\leftrightarrow^j}{\nabla} N \right) \Big] + h.c.\end{aligned} \tag{4.1}$$

where $a \overset{\leftrightarrow}{\nabla} b = a(\overrightarrow{\nabla})b - (\overrightarrow{\nabla}a)b$, and $\mathcal{I} = \mathrm{diag}[1, 1, -2]$ projects out the isotensor contribution. As in the parity-conserving case for three-body interactions one needs to solve an infinite sum of diagrams for the PV amplitude at LO [15, 50], leading to a coupled set of integral equations given in Fig. 4.1. Numerical solution is necessary, as such integral equations cannot be solved analytically. In general we must solve a set of four coupled integral equations. However, since parity-violation is so small, $G_F m_\pi^2 \sim 10^{-7}$ we can ignore second order PV terms. Then the integral equations for the parity-conserving amplitudes decouple [59], and are exactly the same as in previous papers [15, 50, 55]. The remaining coupled PV integral equations at LO

are shown in Fig. 4.2, where the boxes represent PV vertices, the double line the dressed deuteron propagator, the double dashed lines the dressed singlet propagator, and the line with arrow the nucleon propagator. The thick lines represent a sum over both deuteron and singlet propagators. Thus the thick line allows one to represent two Feynman diagrams with a single diagram. There are also diagrams where two dibaryon lines and two nucleon lines meet at a single vertex, due to the three-body force term in the Lagrangian.

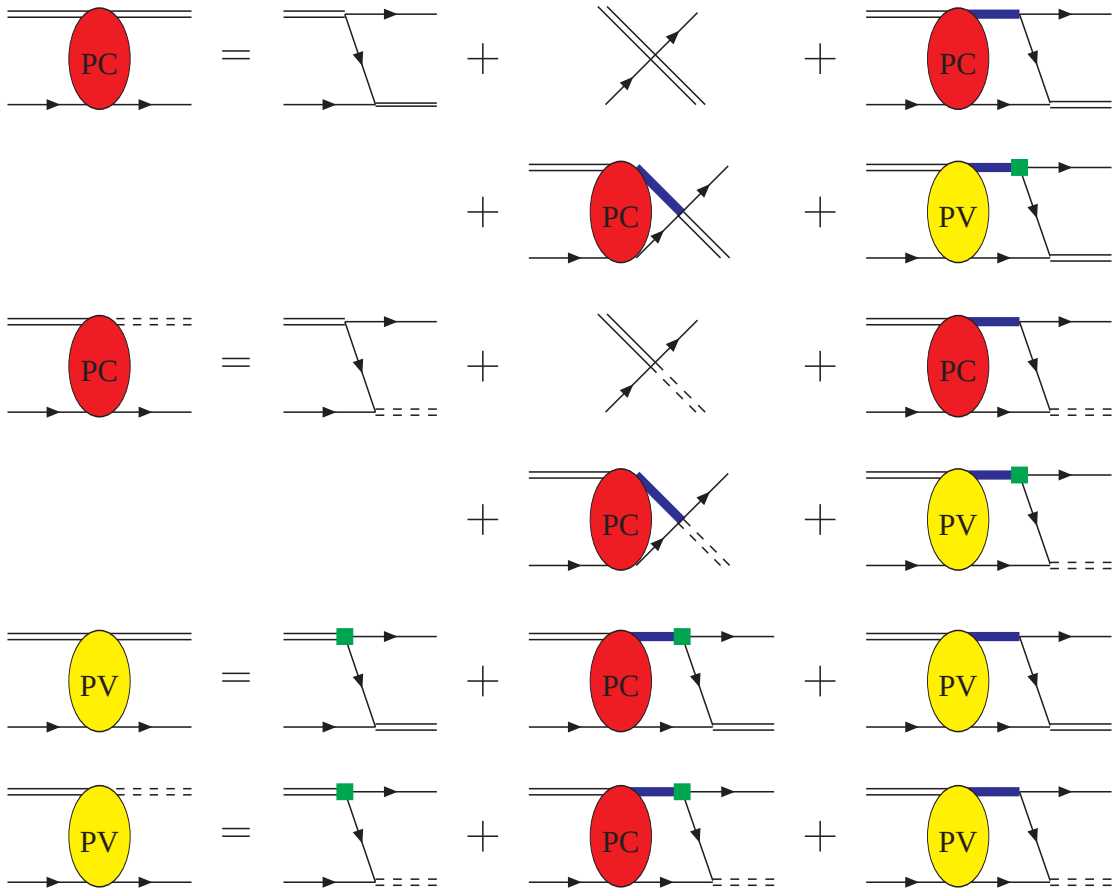

Figure 4.1: Integral equations for parity-violation at LO (Note diagrams where lower vertices are PV are not included)

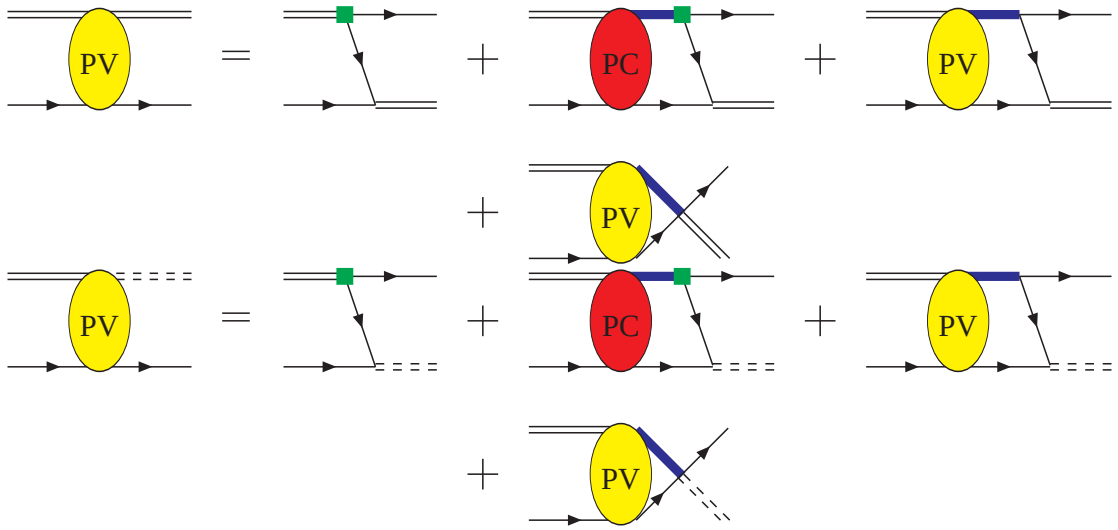

Figure 4.2: Integral equations for parity-violation at LO (Note diagrams where lower vertices are PV are not included)

This three-body force term enters at LO, only in the Doublet S-wave channel. (Note we have not yet projected out any specific channel.) The momentum integrals are regulated

using a sharp cutoff Λ. The three-body force term is cutoff dependent. This cutoff is convenient because it can be implemented straightforwardly numerically. The LO three-body force term in the Doublet S wave channel as given by (3.4) [12, 13] has its cutoff dependence chosen such that the doublet S wave amplitude produces the correct scattering length [14, 15, 55]. There is no need to include a PV three-body force, as it has been explicitly shown that no such term exists up to and including NLO [56].) The cutoff dependence for $H_0(\Lambda)$ is given below in Fig 4.4 from 200 MeV to 1500 MeV.

To first order in parity-violation the integral equation for the PV amplitude is given by the sum of diagrams shown in Fig. 4.3. The first diagram corresponds to a pure PV transition with no scattering in the initial or final channel. The next set of diagrams has a PV transition with scattering either in the initial or final channel but

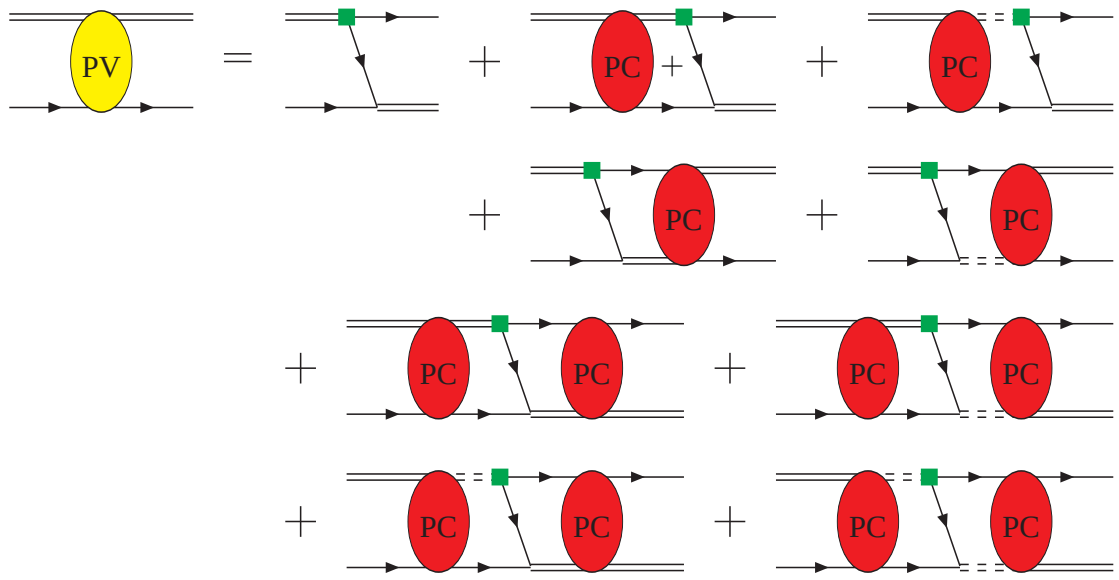

Figure 4.3: PV diagrams at LO (Note diagrams where lower vertices are PV are not included)

not both. (Also note that for these diagrams the singlet field acts as an intermediate state, which can only exist in the doublet channel.) Finally we have the set of diagrams with a PV transition and scattering in both the final and initial channels.

Summing all of these figures one finds the PV amplitude given in Eq. (4.2), where $\vec{\mathbf{k}}$ is the incoming nucleon momentum and $\vec{\mathbf{p}}$ is the outgoing nucleon momentum in the c.m. frame. Since our diagrams are on shell we have $|\vec{\mathbf{k}}| = |\vec{\mathbf{p}}|$, and the total energy in the c.m. frame is given by $E = \frac{3\vec{\mathbf{k}}^2}{4M_N} - \frac{\gamma_t^2}{M_N}$. The vector index letter w (x), represents the initial (final) deuteron auxiliary field polarization. Finally the Greek index α (β) is the initial (final) spinor index and a (b) is the initial (final) isospinor index.

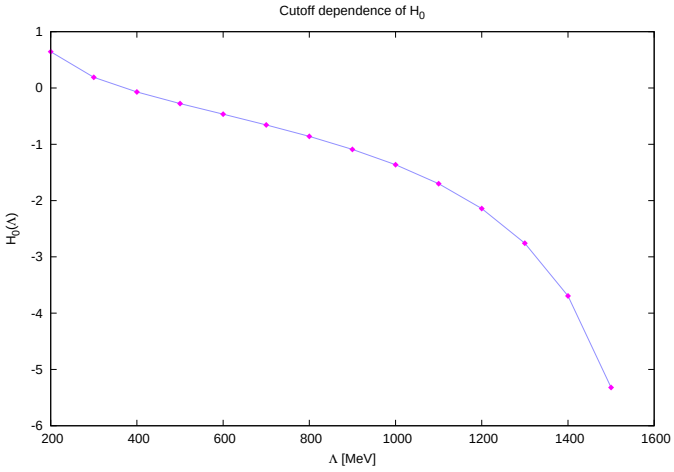

Figure 4.4: Cutoff dependence of three-body force term $H_0(\Lambda)$

$$
\begin{aligned}
(it_{PV}^{xw})_{\alpha a}^{\beta b}(\vec{\mathbf{k}},\vec{\mathbf{p}}) = {} & \frac{4M_N}{\sqrt{8}}\frac{i}{\vec{\mathbf{k}}^2+\vec{\mathbf{k}}\cdot\vec{\mathbf{p}}+\vec{\mathbf{p}}^2-M_NE-i\epsilon}\left(\mathcal{K}_{PV}^{11\ xw}\right)_{\alpha a}^{\beta b}(\vec{\mathbf{p}},\vec{\mathbf{k}}) \\
& + \frac{4M_N}{\sqrt{8}}\int\frac{d^4q}{(2\pi)^4}\mathbf{v}_p^T(i\tilde{\boldsymbol{\mathcal{K}}}^{xy})_{\gamma c}^{\beta b}(\vec{\mathbf{q}},\vec{\mathbf{p}},q_0)i\mathbf{D}\left(\frac{\vec{\mathbf{k}}^2}{4M_N}-\frac{\gamma_t^2}{M_N}+q_0,\vec{\mathbf{q}}\right) \\
& \qquad \left((it^{yw})_{\alpha a}^{\gamma c}(\vec{\mathbf{k}},\vec{\mathbf{q}})\right)\frac{i}{\frac{\vec{\mathbf{k}}^2}{2M_N}-q_0-\frac{\vec{\mathbf{q}}^2}{2M_N}+i\epsilon} \\
& + \frac{4M_N}{\sqrt{8}}\int\frac{d^4q}{(2\pi)^4}\left((it^{xy})_{\gamma c}^{\beta b}(\vec{\mathbf{p}},\vec{\mathbf{q}})\right)^T i\mathbf{D}\left(\frac{\vec{\mathbf{k}}^2}{4M_N}-\frac{\gamma_t^2}{M_N}+q_0,\vec{\mathbf{q}}\right) \\
& \qquad (i\tilde{\boldsymbol{\mathcal{K}}}^{yw})_{\alpha a}^{\gamma c}(\vec{\mathbf{k}},\vec{\mathbf{q}},q_0)\mathbf{v}_p\times\frac{i}{\frac{\vec{\mathbf{k}}^2}{2M_N}-q_0-\frac{\vec{\mathbf{q}}^2}{2M_N}+i\epsilon} \\
& + \frac{4M_N}{\sqrt{8}}\int\frac{d^4q}{(2\pi)^4}\int\frac{d^4\ell}{(2\pi)^4}\left((it^{xz})_{\delta d}^{\beta b}(\vec{\mathbf{p}},\vec{\boldsymbol{\ell}})\right)^T i\mathbf{D}\left(\frac{\vec{\mathbf{k}}^2}{4M_N}-\frac{\gamma_t^2}{M_N}+q_0,\vec{\mathbf{q}}\right) \\
& \qquad (i\tilde{\boldsymbol{\mathcal{K}}}^{zy})_{\gamma c}^{\delta d}(\vec{\mathbf{q}},\vec{\boldsymbol{\ell}},q_0+\ell_0)i\mathbf{D}\left(\frac{\vec{\mathbf{k}}^2}{4M_N}-\frac{\gamma_t^2}{M_N}+\ell_0,\vec{\boldsymbol{\ell}}\right) \\
& \qquad \left((it^{yw})_{\alpha a}^{\gamma c}(\vec{\mathbf{k}},\vec{\mathbf{q}})\right)\frac{i}{\frac{\vec{\mathbf{k}}^2}{2M_N}-q_0-\frac{\vec{\mathbf{q}}^2}{2M_N}+i\epsilon}\frac{i}{\frac{\vec{\mathbf{k}}^2}{2M_N}-\ell_0-\frac{\vec{\boldsymbol{\ell}}^2}{2M_N}+i\epsilon}
\end{aligned}
\tag{4.2}
$$

The vector $\mathbf{v}_p$ projects out the nucleon-deuteron amplitude in cluster-configuration space and is defined as [55]

$$\mathbf{v}_p = \begin{pmatrix} 1 \\ 0 \end{pmatrix} \tag{4.3}$$

and the parity-conserving amplitudes t are a vector defined as follows

$$\left((it^{xw})^{\beta b}_{\alpha a}(\vec{\mathbf{k}},\vec{\mathbf{q}})\right) = \begin{pmatrix} (it^{xw}_{Nt\to Nt})^{\beta b}_{\alpha a}(\vec{\mathbf{k}},\vec{\mathbf{q}}) \\ (it^{xw}_{Nt\to Ns})^{\beta b}_{\alpha a}(\vec{\mathbf{k}},\vec{\mathbf{q}}) \end{pmatrix} \tag{4.4}$$

where $t_{Nt\to Nt}$ is the amplitude for nd scattering and $t_{Nt\to Ns}$ is the amplitude for nd going to a nucleon and a singlet combination of the remaining nucleons. (Note that we have not yet projected out quartet or doublet channels.) The expressions $\mathbf{D}(E,\vec{\mathbf{q}})$ and $(i\tilde{\boldsymbol{\mathcal{K}}}^{xw})^{\beta b}_{\alpha a}(\vec{\mathbf{q}},\vec{\boldsymbol{\ell}},q_0)$ are both matrices defined via.

$$i\mathbf{D}(E,\vec{\mathbf{q}}) = \begin{pmatrix} i\Delta_t^{LO}(E,\vec{\mathbf{q}}) & 0 \\ 0 & i\Delta_s^{LO}(E,\vec{\mathbf{q}}) \end{pmatrix} \tag{4.5}$$

$$\begin{aligned}(i\tilde{\boldsymbol{\mathcal{K}}}^{xw})^{\beta b}_{\alpha a}(\vec{\mathbf{q}},\vec{\boldsymbol{\ell}},q_0) =& \frac{i}{\frac{1}{2}\vec{\mathbf{q}}^2 + \vec{\mathbf{q}}\cdot\vec{\boldsymbol{\ell}} + \frac{1}{2}\vec{\boldsymbol{\ell}}^2 + \frac{1}{4}\vec{\mathbf{k}}^2 + \gamma_t^2 - M_N q_0 - i\epsilon}\times \\ & \times \begin{pmatrix} (\mathcal{K}_{PV}^{11\,xw})^{\beta b}_{\alpha a}(\vec{\mathbf{q}},\vec{\boldsymbol{\ell}}) & (\mathcal{K}_{PV}^{12\,xw})^{\beta b}_{\alpha a}(\vec{\mathbf{q}},\vec{\boldsymbol{\ell}}) \\ (\mathcal{K}_{PV}^{21\,xw})^{\beta b}_{\alpha a}(\vec{\mathbf{q}},\vec{\boldsymbol{\ell}}) & (\mathcal{K}_{PV}^{22\,xw})^{\beta b}_{\alpha a}(\vec{\mathbf{q}},\vec{\boldsymbol{\ell}}) \end{pmatrix}\end{aligned} \tag{4.6}$$

where the functions $\left(\mathcal{K}_{PV}^{XY\,xw}\right)^{\beta b}_{\alpha a}(\vec{\mathbf{q}},\vec{\boldsymbol{\ell}})$, which contain all of the PV dependence are defined as

$$\begin{aligned}\left(\mathcal{K}_{PV}^{11\,xw}\right)^{\beta b}_{\alpha a}(\vec{\mathbf{k}},\vec{\mathbf{p}}) = y_t^2 \Big(& g_1(\sigma^x)^\beta_\alpha \delta^b_a (\vec{\mathbf{k}}+2\vec{\mathbf{p}})^w + ig_2\epsilon^{w\ell y}(\sigma^y\sigma^x)^\beta_\alpha(\tau_3)^b_a(\vec{\mathbf{k}}+2\vec{\mathbf{p}})^\ell \\ & + g_1(\sigma^w)^\beta_\alpha\delta^b_a(2\vec{\mathbf{k}}+\vec{\mathbf{p}})^x - ig_2\epsilon^{x\ell y}(\sigma^w\sigma^y)^\beta_\alpha(\tau_3)^b_a(2\vec{\mathbf{k}}+\vec{\mathbf{p}})^\ell\Big)\end{aligned} \tag{4.7a}$$

$$\left(\mathcal{K}_{PV}^{12\ xA}\right)_{\alpha a}^{\beta b}(\vec{\mathbf{k}},\vec{\mathbf{p}}) = y_t y_s \left(g_3(\sigma^\ell\sigma^x)_\alpha^\beta(\tau^A)_a^b + ig_4\epsilon^{3AC}(\sigma^\ell\sigma^x)_\alpha^\beta(\tau^C)_a^b\right)(\vec{\mathbf{k}}+2\vec{\mathbf{p}})^\ell \quad (4.7b)$$
$$+ y_s y_t \left(g_1\delta_\alpha^\beta(\tau^A)_a^b(2\vec{\mathbf{k}}+\vec{\mathbf{p}})^x - ig_2\epsilon^{x\ell y}(\tau^A\tau_3)_a^b(\sigma^y)_\alpha^\beta(2\vec{\mathbf{k}}+\vec{\mathbf{p}})^\ell\right)$$

$$\left(\mathcal{K}_{PV}^{21\ Bw}\right)_{\alpha a}^{\beta b}(\vec{\mathbf{k}},\vec{\mathbf{p}}) = y_s y_t \left(g_1(\tau^B)_a^b\delta_\alpha^\beta(\vec{\mathbf{k}}+2\vec{\mathbf{p}})^w + ig_2\epsilon^{w\ell y}(\sigma^y)_\alpha^\beta(\tau_3\tau^B)_a^b(\vec{\mathbf{k}}+2\vec{\mathbf{p}})^\ell\right) \quad (4.7c)$$
$$+ y_t y_s \left(g_3(\sigma^w\sigma^\ell)_\alpha^\beta(\tau^B)_a^b - ig_4\epsilon^{3BC}(\sigma^w\sigma^\ell)_b^\beta(\tau^C)_a^b\right)(2\vec{\mathbf{k}}+\vec{\mathbf{p}})^\ell$$

$$\left(\mathcal{K}_{PV}^{22\ BA}\right)_{\alpha a}^{\beta b}(\vec{\mathbf{k}},\vec{\mathbf{p}}) = y_s^2 \left(g_3(\sigma^\ell)_\alpha^\beta(\tau^A\tau^B)_a^b + ig_4\epsilon^{3AC}(\sigma^\ell)_\alpha^\beta(\tau^C\tau^B)_a^b\right)(\vec{\mathbf{k}}+2\vec{\mathbf{p}})^\ell \quad (4.7d)$$
$$+ y_s^2 \left(g_3(\tau^A\tau^B)_a^b(\sigma^\ell)_\alpha^\beta - ig_4\epsilon^{3BC}(\tau^A\tau^C)_a^b(\sigma^\ell)_\alpha^\beta\right)(2\vec{\mathbf{k}}+\vec{\mathbf{p}})^\ell$$

(Note that the capital letters A,B, and C are used for the singlet auxiliary field polarization and the lowercase letters w,x, and y are used for the deuteron auxiliary field polarization.) where the coefficients g_i are defined in Eq. (4.14). Integrating over the energy and picking up the poles from the nucleon propagators in our diagrams Eq. (4.2) becomes.

$$\begin{aligned}(t_{PV}^{xw})_{\alpha a}^{\beta b}(\vec{\mathbf{k}},\vec{\mathbf{p}}) &= \frac{4M_N}{\sqrt{8}}\mathbf{v}_p^T\left(\boldsymbol{\mathcal{K}}^{xw}\right)_{\alpha a}^{\beta b}(\vec{\mathbf{k}},\vec{\mathbf{p}})\mathbf{v}_p \\ &- \frac{4M_N}{\sqrt{8}}\int\frac{d^3q}{(2\pi)^3}\mathbf{v}_p^T(\boldsymbol{\mathcal{K}}^{xy})_{\gamma c}^{\beta b}(\vec{\mathbf{q}},\vec{\mathbf{p}})\mathbf{D}\left(E-\frac{\vec{\mathbf{q}}^2}{2M_N},\vec{\mathbf{q}}\right)\left((t^{yw})_{\alpha a}^{\gamma c}(\vec{\mathbf{k}},\vec{\mathbf{q}})\right) \\ &- \frac{4M_N}{\sqrt{8}}\int\frac{d^3q}{(2\pi)^3}\left((t^{xy})_{\gamma c}^{\beta b}(\vec{\mathbf{q}},\vec{\mathbf{p}})\right)^T\mathbf{D}\left(E-\frac{\vec{\mathbf{q}}^2}{2M_N},\vec{\mathbf{q}}\right)(\boldsymbol{\mathcal{K}}^{yw})_{\alpha a}^{\gamma c}(\vec{\mathbf{k}},\vec{\mathbf{q}})\mathbf{v}_p \\ &+ \frac{4M_N}{\sqrt{8}}\int\frac{d^3q}{(2\pi)^3}\int\frac{d^3\ell}{(2\pi)^3}\left((t^{xz})_{\delta d}^{\beta b}(\vec{\boldsymbol{\ell}},\vec{\mathbf{p}},)\right)^T\mathbf{D}\left(E-\frac{\vec{\mathbf{q}}^2}{2M_N},\vec{\mathbf{q}}\right) \\ &\qquad (\boldsymbol{\mathcal{K}}^{zy})_{\gamma c}^{\delta d}(\vec{\mathbf{q}},\vec{\boldsymbol{\ell}})\mathbf{D}\left(E-\frac{\vec{\boldsymbol{\ell}}^2}{2M_N},\vec{\boldsymbol{\ell}}\right)\left((t^{yw})_{\alpha a}^{\gamma c}(\vec{\mathbf{k}},\vec{\mathbf{q}})\right)\end{aligned} \quad (4.8)$$

where

$$(\mathcal{K}^{xw})^{\beta b}_{\alpha a}(\vec{\mathbf{q}},\vec{\boldsymbol{\ell}}) = \frac{1}{\vec{\mathbf{q}}^2+\vec{\mathbf{q}}\cdot\vec{\boldsymbol{\ell}}+\vec{\boldsymbol{\ell}}^2 - M_N E - i\epsilon}\times \times \begin{pmatrix} (\mathcal{K}^{11}_{PV}{}^{xw})^{\beta b}_{\alpha a}(\vec{\mathbf{q}},\vec{\boldsymbol{\ell}}) & (\mathcal{K}^{12}_{PV}{}^{xw})^{\beta b}_{\alpha a}(\vec{\mathbf{q}},\vec{\boldsymbol{\ell}}) \\ (\mathcal{K}^{21}_{PV}{}^{xw})^{\beta b}_{\alpha a}(\vec{\mathbf{q}},\vec{\boldsymbol{\ell}}) & (\mathcal{K}^{22}_{PV}{}^{xw})^{\beta b}_{\alpha a}(\vec{\mathbf{q}},\vec{\boldsymbol{\ell}}) \end{pmatrix} \tag{4.9}$$

Now that we have derived the PV amplitude, we note that it contains the related scattering amplitudes from the PC sector. As mentioned earlier such PC scattering amplitudes are calculated in [55], by numerically solving Faddeev's equation in an angular momentum basis. However, as part of this solution one runs into singularities along the real axis. To overcome this difficulty the method of Hetherington and Schick is employed, in which the axis of integration is rotated into the complex plane, therefore avoiding the singularities [1, 21, 64]. One can then use the solutions along the deformed contour to solve for the amplitudes along the real axis. Details of the procedure to calculate these amplitudes can be found in [98]. In order to use the solutions to Faddeev's equations we need to project out our PV amplitude into an angular momentum basis. However, unlike the PC sector, the PV amplitudes mix different angular momentum states. Also, since at leading order, spin and orbital angular momentum mix, the appropriate angular momentum basis to use is the total angular momentum $\vec{\mathbf{J}} = \vec{\mathbf{L}} + \vec{\mathbf{S}}$. Thus we express our PV amplitude as

$$t_{PV}(\vec{\mathbf{k}},\vec{\mathbf{p}}) = \sum_{J=0}^{\infty}\sum_{M=-J}^{M=J}\sum_{L=|J-S|}^{J+S}\sum_{L'=|J-S'|}^{J+S'}\sum_{S,S'} 4\pi t^{JM}_{L'S',LS}(k,p)\mathscr{Y}^{M}_{J,L'S'}(\hat{\mathbf{p}})\left(\mathscr{Y}^{M}_{J,LS}(\hat{\mathbf{k}})\right)^{*} \tag{4.10}$$

where the spin angle functions are given by

$$\mathscr{Y}^{M}_{J,LS}(\hat{\mathbf{k}}) = \sum_{m_L,m_S} C^{m_L,m_S,M}_{L,S,J} Y^{m_L}_{L}(\hat{\mathbf{k}})\chi^{m_S}_{S} \tag{4.11}$$

$\chi_S^{m_S}$ being the spinor part of the spin-angle functions, $C_{L,S,J}^{m_L,m_S,M}$ the appropriate Clebsch-Gordan coefficient, and $Y_L^{m_L}(\hat{\mathbf{k}})$ is the appropriate spherical harmonic. Since the spin-angle functions are orthogonal, we can project out the amplitudes in our angular momentum basis via

$$t^{JM}_{L'S',LS}(k,p) = \frac{1}{4\pi}\int d\Omega_k \int d\Omega_p \left(\mathscr{Y}^M_{J,L'S'}(\hat{\mathbf{p}})\right)^* t_{PV}(\vec{\mathbf{k}},\vec{\mathbf{p}})\mathscr{Y}^M_{J,LS}(\hat{\mathbf{k}}) \tag{4.12}$$

At sufficiently low energies S-P mixing will dominate. Thus we will calculate only the amplitudes $t^{SM}_{1S',0S}$ (Note J=S here since L=0) for all possible values of S and S'. All spin and angle dependence is contained within the matrix $(\boldsymbol{\mathcal{K}}^{xw})^{\beta b}_{\alpha a}(\vec{\mathbf{q}},\vec{\boldsymbol{\ell}})$, and the appropriate projections in $\vec{\mathbf{J}}$, $\vec{\mathbf{L}}$,and $\vec{\mathbf{S}}$ can be found in the appendix. Going to a partial wave basis we finally obtain Eq. (4.13) for the PV partial wave amplitudes.

$$\begin{aligned}
{t_{PV}}^{JM}_{L'S',LS}(k,p) = {} & \frac{M_N}{\sqrt{8}\pi}\mathbf{v}_p^T\boldsymbol{\mathcal{K}}(k,p)^J_{L'S',LS}\mathbf{v}_p + \\
& - \frac{M_N}{2\sqrt{8}\pi^3}\int_0^\infty dqq^2\mathbf{v}_p^T\boldsymbol{\mathcal{K}}(q,p)^J_{L'S',LS}\mathbf{D}\left(E-\frac{\vec{\mathbf{q}}^2}{2M_N},\vec{\mathbf{q}}\right)\left(t_{PC}{}^{JM}_{LS,LS}(k,q)\right) \\
& - \frac{M_N}{2\sqrt{8}\pi^3}\int_0^\infty dqq^2\left(t_{PC}{}^{JM}_{L'S',L'S'}(q,p)\right)^T\mathbf{D}\left(E-\frac{\vec{\mathbf{q}}^2}{2M_N},\vec{\mathbf{q}}\right) \\
& \quad \boldsymbol{\mathcal{K}}(k,q)^J_{L'S',LS}\mathbf{v}_p \\
& + \frac{M_N}{4\sqrt{8}\pi^5}\int_0^\infty dqq^2\int_0^\infty d\ell\ell^2\left(t_{PC}{}^{JM}_{L'S',L'S'}(p,\ell)\right)^T\mathbf{D}\left(E-\frac{\vec{\mathbf{q}}^2}{2M_N},\vec{\mathbf{q}}\right) \\
& \quad \boldsymbol{\mathcal{K}}(q,\ell)^{JM}_{L'S',LS}\mathbf{D}\left(E-\frac{\vec{\boldsymbol{\ell}}^{\mathbf{2}}}{2M_N},\vec{\boldsymbol{\ell}}\right)\left(t_{PC}{}^{JM}_{LS,LS}(k,q)\right)
\end{aligned} \tag{4.13}$$

This expression contains the PC amplitudes in the partial wave basis of total angular momentum $\vec{\mathbf{J}} = \vec{\mathbf{L}} + \vec{\mathbf{S}}$. (These are equivalent to the PC amplitudes in the partial wave basis of orbital angular momentum.) It can be shown straightforwardly that the PC amplitudes are independent of total angular momentum $\vec{\mathbf{J}}$. Thus we can use the

PC amplitudes as calculated numerically by [15, 50, 55] and perform the integration numerically in order to obtain the associated PV amplitudes.

Before integrating Eq. (4.13) we multiply by the LO deuteron renormalization $Z_D = (8\pi\gamma_d)/(M_N^2 y_t^2)$ [50], and use the renormalized PC amplitudes. We find that all the PV LEC's occur in the combinations.

$$\frac{g^{^3S_1-{}^1P_1}}{y_t}, \frac{g^{^3S_1-{}^3P_1}}{y_t}, \frac{g^{^1S_0-{}^3P_0}_{(\Delta I=0)}}{y_s}, \frac{g^{^1S_0-{}^3P_0}_{(\Delta I=1)}}{y_s}$$

(Note $g^{^1S_0-{}^3P_0}_{(\Delta I=2)}$ does not appear as a $\Delta I = 2$ transition is not allowed for a first order PV transition in nd scattering.) For the sake of convenience we find it useful to make the following definitions.

$$g_1 = \frac{g^{^3S_1-{}^1P_1}}{y_t}, g_2 = \frac{g^{^3S_1-{}^3P_1}}{y_t}, g_3 = \frac{g^{^1S_0-{}^3P_0}_{(\Delta I=0)}}{y_s}, g_4 = \frac{g^{^1S_0-{}^3P_0}_{(\Delta I=1)}}{y_s}, g_5 = \frac{g^{^1S_0-{}^3P_0}_{(\Delta I=2)}}{y_s} \tag{4.14}$$

Since these coefficients are unknown, we will write the PV partial wave amplitudes as follows, where $\left(t_{PV}{}^{JM}_{L'S',LS}(k,p)\right)^i$ is calculated by setting $g_j = 0, j \neq i$ and $g_i = 1$ in the PV partial wave amplitude. Thus the PV amplitude can be written as.

$$t_{PV}{}^{JM}_{L'S',LS}(k,p) = \sum_{i=1}^{4} g_i \left(t_{PV}{}^{JM}_{L'S',LS}(k,p)\right)^i \tag{4.15}$$

4.2 Parity-Violating Potential

It is clear from Eq. (4.15) that in order to obtain numerical values for the PV amplitude one needs to know the size of the coefficients g_i, which at this time are not determined from either theory or experiment. Nevertheless, we can obtain estimates by matching the g_i onto the familiar DDH coefficients. We will carry out this procedure in three steps. First we match the DDH coefficients onto the coefficients

of the Zhu potential [110]. Then we match the Zhu potential on to the Girlanda potential [95, 96]. Finally we project the coefficients of the Girlanda potential onto the coefficients of the auxiliary field formalism. We also show how all these formalisms can be matched to the familiar Danilov parameters

The DDH model [31] is a single-meson-exchange picture, limited to exchange of the lightest mesons π, ρ, and ω.[1] The strong Hamiltonian is given by

$$\begin{aligned}\mathcal{H}_{st} =& ig_{\pi NN}\bar{N}\gamma_5\tau\cdot\pi N + g_\rho\bar{N}\left(\gamma_\mu + i\frac{(1+\chi_\rho)}{2M_N}\sigma_{\mu\nu}k^\nu\right)\tau\cdot\rho^\mu N \\ &+ g_\omega\bar{N}\left(\gamma_\mu + i\frac{(1+\chi_\omega)}{2M_N}\sigma_{\mu\nu}k^\nu\right)\omega^\mu N\end{aligned} \tag{4.16}$$

with the strong couplings given approximately by $g^2_{\pi NN}/4\pi \simeq 13.5$ and $g^2_\rho/4\pi = \frac{1}{9}g^2_\omega/4\pi \simeq .67$, while the magnetic moment terms are approximately $\chi_\rho = \kappa_p - \kappa_n = 3.7$ and $\chi_\omega = \kappa_p + \kappa_n = -.12$. The phenomenological weak interaction Hamiltonian posited by DDH consists of seven weak coupling terms

$$\begin{aligned}\mathcal{H}_{wk} =& i\frac{f^1_\pi}{\sqrt{2}}\bar{N}(\tau\times\pi)_z N + \bar{N}\left(h^0_\rho\tau\cdot\rho^\mu + h^1_\rho\rho^\mu_z + \frac{h^2_\rho}{2\sqrt{6}}(3\tau_z\rho^\mu_z - \tau\cdot\rho^\mu)\right)\gamma_\mu\gamma_5 N \\ &+ \bar{N}\left(h^0_\omega\omega^\mu + h^1_\omega\tau_z\omega^\mu\right)\gamma_\mu\gamma_5 N - {h'_\rho}^1\bar{N}(\tau\times\rho^\mu)_z\frac{\sigma_{\mu\nu}k^\nu}{2M_N}\gamma_5 N\end{aligned} \tag{4.17}$$

DDH attempted to obtain theoretical predictions for the seven constants using SU(6) symmetry and quark model techniques. (Note ${h'_\rho}^1$ is shown to be small by quark model calculations and is dropped in the following.) However, due to the difficulty

[1] Since CP is conserved there are no neutral pseudoscalar mesons π^0, η, or η' by Barton's theorem [8]

of this calculation they were only able to come up with reasonable ranges and "best" values as shown in Table 4.1. (Also shown are estimates by other groups.)

Coupling	DDH [31] Reasonable Range	DDH [31] "Best" Value	DZ [37]	FCDH [48]
f_π	$0 \to 30$	+12	+3	+7
h^0_ρ	$30 \to -81$	-30	-22	-10
h^1_ρ	$-1 \to 0$	-.5	+1	-1
h^2_ρ	$-20 \to -29$	-25	-18	-18
h^0_ω	$15 \to -27$	-5	-10	-13
h^1_ω	$-5 \to -2$	-3	-6	-6

Table 4.1: Weak nucleon-nucleon-meson (NNM) couplings. All numbers are quoted in units of the "sum rule" value $S_R = 3.8 \times 10^{-8}$

The form of any PV potential can be written as a sum of operators $O^{(n)}_{ij}$ with corresponding coefficients c^α_n, where α refers to the specific potential of interest..

$$V^\alpha_{ij} = \sum_n c^\alpha_n O^{(n)}_{ij} \tag{4.18}$$

At the lowest energies the component of the operators that contain momentum is of two forms.

$$\begin{aligned} \mathbf{X}^{(n)}_{ij,+} &= \{\vec{\mathbf{p}}_{ij}, f^\alpha_n(r_{ij})\} \\ \mathbf{X}^{(n)}_{ij,-} &= i[\vec{\mathbf{p}}_{ij}, f^\alpha_n(r_{ij})] \end{aligned} \tag{4.19}$$

where $\vec{\mathbf{p}}_{ij} = (\vec{\mathbf{p}}_1 - \vec{\mathbf{p}}_2)/2$ is the momentum of the nucleon-nucleon system in the c.m. frame.

The coefficients, operators, and regulator functions $f^{DDH}_n(r_{ij})$ for the DDH potential and $f^{Zhu}_n(r_{ij})$ for the Zhu potential are given in Table 4.2. The functions $f^{DDH}_n(r_{ij})$ are Yukawa functions, where the mass corresponds to the appropriate meson [67].

Table 4.2: PV potential in DDH and Zhu formalism. $\mathcal{T}_{ij} \equiv (3\tau_i^z\tau_j^z - \tau_i \cdot \tau_j)$. (Note $\Lambda_\chi \sim 4\pi F_\pi$ is the chiral scale [33,82], where $F_\pi = 92.4MeV$ is the pion decay constant)

n	c_n^{DDH}	c_n^{Zhu}	$f_n^{DDH}(r)$	f_n^{Zhu}	$O_{ij}^{(n)}$
1	$+\frac{g_{\pi NN}}{2\sqrt{2}M_N} f_\pi$	$\frac{m^2}{\Lambda_\chi^3} 2\tilde{C}_6$	$f_\pi(r)$	$f_m(r)$	$(\tau_i \times \tau_j)^z(\vec{\boldsymbol{\sigma}}_i + \vec{\boldsymbol{\sigma}}_j) \cdot \boldsymbol{X}_{ij,-}^{(1)}$
2	$-\frac{g_\rho}{M_N} h_\rho^0$	$\frac{m^2}{\Lambda_\chi^3} 2C_3$	$f_\rho(r)$	$f_m(r)$	$(\tau_i \cdot \tau_j)(\vec{\boldsymbol{\sigma}}_i - \vec{\boldsymbol{\sigma}}_j) \cdot \boldsymbol{X}_{ij,+}^{(2)}$
3	$-\frac{g_\rho(1+\chi_\rho)}{M_N} h_\rho^0$	$\frac{m^2}{\Lambda_\chi^3} 2\tilde{C}_3$	$f_\rho(r)$	$f_m(r)$	$(\tau_i \cdot \tau_j)(\vec{\boldsymbol{\sigma}}_i \times \vec{\boldsymbol{\sigma}}_j) \cdot \boldsymbol{X}_{ij,-}^{(3)}$
4	$-\frac{g_\rho}{2M_N} h_\rho^1$	$\frac{m^2}{\Lambda_\chi^3} C_4$	$f_\rho(r)$	$f_m(r)$	$(\tau_i + \tau_j)^z(\vec{\boldsymbol{\sigma}}_i - \vec{\boldsymbol{\sigma}}_j) \cdot \boldsymbol{X}_{ij,+}^{(4)}$
5	$-\frac{g_\rho(1+\chi_\rho)}{2M_N} h_\rho^1$	$\frac{m^2}{\Lambda_\chi^3} \tilde{C}_4$	$f_\rho(r)$	$f_m(r)$	$(\tau_i + \tau_j)^z(\vec{\boldsymbol{\sigma}}_i \times \vec{\boldsymbol{\sigma}}_j) \cdot \boldsymbol{X}_{ij,-}^{(5)}$
6	$-\frac{g_\rho}{2\sqrt{6}M_N} h_\rho^2$	$-\frac{m^2}{\Lambda_\chi^3} 2C_5$	$f_\rho(r)$	$f_m(r)$	$\mathcal{T}_{ij}(\vec{\boldsymbol{\sigma}}_i - \vec{\boldsymbol{\sigma}}_j) \cdot \boldsymbol{X}_{ij,+}^{(6)}$
7	$-\frac{g_\rho(1+\chi_\rho)}{2\sqrt{6}M_N} h_\rho^2$	$-\frac{m^2}{\Lambda_\chi^3} 2\tilde{C}_5$	$f_\rho(r)$	$f_m(r)$	$\mathcal{T}_{ij}(\vec{\boldsymbol{\sigma}}_i \times \vec{\boldsymbol{\sigma}}_j) \cdot \boldsymbol{X}_{ij,-}^{(7)}$
8	$-\frac{g_\omega}{M_N} h_\omega^0$	$\frac{m^2}{\Lambda_\chi^3} 2C_1$	$f_\omega(r)$	$f_m(r)$	$(\vec{\boldsymbol{\sigma}}_i - \vec{\boldsymbol{\sigma}}_j) \cdot \boldsymbol{X}_{ij,+}^{(8)}$
9	$-\frac{g_\omega(1+\chi_\omega)}{M_N} h_\omega^0$	$\frac{m^2}{\Lambda_\chi^3} 2\tilde{C}_1$	$f_\omega(r)$	$f_m(r)$	$(\vec{\boldsymbol{\sigma}}_i \times \vec{\boldsymbol{\sigma}}_j) \cdot \boldsymbol{X}_{ij,-}^{(9)}$
10	$-\frac{g_\omega}{2M_N} h_\omega^1$	$\frac{m^2}{\Lambda_\chi^3} C_2$	$f_\omega(r)$	$f_m(r)$	$(\tau_i + \tau_j)^z(\vec{\boldsymbol{\sigma}}_i - \vec{\boldsymbol{\sigma}}_j) \cdot \boldsymbol{X}_{ij,+}^{(10)}$
11	$-\frac{g_\omega(1+\chi_\omega)}{2M_N} h_\omega^1$	$\frac{m^2}{\Lambda_\chi^3} \tilde{C}_2$	$f_\omega(r)$	$f_m(r)$	$(\tau_i + \tau_j)^z(\vec{\boldsymbol{\sigma}}_i \times \vec{\boldsymbol{\sigma}}_j) \cdot \boldsymbol{X}_{ij,-}^{(11)}$
12	$-\frac{g_\omega h_\omega^1 - g_\rho h_\rho^1}{2M_N}$	$\frac{m^2}{\Lambda_\chi^3}(C_2 - C_4)$	$f_\rho(r)$	$f_m(r)$	$(\tau_i - \tau_j)^z(\vec{\boldsymbol{\sigma}}_i + \vec{\boldsymbol{\sigma}}_j) \cdot \boldsymbol{X}_{ij,+}^{(12)}$
13	$-\frac{g_\rho}{2M_N} h_\rho'^1$	0	$f_\rho(r)$	0	$(\tau_i \times \tau_j)^z(\vec{\boldsymbol{\sigma}}_i + \vec{\boldsymbol{\sigma}}_j) \cdot \boldsymbol{X}_{ij,-}^{(13)}$

However, at the lowest energies the functions for the DDH potential can be written as $f_i(r) = \frac{1}{m_i^2}\delta^3(\vec{\mathbf{r}})$, where $i = \pi$,ρ, or ω [67]. Likewise the functions $f_m(r)$ for the Zhu potential become delta functions, with $f_m(r) = \frac{1}{m^2}\delta^3(\vec{\mathbf{r}})$ in the low energy limit, where m is a mass sufficiently greater than our energies of interest such that the delta function approximation is valid (for our low energies of interest $m = m_\pi$ is sufficient). Thus at low energies the DDH potential and the Zhu potential can be trivially matched yielding [110]

$$\frac{\tilde{C}_1}{C_1} = \frac{\tilde{C}_2}{C_2} = 1 + \chi_\omega \simeq .88 \tag{4.20}$$

$$\frac{\tilde{C}_3}{C_3} = \frac{\tilde{C}_4}{C_4} = \frac{\tilde{C}_5}{C_5} = 1 + \chi_\rho \simeq 4.7 \tag{4.21}$$

$$
\begin{aligned}
C_1^{DDH} &= -\frac{\Lambda_\chi^3}{2M_N m_\omega^2} g_\omega h_\omega^0 \overset{\text{bestguess}}{\longrightarrow} 2.25\times 10^{-6} \\
C_2^{DDH} &= -\frac{\Lambda_\chi^3}{2M_N m_\omega^2} g_\omega h_\omega^1 \overset{\text{bestguess}}{\longrightarrow} 1.35\times 10^{-6} \\
C_3^{DDH} &= -\frac{\Lambda_\chi^3}{2M_N m_\rho^2} g_\rho h_\rho^0 \overset{\text{bestguess}}{\longrightarrow} 4.58\times 10^{-6} \\
C_4^{DDH} &= -\frac{\Lambda_\chi^3}{2M_N m_\rho^2} g_\rho h_\rho^1 \overset{\text{bestguess}}{\longrightarrow} 7.64\times 10^{-8} \\
C_5^{DDH} &= \frac{\Lambda_\chi^3}{4\sqrt{6} M_N m_\rho^2} g_\rho h_\rho^0 \overset{\text{bestguess}}{\longrightarrow} -7.80\times 10^{-7} \\
\tilde{C}_6^{DDH} &\simeq \frac{\Lambda_\chi^3}{4\sqrt{2} M_N m_\pi^2} g_{\pi NN} f_\pi \overset{\text{bestguess}}{\longrightarrow} 9.19\times 10^{-5}
\end{aligned}
\tag{4.22}
$$

As first pointed out by Danilov, one needs five PV terms at the lowest energies in the two-body sector [28], since only S-P mixing is involved. By conservation of angular momentum the state ${}^3S_1$, can only connect with the states ${}^1P_1$ or ${}^3P_1$. Since ${}^3S_1$ is an isosinglet there is a unique way to get to the isosinglet state ${}^1P_1$ and isotriplet state ${}^3P_1$. Similarly, the state ${}^1S_0$ can only connect with the state ${}^3P_0$. However, both ${}^1S_0$ and ${}^3P_0$ are isotriplet states so the operator connecting these states can carry $\Delta I = 0, 1,$ or 2. The existence of five unique operators which characterize parity violation at low energy appears to be in contradiction with the DDH and Zhu potential, which involve ten different operators. However, at low energies five of these operator structures are redundant as shown by Girlanda [53]. In this procedure one begins with all possible up to one-derivative P violating CP conserving relativistic terms.

$$
\begin{aligned}
\mathcal{O}_1 &= \bar{\psi}\gamma^\mu\psi\bar{\psi}\gamma_\mu\gamma_5\psi & \tilde{\mathcal{O}}_1 &= \bar{\psi}\gamma^\mu\gamma_5\psi\partial^\nu(\bar{\psi}\sigma_{\mu\nu}\psi) \\
\mathcal{O}_2 &= \bar{\psi}\gamma^\mu\psi\bar{\psi}\tau_3\gamma_\mu\gamma_5\psi & \tilde{\mathcal{O}}_2 &= \bar{\psi}\gamma^\mu\gamma_5\psi\partial^\nu(\bar{\psi}\tau_3\sigma_{\mu\nu}\psi) \\
\mathcal{O}_3 &= \bar{\psi}\tau_a\gamma^\mu\psi\bar{\psi}\tau^a\gamma_\mu\gamma_5\psi & \tilde{\mathcal{O}}_3 &= \bar{\psi}\tau_a\gamma^\mu\gamma_5\psi\partial^\nu(\bar{\psi}\tau^a\sigma_{\mu\nu}\psi) \\
\mathcal{O}_4 &= \bar{\psi}\tau_3\gamma^\mu\psi\bar{\psi}\gamma_\mu\gamma_5\psi & \tilde{\mathcal{O}}_4 &= \bar{\psi}\tau_3\gamma^\mu\gamma_5\psi\partial^\nu(\bar{\psi}\sigma_{\mu\nu}\psi) \\
\mathcal{O}_5 &= \mathcal{I}_{ab}\bar{\psi}\tau_a\gamma^\mu\psi\bar{\psi}\tau_b\gamma_\mu\gamma_5\psi & \tilde{\mathcal{O}}_5 &= \mathcal{I}_{ab}\bar{\psi}\tau_a\gamma^\mu\gamma_5\psi\partial^\nu(\bar{\psi}\tau_b\sigma_{\mu\nu}\psi) \\
\mathcal{O}_6 &= i\epsilon_{ab3}\bar{\psi}\tau_a\gamma^\mu\psi\bar{\psi}\tau_b\gamma_\mu\gamma_5\psi & \tilde{\mathcal{O}}_6 &= i\epsilon_{ab3}\bar{\psi}\tau_a\gamma^\mu\gamma_5\psi\partial^\nu(\bar{\psi}\tau_b\sigma_{\mu\nu}\psi)
\end{aligned}
\tag{4.23}
$$

Using Fierz transformations and the equations of motion, there exist six identities

$$
\begin{aligned}
\mathcal{O}_3 &= \mathcal{O}_1 & \tilde{\mathcal{O}}_2 + \tilde{\mathcal{O}}_4 &= M_N(\mathcal{O}_2 + \mathcal{O}_4) \\
\mathcal{O}_2 - \mathcal{O}_4 &= 2\mathcal{O}_6 & \tilde{\mathcal{O}}_2 - \tilde{\mathcal{O}}_4 &= -2M_N\mathcal{O}_6 - \tilde{\mathcal{O}}_6 \\
\tilde{\mathcal{O}}_3 + 3\tilde{\mathcal{O}}_1 &= 2M_N(\mathcal{O}_1 + \mathcal{O}_3) & \tilde{\mathcal{O}}_5 &= M_N\mathcal{O}_5
\end{aligned}
\tag{4.24}
$$

reducing the number of unique operators to six. However, in a non-relativistic reduction it turns out that two of the operators have equivalent structures leaving five unique operators at the lowest energies. The resulting PV Lagrangian in the Girlanda formalism is given by

$$
\begin{aligned}
\mathcal{L}_{\rm PV}^{\rm Gir} = {} & \mathcal{G}_1(N^\dagger\vec{\boldsymbol{\sigma}}N\cdot N^\dagger i\overleftrightarrow{\nabla}N - N^\dagger NN^\dagger i\overleftrightarrow{\nabla}\cdot\vec{\boldsymbol{\sigma}}N) - \tilde{\mathcal{G}}_1\epsilon_{ijk}N^\dagger\sigma_i N\nabla_j(N^\dagger\sigma_k N) \\
& - \mathcal{G}_2\epsilon_{ijk}[N^\dagger\tau_3\sigma_i N\nabla_j(N^\dagger\sigma_k N) + N^\dagger\sigma_i N\nabla_j(N^\dagger\tau_3\sigma_k N)] \\
& - \tilde{\mathcal{G}}_5\mathcal{I}_{ab}\epsilon_{ijk}N^\dagger\tau_a\sigma_i N\nabla_j(N^\dagger\tau_b\sigma_k N) + \mathcal{G}_6\epsilon_{ab3}\overrightarrow{\nabla}(N^\dagger\tau_a N)\cdot N^\dagger\tau_b\vec{\boldsymbol{\sigma}}N
\end{aligned}
\tag{4.25}
$$

(In Eq. (4.25) a factor of $1/\Lambda_\chi^3$ has been absorbed into the coefficients. This notation agrees with the notation of Phillips, Schindler, and Springer [88].) With this PV

Lagrangian one can compute the Girlanda potential which takes on the following form given by Table 4.3 and Eq. (4.18), where n runs from one to five, and μ is a mass chosen to be much larger than the energies of interest (again for our purposes we choose $\mu = m_\pi$).

Table 4.3: Parity violating potential in Girlanda formalism. $\mathcal{T}_{ij} \equiv (3\tau_i^z\tau_j^z - \tau_i \cdot \tau_j)$.

n	c_n^{Gir}	$f_n^{Gir}(r)$	$O_{ij}^{(n)}$
1	$-\mu^2\mathcal{G}_6$	$\frac{1}{\mu^2}\delta^3(\vec{\mathbf{r}})$	$(\tau_i \times \tau_j)^z(\vec{\boldsymbol{\sigma}}_i + \vec{\boldsymbol{\sigma}}_j) \cdot \boldsymbol{X}_{ij,-}^{(1)}$
2	$2\mu^2\mathcal{G}_2$	$\frac{1}{\mu^2}\delta^3(\vec{\mathbf{r}})$	$(\tau_i + \tau_j)^z(\vec{\boldsymbol{\sigma}}_i - \vec{\boldsymbol{\sigma}}_j) \cdot \boldsymbol{X}_{ij,+}^{(2)}$
3	$-2\mu^2\mathcal{G}_5$	$\frac{1}{\mu^2}\delta^3(\vec{\mathbf{r}})$	$\mathcal{T}_{ij}(\vec{\boldsymbol{\sigma}}_i - \vec{\boldsymbol{\sigma}}_j) \cdot \boldsymbol{X}_{ij,+}^{(3)}$
4	$2\mu^2\mathcal{G}_1$	$\frac{1}{\mu^2}\delta^3(\vec{\mathbf{r}})$	$(\vec{\boldsymbol{\sigma}}_i - \vec{\boldsymbol{\sigma}}_j) \cdot \boldsymbol{X}_{ij,+}^{(4)}$
5	$2\mu^2\tilde{\mathcal{G}}_1$	$\frac{1}{\mu^2}\delta^3(\vec{\mathbf{r}})$	$(\vec{\boldsymbol{\sigma}}_i \times \vec{\boldsymbol{\sigma}}_j) \cdot \boldsymbol{X}_{ij,-}^{(5)}$

Using (4.24) and the nonrelativistic reduction one can reduce the Zhu potential to a set of five operators, allowing the matching of the Zhu coefficients onto the Girlanda coefficients as shown in Table 4.5.

For our calculations, we also require the coefficients in the auxiliary field formalism Eq. (4.1). This matching of the $\mathcal{G}_i$ and g_i requires two steps. One first performs Gaussian integration over the auxiliary fields followed by a field redefinition to rewrite the Lagrangian, Eq (4.1) in terms of nucleon fields, as done by Schindler, and Springer [97]. Then one can match this partial wave formalism onto the Girlanda formalism by performing Fierz rearrangements and using the constraints Eq. (4.24) with a non-relativistic reduction, yielding the results in Table 4.5. The matching of the partial wave and Girlanda formalism is carried out in greater detail in the appendix. (This has also been done using a different method by Phillips, Schindler, and Springer [88].)

Finally we wish to match the Girlanda potential onto the Danilov potential which is given by Table 4.4 and Eq. (4.18), where n runs from one to five.

In order to match the Girlanda formalism to the Danilov formalism we note the identity

Table 4.4: Parity violating potential in Danilov formalism. $\mathcal{T}_{ij} \equiv (3\tau_i^z\tau_j^z - \tau_i \cdot \tau_j)$, $P_0 = \frac{1}{4}(1 - \vec{\boldsymbol{\sigma}}_i \cdot \vec{\boldsymbol{\sigma}}_j)$, $P_1 = \frac{1}{4}(3 + \vec{\boldsymbol{\sigma}}_i \cdot \vec{\boldsymbol{\sigma}}_j)$, and $a_t = 5.423$ fm is the ${}^3S_1$ scattering length.

n	c_n^{Dan}	$f_n^{Dan}(r)$	$O_{ij}^{(n)}$
1	$\frac{1}{2}a_t\rho_t$	$\frac{4\pi}{M_N}\delta^3(\vec{\mathbf{r}})$	$(\tau_i - \tau_j)^z(\vec{\boldsymbol{\sigma}}_i + \vec{\boldsymbol{\sigma}}_j) \cdot \boldsymbol{X}_{ij,+}^{(1)}$
2	$\frac{1}{2}\lambda_s^1/\gamma_s$	$\frac{4\pi}{M_N}\delta^3(\vec{\mathbf{r}})$	$(\tau_i + \tau_j)^z(\vec{\boldsymbol{\sigma}}_i - \vec{\boldsymbol{\sigma}}_j) \cdot \boldsymbol{X}_{ij,+}^{(2)}$
3	$\frac{1}{2\sqrt{6}}\lambda_s^2/\gamma_s$	$\frac{4\pi}{M_N}\delta^3(\vec{\mathbf{r}})$	$\mathcal{T}_{ij}(\vec{\boldsymbol{\sigma}}_i - \vec{\boldsymbol{\sigma}}_j) \cdot \boldsymbol{X}_{ij,+}^{(3)}$
4	$a_t\lambda_t$	$\frac{4\pi}{M_N}\delta^3(\vec{\mathbf{r}})$	$(\vec{\boldsymbol{\sigma}}_i - \vec{\boldsymbol{\sigma}}_j)P_1 \cdot \boldsymbol{X}_{ij,+}^{(4)}$
5	λ_s^0/γ_s	$\frac{4\pi}{M_N}\delta^3(\vec{\mathbf{r}})$	$(\vec{\boldsymbol{\sigma}}_i - \vec{\boldsymbol{\sigma}}_j)P_0 \cdot \boldsymbol{X}_{ij,+}^{(5)}$

$$\langle P|[-i\boldsymbol{\nabla}, \delta^3(\vec{\mathbf{r}})]|S\rangle = \langle P|\left\{-i\boldsymbol{\nabla}, \delta^3(\vec{\mathbf{r}})\right\}|S\rangle \tag{4.26}$$

which follows trivially since P waves are zero at the origin. Next we make use of the identical identities in spin and isospin space. (Note $P_0^\tau = \frac{1}{4}(1 - \vec{\boldsymbol{\tau}}_i \cdot \vec{\boldsymbol{\tau}}_j)$, and $P_1^\tau = \frac{1}{4}(3 + \vec{\boldsymbol{\tau}}_i \cdot \vec{\boldsymbol{\tau}}_j)$)

$$i(\vec{\boldsymbol{\sigma}}_i \times \vec{\boldsymbol{\sigma}}_j) = (\vec{\boldsymbol{\sigma}}_i - \vec{\boldsymbol{\sigma}}_j)(P_0 - P_1) \tag{4.27}$$

$$i(\vec{\boldsymbol{\tau}}_i \times \vec{\boldsymbol{\tau}}_j)^z = (\vec{\boldsymbol{\tau}}_i - \vec{\boldsymbol{\tau}}_j)^z(P_0^\tau - P_1^\tau) \tag{4.28}$$

The isospin operator $i(\vec{\boldsymbol{\tau}}_i \times \vec{\boldsymbol{\tau}}_j)^z$ only appears with the spin operator $(\vec{\boldsymbol{\sigma}}_i + \vec{\boldsymbol{\sigma}}_j)$ in the Girlanda potential. Since this spin operator only projects out the triplet state of the S wave, only the isosinglet part of the operator $i(\vec{\boldsymbol{\tau}}_i \times \vec{\boldsymbol{\tau}}_j)^z$ is projected out. Thus by Eq. (4.28) we find that in combination with the spin operator $(\vec{\boldsymbol{\sigma}}_i + \vec{\boldsymbol{\sigma}}_j)$ the isospin operator $i(\vec{\boldsymbol{\tau}}_i \times \vec{\boldsymbol{\tau}}_j)^z = (\vec{\boldsymbol{\tau}}_i - \vec{\boldsymbol{\tau}}_j)^z$. Finally using Eqs. (4.26), (4.27), and the fact that the identity I is $I = P_0 + P_1$ one can straightforwardly match the Girlanda coefficients to the Danilov coefficients, giving the results shown in Table 4.5. Also shown in Table 4.5 are the relation between the Zhu, Girlanda, Auxiliary, and Danilov formalisms. The primary goal in low energy hadronic parity violation is to determine the value of

the Danilov parameters. At low energies all of these different EFT formalisms can be shown to be equivalent to the Danilov parameters, as shown in Table 4.5. Thus one can use whichever formalism is more convenient.

Table 4.5: Translation between various formalisms of PV potential

Zhu	Girlanda	Auxiliary	Danilov
$\frac{M_N(\frac{1}{a_t}-\mu)}{2\pi\Lambda_\chi^3}\left(C_1-\tilde{C}_1-3(C_3-\tilde{C}_3)\right)$	$\frac{M_N(\frac{1}{a_t}-\mu)}{2\pi}\left(\mathcal{G}_1-\tilde{\mathcal{G}}_1\right)$	$-2\sqrt{2}g_1$	$\lambda_t a_t(\frac{1}{a_t}-\mu)$
$\frac{M_N(\frac{1}{a_t}-\mu)}{2\pi\Lambda_\chi^3}\left(2\tilde{C}_6+(C_2-C_4)\right)$	$-\frac{M_N(\frac{1}{a_t}-\mu)}{2\pi}\mathcal{G}_6$	$2\sqrt{2}g_2$	$\rho_t a_t(\frac{1}{a_t}-\mu)$
$\frac{M_N(\gamma_s-\mu)}{2\pi\Lambda_\chi^3}\left(C_1+\tilde{C}_1+(C_3+\tilde{C}_3)\right)$	$\frac{M_N(\gamma_s-\mu)}{2\pi}\left(\tilde{\mathcal{G}}_1+\mathcal{G}_1\right)$	$-2\sqrt{2}g_3$	$\lambda_s^1\frac{1}{\gamma_s}(\gamma_s-\mu)$
$\frac{M_N(\gamma_s-\mu)}{2\pi\Lambda_\chi^3}\left(C_2+C_4+\tilde{C}_2+\tilde{C}_4\right)$	$\frac{M_N(\gamma_s-\mu)}{\pi}\mathcal{G}_2$	$-2\sqrt{2}g_4$	$\lambda_s^1\frac{1}{\gamma_s}(\gamma_s-\mu)$
$-\frac{M_N(\gamma_s-\mu)\sqrt{6}}{\pi\Lambda_\chi^3}\left(C_5+\tilde{C}_5\right)$	$-\frac{M_N(\gamma_s-\mu)\sqrt{6}}{\pi}\mathcal{G}_5$	$-4\sqrt{3}g_5$	$\lambda_s^2\frac{1}{\gamma_s}(\gamma_s-\mu)$

Having matched the auxiliary coefficients g_i to the Zhu coefficients we can now use the matching of the Zhu coefficients to the DDH "best" values to obtain estimates for the auxiliary coefficients which yields.

$$g_1 = -\frac{M_N(\frac{1}{a_t}-\mu)}{8\sqrt{2}\pi}\left[\frac{g_\omega\chi_\omega}{M_N m_\omega^2}h_\omega^0 - \frac{3g_\rho\chi_\rho}{M_N m_\rho^2}h_\rho^0\right] \sim 1.75\times10^{-10}\text{MeV}^{-1} \tag{4.29a}$$

$$g_2 = \frac{M_N(\frac{1}{a_t}-\mu)}{8\sqrt{2}\pi}\left[\frac{g_{\pi NN}}{\sqrt{2}M_N m_\pi^2}f_\pi + \frac{g_\rho}{M_N m_\rho^2}h_\rho^1 - \frac{g_\omega}{M_N m_\omega^2}h_\omega^1\right] \sim -6.34\times10^{-10}\text{MeV}^{-1} \tag{4.29b}$$

$$g_3 = \frac{M_N(\gamma_s-\mu)}{8\sqrt{2}\pi}\left[\frac{g_\omega(2+\chi_\omega)}{M_N m_\omega^2}h_\omega^0 + \frac{g_\rho(2+\chi_\rho)}{M_N m_\rho^2}h_\rho^0\right] \sim 1.50\times10^{-10}\text{MeV}^{-1} \tag{4.29c}$$

$$g_4 = \frac{M_N(\gamma_s-\mu)}{8\sqrt{2}\pi}\left[\frac{g_\rho(2+\chi_\rho)}{M_N m_\rho^2}h_\rho^1 + \frac{g_\omega(2+\chi_\omega)}{M_N m_\omega^2}h_\omega^1\right] \sim 1.47\times10^{-11}\text{MeV}^{-1} \tag{4.29d}$$

$$g_5 = \frac{M_N(\gamma_s-\mu)}{8\sqrt{2}\pi}\left[\frac{g_\rho(2+\chi_\rho)}{\sqrt{6}M_N m_\rho^2}h_\rho^2\right] \sim 4.39\times10^{-11}\text{MeV}^{-1} \tag{4.29e}$$

4.3 Spin Observables

Now that we have the PV amplitudes calculated we, of course, need to relate them to observables. We wish to find quantities that would be zero in the absence of parity violation. One such observable is the neutron asymmetry A_N [94], wherein we scatter longitudinally polarized neutrons from an unpolarized deuteron target. Then we measure the difference of the two cross sections σ_+ and σ_- defined below. The observable is defined as

$$A_N = \frac{\sigma_+ - \sigma_-}{\sigma_+ + \sigma_-} \tag{4.30}$$

where σ_+ (σ_-) represents the cross section of positive (negative) helicity nucleons

In order to calculate observables we need to write them in terms of the partial wave amplitudes calculated above. We denote the transition matrix with the addition of spin by the operator $\mathbf{M}$, which is not diagonal in the orbital angular momentum basis, but rather diagonal in the total angular momentum basis where the total angular momentum is $\vec{\mathbf{J}} = \vec{\mathbf{L}} + \vec{\mathbf{S}}$. The basis states for the total angular momentum are given by.

$$|JMLS\rangle = \sum_{m_L, m_S} C_{L,S,J}^{m_L, m_S, M} |L, m_L\rangle |S, m_S\rangle \tag{4.31}$$

Plugging in a complete set of states around $\mathbf{M}$ we find the following. (Note the inclusion of the factor 4π is arbitrary, but is is included so our PC amplitudes will be equivalent to the PC amplitudes in the standard partial wave expansion in orbital angular momentum.)

$$\langle p, S', m'_S|\mathbf{M}|k, S, m_S\rangle = 4\pi \sum_{J,M}\sum_{L,L'}\sum_{\tilde{S},\tilde{S}'}\langle p, S', m'_S|JML'\tilde{S}'\rangle\langle JML'\tilde{S}'|\mathbf{M}|JML\tilde{S}\rangle\times \tag{4.32}$$

$$\times\, \langle JML\tilde{S}|k, S, m_S\rangle$$

Then using Eq. (4.31) we find

$$\langle p, S', m'_S|\mathbf{M}|k, S, m_S\rangle = 4\pi \sum_{J,M}\sum_{L,L'}\sum_{\tilde{S},\tilde{S}'}\sum_{m_L,m_{\tilde{S}}}\sum_{m_{L'},m_{\tilde{S}'}} C^{m_L,m_{\tilde{S}},M}_{L,\tilde{S},J} C^{m_{L'},m_{\tilde{S}'},M}_{L',\tilde{S}',J}\times \tag{4.33}$$

$$\times\, \langle S', m'_S|\tilde{S}', m_{\tilde{S}'}\rangle\langle p|L', m'_L\rangle\langle L, m_L|k\rangle\langle \tilde{S}, m_{\tilde{S}}|S, m_S\rangle M^{JM}_{L'\tilde{S}',L\tilde{S}}$$

Setting $\hat{\mathbf{k}} = \hat{\mathbf{z}}$ we obtain Eq. (4.34), where θ is the angle between $\vec{\mathbf{k}}$ and $\vec{\mathbf{p}}$

$$\langle p, S', m'_S|\mathbf{M}|k, S, m_S\rangle = \sqrt{4\pi}\sum_{J}\sum_{L,L'}\sum_{m'_L}\sqrt{2L+1}C^{0,m_S,M}_{L,S,J} C^{m'_L,m'_S,M}_{L',S',J}\times \tag{4.34}$$

$$\times\, Y^{m'_L}_{L'}(\theta,\phi) M^{J}_{L'S',LS}$$

We now define $M_{m'_1,m'_2;m_1,m_2}$ as the T matrix where the nucleon has initial (final) spin m_2, (m'_2), and the deuteron has initial (final) spin m_1, (m'_1).

$$M_{m'_1,m'_2;m_1,m_2} = \sqrt{4\pi}\sum_{J}\sum_{L,L'}\sum_{S,S'}\sum_{m_s,m'_S}\sum_{m'_L}\sqrt{2L+1}C^{m_1,m_2,m_S}_{1,1/2,S} C^{m'_1,m'_2,m'_S}_{1,1/2,S'}\times \tag{4.35}$$

$$\times\, C^{0,m_S,M}_{L,S,J} C^{m'_L,m'_S,M}_{L',S',J} Y^{m'_L}_{L'}(\theta,\phi) M^{J}_{L'S',LS}$$

Observables are most easily defined in terms of $M_{m'_1,m'_2;m_1,m_2}$. Having $M_{m'_1,m'_2;m_1,m_2}$ in terms of the calculated functions $M^J_{L'S',LS}$, we can calculate observables by truncating

the sum over J, L, and L' at some reasonable level. The observable A_N is defined in terms of these matrix elements via

$$A_N = \frac{\sum\limits_{m_1',m_2'} \sum\limits_{m_1,m_2} (-1)^{1/2-m_2} \int d\Omega |M_{m_1',m_2';,m_2,m_2}|^2}{\sum\limits_{m_1',m_2'} \sum\limits_{m_1,m_2} \int d\Omega |M_{m_1',m_2';,m_2,m_2}|^2} \tag{4.36}$$

Combining our expressions and explicitly summing over values of angular momentum from 0 to 1, and spin and J from $1/2$ to $3/2$ we find.

$$\begin{aligned} A_N = \frac{2}{3}\mathrm{Re}\Big[&\left(M^{1/2}_{0^{1/2},0^{1/2}} + M^{1/2}_{1^{1/2},1^{1/2}}\right)\left(M^{1/2}_{1^{1/2},0^{1/2}}\right)^* \\ &+ 2\sqrt{2}\left(M^{1/2}_{0^{1/2},0^{1/2}} + M^{1/2}_{1^{3/2},1^{3/2}}\right)\left(M^{1/2}_{1^{3/2},0^{1/2}}\right)^* \\ &- 4\left(M^{3/2}_{0^{3/2},0^{3/2}} + M^{1/2}_{1^{1/2},1^{1/2}}\right)\left(M^{3/2}_{1^{1/2},0^{3/2}}\right)^* \\ &-2\sqrt{5}\left(M^{3/2}_{0^{3/2},0^{3/2}} + M^{3/2}_{1^{3/2},1^{3/2}}\right)\left(M^{3/2}_{1^{3/2},0^{3/2}}\right)^*\Big] / \\ &\Big[|M^{1/2}_{0^{1/2},0^{1/2}}|^2 + 2|M^{3/2}_{0^{3/2},0^{3/2}}|^2 + 3|M^{1/2}_{1^{1/2},1^{1/2}}|^2 + 3|M^{3/2}_{1^{3/2},1^{3/2}}|^2\Big] \end{aligned} \tag{4.37}$$

At this point it would be useful to know if the amplitudes are at least reasonable. The amplitudes should satisfy unitarity to a large degree (Violation is due to numerics and excluding higher order PV terms). A simple test for unitarity is given by the optical theorem, which requires that

$$A_N = \frac{\sum_m \mathrm{Im}\left(M_{m,1/2;m,1/2}|_{\theta=0} - M_{m,-1/2;m,-1/2}|_{\theta=0}\right)}{\sum_m \mathrm{Im}\left(M_{m,1/2;m,1/2}|_{\theta=0} + M_{m,-1/2;m,-1/2}|_{\theta=0}\right)} \tag{4.38}$$

Again explicitly summing over angular momentum from 0 to 1, spin, and total angular momentum from $J = 1/2$ to $J = 3/2$ we find

$$A_N = \frac{2}{3}\mathrm{Im}\left[M^{1/2}_{1^1/_2,0^1/_2} + 2\sqrt{2}M^{1/2}_{1^3/_2,0^1/_2} - 4M^{3/2}_{1^1/_2,0^3/_2} - 2\sqrt{5}M^{3/2}_{1^3/_2,0^1/_2}\right] / \qquad (4.39)$$
$$\mathrm{Im}\left[M^{1/2}_{0^1/_2,0^1/_2} + 2M^{3/2}_{0^3/_2,0^3/_2} + 3M^{1/2}_{1^1/_2,1^1/_2} + 3M^{1/2}_{1^3/_2,1^3/_2}\right]$$

Another possible PV observable is the spin rotation. At low energies a neutron traveling through matter can be described by an index of refraction [65]. If a neutron passes through a slab of matter of thickness d, the form of the asymptotic wavefunction is given by

$$e^{ik(z-d)}e^{ikdn_{m_2}}|m_2\rangle \qquad (4.40)$$

where m_2 represents the spin of the neutron in the direction of momentum $\vec{\mathbf{k}}$ which is chosen to be the z-axis. The index of refraction in the case of neutron deuteron scattering is given by

$$n_{m_2} - 1 = \frac{2\pi N}{k^2}\frac{1}{3}\sum_{m_1} M_{m1,m2;m1,m2}\big|_{\theta=0} \qquad (4.41)$$

where $N = .4 \times 10^{23}$ atoms cm^{-3} is the number density of liquid deuterium and k is the magnitude of the momentum of the neutron in the c.m. coordinates. Now suppose that the neutron is polarized transversely to the neutron momentum. Without loss of generality we assume that the neutron is polarized along the positive x-axis, then the initial wavefunction of the neutron is

$$e^{ikz}\frac{1}{\sqrt{2}}\left(|+{}^1/_2\rangle + |-{}^1/_2\rangle\right) \qquad (4.42)$$

After it passes through the slab of thickness d the neutron wavefunction becomes.

$$e^{ik(z-d)}e^{ikd(n_{+1/2}+n_{-1/2})/2}\frac{1}{\sqrt{2}}\left(e^{ikd(n_{+1/2}-n_{-1/2})/2}|1/2\rangle + e^{-ikd(n_{+1/2}-n_{-1/2})/2}|-1/2\rangle\right) \tag{4.43}$$

In the case of parity violation it is generally true that $n_{+1/2} \neq n_{-1/2}$. This leads to a rotation in the polarization of the neutron, where the angle of rotation ϕ is given by [94].

$$\frac{d\phi}{dz} = -\frac{2M_N N}{9k}\sum_m \mathrm{Re}\left[M_{m,1/2;m,1/2}|_{\theta=0} - M_{m,-1/2;m,-1/2}|_{\theta=0}\right] \tag{4.44}$$

Using Eq. (4.35) for $M_{m_1',m_2';m_1,m_2}$ and explicitly summing over angular momentum, spin, and J we find

$$\frac{d\phi}{dz} = -\frac{8M_N N}{27k}\mathrm{Re}\left[M^{1/2}_{1^1/_2,0^1/_2} + 2\sqrt{2}M^{1/2}_{1^3/_2,0^1/_2} - 4M^{3/2}_{1^1/_2,0^3/_2} - 2\sqrt{5}M^{3/2}_{1^3/_2,0^1/_2}\right] \tag{4.45}$$

The last PV observable that we will consider is a deuteron asymmetry, wherein an unpolarized beam of neutrons is scattered from a polarized deuteron target. At first the deuteron target is polarized in the positive z direction where the positive z direction is in the direction of the neutron's initial momentum. The neutron scatters from the deuteron target and we measure the cross section σ_1. Then the deuteron target is polarized in the opposite direction and we measure the cross section σ_{-1}. If there is parity violation one will find in general that $\sigma_1 \neq \sigma_{-1}$. leading to the PV observable

$$A_D = \frac{\sigma_1 - \sigma_{-1}}{\sigma_1 + \sigma_{-1}} \tag{4.46}$$

In terms of matrix elements one finds the following expression

$$A_D = \frac{\sum\limits_{m_{1'},m_2'} \sum\limits_{m_2} \int d\Omega \left(|M_{m_1',m_2';1,m_2}|^2 - |M_{m_1',m_2';-1,m_2}|^2 \right)}{\sum\limits_{m_{1'},m_2'} \sum\limits_{m_2} \int d\Omega \left(|M_{m_1',m_2';1,m_2}|^2 + |M_{m_1',m_2';-1,m_2}|^2 \right)} \tag{4.47}$$

Now using equation (4.35) and summing angular momentum from 0 to 1, and spin, and J from $1/2$ to $3/2$ we find

$$\begin{aligned} A_D = -\mathrm{Re} \Big[& 2 \left(M^{1/2}_{1^1/_2,1^1/_2} + M^{1/2}_{0^1/_2,0^1/_2} \right) \left(M^{1/2}_{1^1/_2,0^1/_2} \right)^* \\ & + \sqrt{2} \left(M^{1/2}_{1^3/_2,1^3/_2} + M^{1/2}_{0^1/_2,0^1/_2} \right) \left(M^{1/2}_{1^3/_2,0^1/_2} \right)^* \\ & - 2 \left(M^{3/2}_{1^1/_2,1^1/_2} + M^{3/2}_{0^3/_2,0^3/_2} \right) \left(M^{3/2}_{1^1/_2,0^3/_2} \right)^* \\ & + 2\sqrt{5} \left(M^{3/2}_{1^3/_2,1^3/_2} + M^{3/2}_{0^3/_2,0^3/_2} \right) \left(M^{3/2}_{1^3/_2,0^3/_2} \right)^* \Big] / \\ & \left[|M^{1/2}_{0^1/_2,0^1/_2}|^2 + 2|M_{0^3/_2,0^3/_2}|^2 + 3|M^{1/2}_{1^1/_2,1^1/_2}|^2 + 6|M^{1/2}_{1^3/_2,1^3/_2}|^2 \right] \end{aligned} \tag{4.48}$$

Our observable can also be calculated by means of the optical theorem.

$$A_D = \frac{\sum_{m_2} \mathrm{Im} \left(M_{1,m_2;1,m_2}|_{\theta=0} - M_{-1,m_2;-1,m_2}|_{\theta=0} \right)}{\sum_{m_2} \mathrm{Im} \left(M_{1,m_2;1,m_2}|_{\theta=0} + M_{-1,m_2;-1,m_2}|_{\theta=0} \right)} \tag{4.49}$$

Explicity summing over angular momentum from 0 to 1, spin, and J from $J = 1/2$ to $J = 3/2$ we find

$$\begin{aligned} A_D = & - \mathrm{Im} \left[2M^{1/2}_{1^1/_2,0^1/_2} + \sqrt{2} M^{1/2}_{1^3/_2,0^1/_2} - 2M^{3/2}_{1,1/_2,0^3/_2} + 2\sqrt{5} M^{3/2}_{1^3/_2,0^3/_2} \right] / \\ & \mathrm{Im} \left[M^{1/2}_{0^1/_2,0^1/_2} + 2M^{3/2}_{0^3/_2,0^3/_2} + 3M^{1/2}_{1^1/_2,1^1/_2} + 6M^{1/2}_{1^3/_2,1^3/_2} \right] \end{aligned} \tag{4.50}$$

4.4 Results

Plotting our results for beam and target asymmetry as a function of center of mass energy $E_{c.m}$ we find the plots given in Fig. 4.5. The thickness of the plot

denotes the cutoff variation. The momentum cutoff variation runs from 200 MeV to 1500 MeV. It appears that the results begin to converge after 900 MeV as found by other authors [55]. Also it should be noted that the cutoff variation for the beam and target asymmetries at low energies is actually smaller than as shown in the plots, and is displayed with the given thickness in order that the plot be visible. The plots for the beam and target asymmetries extend all the way to 2.22 MeV, which is the deuteron breakup energy. However, the observables cannot be taken seriously at these high energies as higher partial waves and higher order contributions will become important. (It should also be noted that a significant difference was found at about .32 MeV if P waves were not included in the parity-conserving amplitudes.) The spin rotation observable varied from 1.83×10^{-8} rad cm^{-1} to 1.84×10^{-8} rad cm^{-1} due to cutoff variation. (We use a liquid deuterium number density of $N = .4 \times 10^{23}$atoms cm^{-3} [100].) This value is roughly two times the previous estimates for the spin rotation [95, 96, 100]. Also the beam asymmetry ranges from 2.23×10^{-8} to 2.24×10^{-8} due to cutoff dependence, at $E_{lab} = 15$ keV, and again this is roughly a factor of two greater than previous calculations [100]. Finally the target asymmetry varies due to cutoff dependence at $E_{lab} = 15$ keV with values ranging from roughly 3.97×10^{-8} to 3.99×10^{-8}.

Finally in order to compare with possible experiments Tables 4.6 and 4.7 show all three observables in terms of their contributions from each of the g_i. The spin rotation is given at zero energy and the beam and target asymmetry are given at a lab energy of 15 keV. In order to obtain a prediction for the observable each row is multiplied by the appropriate value of g_i and then these products are added together to yield the observable. Below are two tables with different values for the cutoff. The first table shows the cutoff at 200 MeV and the second at setting the cutoff to 1500 MeV.

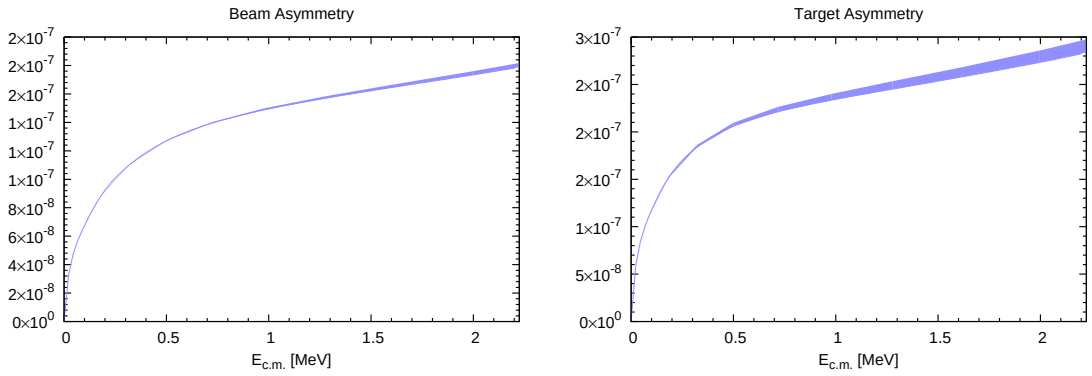

(a) (b)

Figure 4.5: Beam and target asymmetries as function of c.m. energy, $E_{c.m.}$. Estimates for observables are found by using DDH "best" values. The right pane of the plot refers to the deuteron breakup energy

Table 4.6: Values for observables at a cutoff of $\Lambda = 200$ MeV. In order to obtain the corresponding observable each number in a given column is multiplied by the appropriate g_i and then all are added togehter.

g_i	Rotation, $E_{lab} = 0$ keV	A_N, $E_{lab} = 15$ keV	A_D, $E_{lab} = 15$ keV
1	-18.7 rad cm^{-1} MeV	-14.4 MeV	8.92 MeV
2	-36.2 rad cm^{-1} MeV	-39.6 MeV	-59.7 MeV
3	-10.2 rad cm^{-1} MeV	-1.83 MeV	1.65 MeV
4	6.81 rad cm^{-1} MeV	1.22 MeV	-1.10 MeV

We can now compare our results for the spin rotation to previous calculations using a hyperspherical harmonics method or by solving a differential Faddeev equation in configuration space [95, 96, 100]. The authors of both of these papers calculated the spin rotation in terms of the numbers I_n as given by Eq. (4.52)

$$\frac{1}{N}\frac{d\phi}{dz} = \sum_{n=1}^{5} c_n^{Gir} I_n^{Gir} \tag{4.51}$$

where c_n^{Gir} are defined in Table 4.3. Using Tables 4.5, 4.6, and 4.7 it is straightforward to compute the values I_n^{Gir} as predicted by pure EFT$_{\not\pi}$ at LO. The results from the two previous calculations of the nd spin rotation for the values I_n^{Gir} are compared in

Table 4.7: Values for observables at a cutoff of $\Lambda = 1500$ MeV. In order to obtain the corresponding observable each number in a given column is multiplied by the appropriate g_i and then all are added togehter.

g_i	Rotation, $E_{lab} = 0$ keV	A_N, $E_{lab} = 15$ keV	A_D, $E_{lab} = 15$ keV
1	-19.2 rad cm^{-1} MeV	-14.5 MeV	9.15 MeV
2	-38.0 rad cm^{-1} MeV	-39.9 MeV	-59.8 MeV
3	-16.7 rad cm^{-1} MeV	-2.71 MeV	2.47 MeV
4	11.1 rad cm^{-1} MeV	1.81 MeV	-1.65 MeV

Table 4.8 with those given by pure EFT$_{\not\pi}$ at LO as well as with EFT$_{\not\pi}$ at NLO which has been calculated in [57].

$$\frac{1}{N}\frac{d\phi}{dz} = \sum_{n=1}^{5} c_n^{Gir} I_n^{Gir} \tag{4.52}$$

Table 4.8: For EFT$_{\not\pi}$-I, $\mu = 138$ MeV. Also I_n^{Gir} is given in units of fm

$I_n^{\rm Gir}$	EFT$_{\not\pi}$-I/AV18		EFT$_{\not\pi}$-I/AV18+UIX		EFT$_{\not\pi}$	
$n =$	Song [100]	Schiavilla [95]	Song	Schiavilla	LO	NLO [57]
1	61.6	65.6	60.0	63.2	129.3 - 135.7	98.5 - 120.3
2	60.6	62.3	58.8	57.8	35.0 - 57.1	33.4 - 51.9
4	-76.1	-77.9	-75.7	-75.2	-59.6 - -77.2	-48.2 - -67.2
5	-9.46	-9.89	-6.62	-6.12	7.16 - -8.66	-1.85 - -10.6

The manner by which all these results are matched is outlined in the appendix. The range of numbers given for EFT$_{\not\pi}$ at LO and NLO is simply due to cutoff variation in the numerical integration. Looking at the table we see that with the exception of the $n = 1$ term the EFT$_{\not\pi}$ approach gives very similar results within the cutoff variation. However, at low cutoff values for the LO $n = 5$ term we see that it has a different sign than the other results. This is likely due to the fact that in EFT$_{\not\pi}$ this term is calculated by subtracting two terms one of which has a larger cutoff variation. We also note the $n = 2$ term for large cutoff values at LO clearly agrees with the

other schemes where three body forces are included. This should come as no surprise as the EFT$_{\not\pi}$ approach at LO necessarily includes a three-body force term. At larger values of cutoff it is clear the EFT$_{\not\pi}$ approach seems to converge towards the other approaches. At LO the largest cutoff variation comes from the g_3 and g_4 terms, and the terms $n = 2$ through $n = 5$ all contain one of these terms, thus they have a much larger cutoff variation than the $n = 1$ term. The $n = 1$ term in the EFT$_{\not\pi}$ approaches is roughly a factor of two larger than in the other approaches. This result is consistent with our spin rotation and beam asymmetry predictions which were roughly a factor of two larger than the predictions given by the other authors in Table 4.8. The NLO EFT$_{\not\pi}$ results do not seem to differ greatly from the LO predictions. However, we note that the NLO results seem to under predict the results of Song et al. and Schiavilla et al. Also the cutoff variation for the $n = 1$ term seems to be much larger than that at LO. This is concerning as one naivley expects the cutoff variation to get smaller as one goes to higher orders in EFT$_{\not\pi}$.

Finally we should note that the calculation for the beam and target asymmetries were done using both the standard cross section methods and the optical theorem. Plotting the results from both, we found they were indistinguishable. This agreement confirms that our amplitudes are unitary and acts as a check on the validity of our results. For the values quoted in the table, it was found that for the beam and target asymmetries, as well as the values from either the cross sections or optical theorem agreed to less than one percent.

Looking at our results we see from Tables 4.6 and 4.7 that the dominant contribution to all the observables comes from the g_2 term. The dominant contribution to this coefficient comes in particular from the quartet S to quartet P channel. Thus the dominant contribution to all the observables comes from the quartet S to quartet P contribution to the g_2 term. Also looking at the estimates of the g_i we see that g_2 is the only term that contains the pion exchange term from the DDH potential.

Thus the dominant contribution to all of the observables is given by pion exchange in agreement with previous findings [95, 96, 100]. Finally we note that the target asymmetry is larger than the other two observables calculated. Thus this could be a useful observable to find hadronic parity violation. However, experimentally a polarized target experiment would be more difficult than a polarized beam experiment.

4.5 Conclusions and Future Directions

Above we calculated the low energy PV nd transition amplitudes using EFT$_{\not\pi}$. Matching the auxiliary field formalism onto the DDH potential, we obtained estimates for the coefficients of the auxiliary field formalism. Using these amplitudes and estimates for g_i, we were able to make predictions for the spin rotation, beam asymmetry, and target asymmetry in low energy nd interactions. The values obtained for the neutron spin rotation and beam asymmetry were roughly a factor of two larger than those found by other authors, making them possibly more accessible to experiment [95, 96, 100]. Unfortunately due to the smallness of these values they will still require very precise experiments to measure. However, the five LEC's used in parity-violation at LO are not very well determined. Thus upon further experiments it may be found that the values of the LEC's are such that the observables for nd interactions are larger than predicted.

The largest contribution to parity violation was shown to come from the coefficient g_2, which contains the pion contribution, and such experiments should then allow one to determine its value. It is noted that to first order in parity violation the $\Delta I = 2$ (g_5) term does not contribute. Thus nd scattering is sensitive to four out of the five PV coefficients.

In principle we should be able to calculate to NLO in EFT$_{\not\pi}$ without the need for PV three-body forces [56]. Griesshammer, Schindler, and Springer calculated the NLO PV amplitudes using the partially resummed approach which introduces

higher order contributions at NLO [57]. However, to calculate the NLO contributions without higher order contributions, one must calculate the full off shell LO amplitude. Since a calculation of the full off shell LO amplitude is numerically expensive, it will be left to a future publication.

Other possible future directions are to calculate parity violating effects in the pd channel. In the pd channel one has the extra complication of the coulomb force. Parity conserving pd scattering has been carried out by Rupak and Kong and more recently by Konig and Hammer [76, 91]. In each of these papers the coulomb effect is treated perturbatively. Also the infrared singularities from the photon are reuglated by giving the photon a small mass. The results are extrapolated by making the photon mass smaller and smaller until the results begin to converge. In the paper of Konig and Hammer they did both the Quartet and Doublet channel. They also used a special integration mesh that put many points near the singuarltiy introduced by the photon propagator therefore leading to better convergence.

The coulomb force has also been treated nonpertubatively in the case of the bound state of ^{3}He by Ando and Birse [5]. By using the same three-body force at LO for the nd and pd channel they showed that the binding energy of both the triton and ^{3}He can be predicted to the 1% level, thus showing that an isospin violating three-body force term is not required at LO. Since they were performing a bound state calculation the form for their off shell couloumb T-matrix was only valid at energies below zero. Also the infrared singularities from the photon were regulated by the finite extent of the bound state wavefunctions. To extend this nonpertubative approach to the scattering regime would require one to use the off shell coulomb T matrix for energies greater than zero. The singularities introduced by the off shell coulomb T matrix would introduce new complications into the numerical solution. In particular at zero energy the off shell coulomb T matrix posseses an essential singularity which is very problematic [75]. It may be necessary at higher orders to calculate the amplitudes at

zero energy in order to fit potential new three-body forces to pd scattering data at zero energy.

Ultimately one would like to predict the LEC's of our EFT from QCD. This would most likely be done by the use of lattice QCD. A possible route to obtain a prediction for the long range pion coupling found in pionful EFT has been outlined by Beane and Savage [10]. The prediction of the five LEC's from lattice QCD is far from feasable at this point in time. Predicting the LEC's constants from lattice QCD would connect high energy pertubative QCD with low energy non-perturbative EFT techniques for QCD thus leading to further credence that QCD is the correct theory of nuclear forces.

APPENDIX A

PARITY VIOLATING POTENTIAL

A.1 Matching Auxiliary to Girlanda

The matching of the Girlanda LEC's onto the auxiliary field coefficients is outlined here. Performing the non-relativistic reduction on the constraints derived by Girlanda Eqs. (4.24) one finds the results Eqs. (A.1).

$$N_3^{(2)} - N_3^{(1)} = -\left(N_1^{(2)} - N_1^{(1)}\right) - 2N_1^{(3)} \tag{A.1a}$$

$$N_3^{(3)} = -2(N_1^{(2)} - N_1^{(1)}) - N_1^{(3)} \tag{A.1b}$$

$$-N_4^{(1)} - N_4^{(2)} = \quad 2N_6^{(1)} \tag{A.1c}$$

$$N_5^{(2)} - N_5^{(1)} = -N_5^{(3)} \tag{A.1d}$$

$$N_2^{(2)} - N_2^{(1)} = -N_2^{(3)} \tag{A.1e}$$

where the operators $N_i^{(j)}$ are defined as

$$N_i^{(1)} = F_i \otimes N^\dagger N N^\dagger i \overleftrightarrow{\nabla} . \vec{\boldsymbol{\sigma}} N \tag{A.2a}$$

$$N_i^{(2)} = F_i \otimes N^\dagger \vec{\boldsymbol{\sigma}} N \cdot N^\dagger i \overleftrightarrow{\nabla} N \tag{A.2b}$$

$$N_i^{(3)} = F_i \otimes \epsilon_{ijk} N^\dagger \sigma_i N \nabla_j (N^\dagger \sigma_k N) \tag{A.2c}$$

$$N_6^{(1)} = F_6 \otimes i \overrightarrow{\nabla} (N^\dagger N) N^\dagger \vec{\boldsymbol{\sigma}} N \tag{A.2d}$$

and the operators $F_n^{ij,kl}$ represent the isospin operators

$$F_1^{ij,kl} = \delta_{ij}\delta_{kl} \tag{A.3a}$$

$$F_2^{ij,kl} = \delta_{ij}\tau_{kl}^3 + \delta_{kl}\tau_{ij}^3 \tag{A.3b}$$

$$F_3^{ij,kl} = \tau_{ij}^a\tau_{kl}^a \tag{A.3c}$$

$$F_4^{ij,kl} = \delta_{ij}\tau_{kl}^3 - \delta_{kl}\tau_{ij}^3 \tag{A.3d}$$

$$F_5^{ij,kl} = \mathcal{I}^{ab}\tau_{ij}^a\tau_{kl}^b \tag{A.3e}$$

$$F_6^{ij,kl} = i\epsilon^{ab3}\tau_{ij}^a\tau_{kl}^b \tag{A.3f}$$

Combining the constraints derived by Girlanda Eqs. (A.1) with appropriate SU(2) Fierz identities one can match the partial wave EFT$_{\not\pi}$ given by the Lagrangian Eq. (A.4) onto the Girlanda Lagrangian given by Eq. (4.25). They are also matched using a different approach in [88]

$$\begin{aligned}\mathcal{L}_{\rm PV}^{\rm PW} = -\Big[& C^{(^3S_1-{}^1P_1)}(N^T\sigma_2\vec{\boldsymbol{\sigma}}\tau_2 N)^\dagger\cdot(N^T\sigma_2 i\overset{\leftrightarrow}{\nabla}\tau_2 N) \\ & + C_{(\Delta I=0)}^{(^1S_0-{}^3P_0)}(N^T\sigma_2\tau_2\vec{\boldsymbol{\tau}}N)^\dagger(N^T\sigma_2\vec{\boldsymbol{\sigma}}\cdot i\overset{\leftrightarrow}{\nabla}\tau_2\vec{\boldsymbol{\tau}}N) \\ & + C_{(\Delta I=1)}^{(^1S_0-{}^3P_0)}\epsilon^{3ab}(N^T\sigma_2\tau_2\tau^a N)^\dagger(N^T\sigma_2\vec{\boldsymbol{\sigma}}\cdot\overset{\leftrightarrow}{\nabla}\tau_2\tau^b N) \\ & + C_{(\Delta I=2)}^{(^1S_0-{}^3P_0)}\mathcal{I}^{ab}(N^T\sigma_2\tau_2\tau^a N)^\dagger(N^T\sigma_2\vec{\boldsymbol{\sigma}}\cdot i\overset{\leftrightarrow}{\nabla}\tau_2\tau^b N) \\ & + C^{(^3S_1-{}^3P_1)}\epsilon^{ijk}(N^T\sigma_2\sigma^i\tau_2 N)^\dagger(N^T\sigma_2\sigma^k\tau_2\tau_3\overset{\leftrightarrow}{\nabla}{}^j N)\Big] + h.c.\end{aligned} \tag{A.4}$$

The necessary SU(2) Fierz transformations are given below (Note there is an extra minus sign due to the anticommutivity of the nucleon fields.)

$$(\sigma_i\sigma_2)[\sigma_2] = \frac{1}{2}\Big\{(\sigma_i][) - (][\sigma_i) + i\epsilon_{ijk}(\sigma_j][\sigma_k)\Big\} \tag{A.5a}$$

$$\epsilon_{ijk}(\sigma_j\sigma_2)[\sigma_2\sigma_k] = \Big\{i(\sigma_i][) + i(][\sigma_i)\Big\} \tag{A.5b}$$

$$(\sigma_2)[\sigma_2\sigma_i] = \frac{1}{2}\Big\{(\sigma_i][) - (][\sigma_i) - i\epsilon_{ijk}(\sigma_j][\sigma_k)\Big\} \tag{A.5c}$$

$$(\tau_2)[\tau_2] = \frac{1}{2}\Big\{(][) - (\tau_a][\tau^a)\Big\} \tag{A.5d}$$

$$(\tau_2)[\tau_2\tau_3] = \frac{1}{2}\Big\{(\tau_3][) - (][\tau_3) - i\epsilon_{ab3}(\tau_a][\tau_b)\Big\} \tag{A.5e}$$

$$(\tau_3\tau_2)[\tau_2] = \frac{1}{2}\Big\{(\tau_3][) - (][\tau_3) + i\epsilon_{ab3}(\tau_a][\tau_b)\Big\} \tag{A.5f}$$

$$(\tau_a\tau_2)[\tau_2\tau^a] = \frac{1}{2}\Big\{3(][) + (\tau_a][\tau^a)\Big\} \tag{A.5g}$$

$$\epsilon_{3ab}(\tau_a\tau_2)[\tau_2\tau_b] = \Big\{i(\tau_3][) + i(][\tau_3)\Big\} \tag{A.5h}$$

$$\mathcal{I}_{ab}(\tau_a\tau_2)[\tau_2\tau_b] = -\mathcal{I}_{ab}(\tau_a][\tau_b) \tag{A.5i}$$

where "(" ,")","[","]" stands for $N_1^\dagger$, N_2, $N_3^\dagger$, and N_4 respectively. Using these Fierz transformations Eqs. (A.5) and the identities derived by Girlanda Eqs. (A.1) we find the following relationship between the partial wave basis and the Girlanda Lagrangian.

$$\begin{aligned}
C^{(^3S_1-{}^1P_1)} &= \frac{1}{4}(\mathcal{G}_1 - \tilde{\mathcal{G}}_1) \\
C^{(^1S_0-{}^3P_0)}_{(\Delta I=0)} &= \frac{1}{4}(\mathcal{G}_1 + \tilde{\mathcal{G}}_1) \\
C^{(^1S_0-{}^3P_0)}_{(\Delta I=1)} &= \frac{1}{2}\mathcal{G}_2 \\
C^{(^1S_0-{}^3P_0)}_{(\Delta I=2)} &= -\frac{1}{2}\tilde{\mathcal{G}}_5 \\
C^{(^3S_1-{}^3P_1)} &= \frac{1}{4}\mathcal{G}_6
\end{aligned} \tag{A.6}$$

Now finally to match the partial wave basis onto the auxiliary field formalism Eq. (4.1) we simply use Gaussian integration on the auxiliary fields and a field redefinition in which higher order terms are thrown out [97]. Performing this we find the following relationship between the PV LEC's in each basis. Note below that X is either $^1S_0$ or

${}^3S_1$ and Y is ${}^1P_1$, ${}^3P_1$, or ${}^3P_0$. The cutoff dependence of the terms comes from using the usual KSW power counting scheme with PDS subtraction. (Also note there is an extra minus sign in Eq. (A.7) compared to [97] because of a difference in convention for the PC auxiliary field Lagrangian.)

$$\frac{g^{(X-Y)}}{y_X} = -\sqrt{8}\frac{\Delta^{(X)}}{y_X^2}C^{(X-Y)} \tag{A.7}$$

$$\frac{\Delta^{({}^3S_1)}}{y_t^2} = \frac{M_N}{4\pi}\left(\frac{1}{a_t} - \mu\right) \tag{A.8}$$

$$\frac{\Delta^{({}^1S_0)}}{y_s^2} = \frac{M_N}{4\pi}\left(\frac{1}{a_s} - \mu\right) \tag{A.9}$$

Combing Eqs. (A.6) and (A.7) we match the coefficients of the Girlanda Lagrangian onto those of the auxiliary field Lagrangian. Note here we have used the conventions for the auxiliary field coefficients as defined in Eq. (4.14) to give.

$$\begin{aligned}
g_1 &= -\frac{M_N(\frac{1}{a_t} - \mu)}{4\sqrt{2}\pi}(\mathcal{G}_1 - \tilde{G}_1) \\
g_2 &= -\frac{M_N(\frac{1}{a_t} - \mu)}{4\sqrt{2}\pi}\mathcal{G}_6 \\
g_3 &= -\frac{M_N(\frac{1}{a_s} - \mu)}{4\sqrt{2}\pi}(\mathcal{G}_1 + \tilde{G}_1) \\
g_4 &= -\frac{M_N(\frac{1}{a_s} - \mu)}{2\sqrt{2}\pi}\mathcal{G}_2 \\
g_5 &= \frac{M_N(\frac{1}{a_s} - \mu)}{2\sqrt{2}\pi}\mathcal{G}_5
\end{aligned} \tag{A.10}$$

A.2 Girlanda Potential

In this appendix we will show how to calculate the Girlanda potential from the Girlanda Lagrangian and show discrepancies between the form calculated here and the form that appears in [96]. The Girlanda Lagrangian is given in Eq. (4.25)

and from this we find the tree level amplitude in the c.m. system is given by Eq. (A.11), where (k, c, p) is one nucleons' initial (spin,isospin,momentum), $(l, d, -p)$ is the other nucleons' initial (spin,isospin,momentum), likewise the final (spin,isospin, momentum) of each nucleon is given by (i, a, p') and $(j, b, -p')$ [88].

$$
\begin{aligned}
&2\mathcal{G}_1((\sigma_A)_{ik}\delta_{jl} - \delta_{ik}(\sigma_A)_{jl})(p+p')_A\delta_{ac}\delta_{bd} \\
&- 2\mathcal{G}_1((\sigma_A)_{jk}\delta_{il} - \delta_{jk}(\sigma_A)_{il})(p-p')_A\delta_{bc}\delta_{ad} \\
&+ 2\tilde{\mathcal{G}}_1\epsilon_{ABC}(\sigma_A)_{ik}(\sigma_B)_{jl}(ip'-ip)_C\delta_{ac}\delta_{bd} \\
&- 2\tilde{\mathcal{G}}_1\epsilon_{ABC}(\sigma_A)_{jk}(\sigma_B)_{il}(-ip'-ip)_C\delta_{bc}\delta_{ad} \\
&+ 2\mathcal{G}_2\epsilon_{ABC}(\sigma_A)_{ik}(\sigma_B)_{jl}(ip'-ip)_C((\tau_3)_{ac}\delta_{bd} + \delta_{ac}(\tau_3)_{bd}) \\
&- 2\mathcal{G}_2\epsilon_{ABC}(\sigma_A)_{jk}(\sigma_B)_{il}(-ip'-ip)_C((\tau_3)_{bc}\delta_{ad} + \delta_{bc}(\tau_3)_{ad}) \\
&+ 2\tilde{\mathcal{G}}_5\epsilon_{ABC}(\sigma_A)_{ik}(\sigma_B)_{jl}(ip'-ip)_C\mathcal{I}_{DE}(\tau_D)_{ac}(\tau_E)_{bd} \\
&- 2\tilde{\mathcal{G}}_5\epsilon_{ABC}(\sigma_A)_{jk}(\sigma_B)_{il}(-ip'-ip)_C\mathcal{I}_{DE}(\tau_D)_{bc}(\tau_E)_{ad} \\
&+ 2\mathcal{G}_6\delta_{ik}(\sigma_A)_{jl}(-ip'+ip)\epsilon_{BC3}(\tau_B)_{ac}(\tau_C)_{bd} \\
&- 2\mathcal{G}_6\delta_{jk}(\sigma_A)_{il}(ip'+ip)\epsilon_{BC3}(\tau_B)_{bc}(\tau_C)_{ad}
\end{aligned}
\tag{A.11}
$$

We note that the Fourier transform of the following operators gives

$$
\mathscr{F}\left([-i\vec{\boldsymbol{\nabla}}, \delta^3(r)]\right) = -i\int d^3x e^{-ip'.r}(\vec{\boldsymbol{\nabla}}\delta^3(r))e^{ip.r} = (p'-p) \tag{A.12}
$$

$$
\mathscr{F}\left(\{-i\vec{\boldsymbol{\nabla}}, \delta^3(r)\}\right) = -i\int d^3x e^{-ip'.r}[(\vec{\boldsymbol{\nabla}}\delta^3(r)) + \delta^3(r)]\vec{\boldsymbol{\nabla}}e^{ip.r} = (p'+p) \tag{A.13}
$$

Taking the Fourier transform of the above amplitude Eq. (A.11) and using Eqs. (A.12) and (A.13) one finds the form for the Girlanda potential in Eq. (A.14)

$$
\begin{aligned}
V_{PV}^{\rm Gir}(r) =& 2\mathcal{G}_1(\vec{\boldsymbol{\sigma}}_1 - \vec{\boldsymbol{\sigma}}_2)\cdot\{-i\vec{\boldsymbol{\nabla}}, \delta^3(r)\} \\
&+ 2\tilde{\mathcal{G}}_1(\vec{\boldsymbol{\sigma}}_1 \times \vec{\boldsymbol{\sigma}}_2)\cdot i[-i\vec{\boldsymbol{\nabla}}, \delta^3(r)] \\
&+ 2\mathcal{G}_2(\vec{\boldsymbol{\sigma}}_1 \times \vec{\boldsymbol{\sigma}}_2)(\tau_1 + \tau_2)_z \cdot i[-i\vec{\boldsymbol{\nabla}}, \delta^3(r)] \\
&+ 2\tilde{\mathcal{G}}_5(\vec{\boldsymbol{\sigma}}_1 \times \vec{\boldsymbol{\sigma}}_2)\mathcal{I}_{ab}\tau_1^a\tau_2^b \cdot i[-i\vec{\boldsymbol{\nabla}}, \delta^3(r)] \\
&- 2\mathcal{G}_6\vec{\boldsymbol{\sigma}}_2(\tau_1 \times \tau_2)_z \cdot i[-i\vec{\boldsymbol{\nabla}}, \delta^3(r)]
\end{aligned}
\tag{A.14}
$$

We now use the fact that at low energies (One could also use the constraints derived by Girlanda to obtain the simplification below.)

$$
\langle P|[-i\vec{\boldsymbol{\nabla}}, \delta^3(r)]|S\rangle = \langle P|\{-i\vec{\boldsymbol{\nabla}}, \delta^3(r)\}|S\rangle \tag{A.15}
$$

and using the relation (Note $P_0^\sigma = \frac{1}{4}(1 - \vec{\boldsymbol{\sigma}}_1\cdot\vec{\boldsymbol{\sigma}}_2)$ and $P_1^\sigma = \frac{1}{4}(3 + \vec{\boldsymbol{\sigma}}_1\cdot\vec{\boldsymbol{\sigma}}_2)$)

$$
(\vec{\boldsymbol{\sigma}}_1 - \vec{\boldsymbol{\sigma}}_2) = i(\vec{\boldsymbol{\sigma}}_1 \times \vec{\boldsymbol{\sigma}}_2)(P_0^\sigma - P_1^\sigma) \tag{A.16}
$$

We rewrite Eq. (A.14) to find

$$
\begin{aligned}
V_{PV}^{\rm Gir}(r) =& 2\left\{\left[\mathcal{G}_1 + \mathcal{G}_2(\tau_1+\tau_2)_z + \tilde{\mathcal{G}}_5\mathcal{I}_{ab}\tau_1^a\tau_2^b\right](\vec{\boldsymbol{\sigma}}_1 - \vec{\boldsymbol{\sigma}}_2)\cdot\{-i\vec{\boldsymbol{\nabla}}, \delta^3(r)\}\right. \\
&+ i\mathcal{G}_1(\vec{\boldsymbol{\sigma}}_1 \times \vec{\boldsymbol{\sigma}}_2)\cdot i[-i\vec{\boldsymbol{\nabla}}, \delta^3(r)] \\
&\left.-\mathcal{G}_6\left(\frac{\vec{\boldsymbol{\sigma}}_1 + \vec{\boldsymbol{\sigma}}_2}{2}\right)(\tau_1\times\tau_2)_z \cdot i[-i\vec{\boldsymbol{\nabla}}, \delta^3(r)]\right\}
\end{aligned}
\tag{A.17}
$$

The Girlanda potential quoted by Girlanda et al. is (Note Girlanda uses a Yukawa regulator function instead of a delta function. However, in the limit where $\mu \to \infty$ the μ dependence goes away and one is left with a delta function)

$$V_{PV}^{\rm Gir}(r) =2\left\{\left[\mathcal{G}_1+\mathcal{G}_2\left(\frac{\tau_1+\tau_2}{2}\right)_z+\tilde{\mathcal{G}}_5\mathcal{I}_{ab}\tau_1^a\tau_2^b\right](\vec{\boldsymbol{\sigma}}_1-\vec{\boldsymbol{\sigma}}_2)\cdot\{-i\vec{\boldsymbol{\nabla}},\delta^3(r)\}\right. \quad \text{(A.18)}$$
$$+i\mathcal{G}_1(\vec{\boldsymbol{\sigma}}_1\times\vec{\boldsymbol{\sigma}}_2)\cdot i[-i\vec{\boldsymbol{\nabla}},\delta^3(r)]$$
$$\left.+\mathcal{G}_6(\vec{\boldsymbol{\sigma}}_1+\vec{\boldsymbol{\sigma}}_2)(\tau_1\times\tau_2)_z\cdot i[-i\vec{\boldsymbol{\nabla}},\delta^3(r)]\right\}$$

We see that the $\mathcal{G}_2$ term differs by a factor of $\frac{1}{2}$ and also the $\mathcal{G}_6$ term differs by a sign and a factor of 2

A.3 Spin Rotation Matching

In this section we will show how the results for the spin rotation of a neutron through a deuterium target from this work can be related to the work of Schiavilla et al, Song et al, and Griesshammer et al. [57, 95, 96, 100]. We will first relate our predictions to those of Griesshammer et al. as they are both pure EFT$_{\not\pi}$ calculations and are the easiest to relate. The prediction of Griesshammer et al. for the spin rotation is given by

$$\left[\frac{1}{N}\frac{d\phi}{dz}\right]_{\rm Gri.}=[8.0\pm0.8]\text{rad MeV}^{-\frac{1}{2}}g^{^3S_1-{}^1P_1}+[17.0\pm1.7]\text{rad MeV}^{-\frac{1}{2}}g^{^3S_1-{}^1P_1} \quad \text{(A.19)}$$
$$+[2.3\pm0.5]\text{rad MeV}^{-\frac{1}{2}}\left(3g_{(\Delta I=0)}^{^1S_0-{}^3P_0}-2g_{(\Delta I=0)}^{^1S_0-{}^3P_0}\right)$$

Our prediction for the spin rotation is

$$\left[\frac{1}{N}\frac{d\phi}{dz}\right]_{\rm Van.}=-[18.7-19.2]\text{rad cm}^{-1}\text{MeV}\frac{1}{Ny_t}g^{^3S_1-{}^1P_1} \quad \text{(A.20)}$$
$$-[36.2-38.0]\text{rad cm}^{-1}\text{MeV}\frac{1}{Ny_t}g^{^3S_1-{}^1P_1}$$
$$-[3.4-5.56]\text{rad cm}^{-1}\text{MeV}\frac{1}{Ny_s}\left(3g_{(\Delta I=0)}^{^1S_0-{}^3P_0}-2g_{(\Delta I=0)}^{^1S_0-{}^3P_0}\right)$$

where $N = .4\times10^{23}$ atoms cm^{-3} is the number density of liquid deuterium. In order to match our numbers to that of Griesshammer we must note that their PC Lagrangian differs by a minus sign from ours. Also in their convention $y_s = y_t = \sqrt{4\pi/M_N}$. Taking these conventions into consideration and converting to similar units we find the two values are related by

$$[\text{Gri.}\#] = -[\text{Van.}\#]\frac{1}{N}\sqrt{\frac{M_N}{4\pi}}10^{26}(197.327)^{-2} \tag{A.21}$$

where [Gri.#], [Van.#] is anyone of the numbers quoted by Griesshammer et al. or us respectively in Eqs. (A.19) and (A.20) respectively. Computing our values for the spin rotation in the Griesshammer et al. formalism using Eq. (A.21) we find Table A.1 comparing our predictions to that of Griesshammer et al.

Table A.1: Comparison of Griesshammer et al. and Vanasse spin rotation numbers in Griesshammer et al. formalism (Note range of numbers is due to cutoff variation in numerical integration.)

coefficient	Girlanda et al.	Vanasse
$g^{^3S_1-{}^1P_1}$	7.2 - 8.8	10.4 - 10.7
$g^{^3S_1-{}^3P_1}$	15.3 - 18.7	20.1 - 21.1
$3g^{^1S_0-{}^3P_0}_{(\Delta I=0)}$	1.8 - 2.8	1.89 - 3.09
$-2g^{^1S_0-{}^3P_0}_{(\Delta I=1)}$	1.8 - 2.8	1.89 - 3.09

We see that the values are in rough agreement and therefore as noted before the NLO corrections do not contribute significantly to the the spin rotation.

The spin rotation observable as defined by Girlanda et al. and Song et al. is given by Eq. (4.52) [95, 96, 100]. Plugging in c_n^{Gir} as defined in Table 4.3 into Eq. (4.52) we find the spin rotation observable is given by Eq (A.22).

$$\left[\frac{1}{N}\frac{d\phi}{dz}\right]_{\substack{\text{Song}\\ \text{Schia.}}} = \sum_{n=1}^{5} c_n^{Gir} I_n^{Gir} \tag{A.22}$$
$$= -\mu^2\mathcal{G}_6 I_1 + 2\mu^2\mathcal{G}_2 I_2 + 2\mu^2\mathcal{G}_1 I_4 + 2\mu^2\tilde{\mathcal{G}}_1 I_5$$

Now in order to match the I_n numbers of Schiavilla et al. and Song et al. to the numbers of Griesshammer et al. we insert the relationship between the auxiliary and Girlanda coefficients Eqs. (A.10) into the Griesshammer et al. expression for the spin rotation Eq. (A.19). We also note from the the definition of g_i, Eq. (4.14) we must multiply by a factor of either y_t or y_s to get the PV coefficient appearing in the auxiliary field Lagrangian Eq. (4.1). Finally taking into account that for Griesshammer et al. $y_t = y_s = \sqrt{4\pi/M_N}$ we obtain Eq. (A.23) for the spin rotation from Griesshammer et al.

$$\begin{aligned}\frac{1}{N}\frac{d\phi}{dz} =& [8.0 \pm .8]\frac{(\frac{1}{a_t} - \mu)}{2\sqrt{2}}\sqrt{\frac{M_N}{\pi}}\left(\mathcal{G}_1 - \tilde{\mathcal{G}}_1\right) + [17.0 \pm 1.7]\frac{(\frac{1}{a_t} - \mu)}{2\sqrt{2}}\sqrt{\frac{M_N}{\pi}}\mathcal{G}_6 \\ &+ [6.9 \pm 1.5]\frac{(\frac{1}{a_s} - \mu)}{2\sqrt{2}}\sqrt{\frac{M_N}{\pi}}\left(\mathcal{G}_1 + \tilde{\mathcal{G}}_1\right) - [4.6 \pm 1.0]\frac{(\frac{1}{a_s} - \mu)}{\sqrt{2}}\sqrt{\frac{M_N}{\pi}}\mathcal{G}_2\end{aligned} \tag{A.23}$$

Matching Eqs. (A.22) and (A.23) and taking all necessary conversions we find the following values for I_n in units of femtometers. Note we choose $\mu = 138$ MeV for our cutoff,(roughly the pion mass) as chosen by Schiavilla et al and Song et al. [95,96,100].

$$\begin{aligned} I_1 &= -[17.0 \pm 1.7]\frac{(\frac{1}{a_t} - \mu)}{2\sqrt{2}\mu^2}\sqrt{\frac{M_N}{\pi}}(197.327) \\ I_2 &= -[4.6 \pm 1.0]\frac{(\frac{1}{a_s} - \mu)}{2\sqrt{2}\mu^2}\sqrt{\frac{M_N}{\pi}}(197.327) \\ I_4 &= \left\{[8.0 \pm .8]\left(\frac{1}{a_t} - \mu\right) + [6.9 \pm 1.5]\left(\frac{1}{a_s} - \mu\right)\right\}\frac{1}{4\sqrt{2}\mu^2}\sqrt{\frac{M_N}{\pi}}(197.327) \\ I_5 &= \left\{[6.9 \pm 1.5]\left(\frac{1}{a_s} - \mu\right) - [8.0 \pm .8]\left(\frac{1}{a_t} - \mu\right)\right\}\frac{1}{4\sqrt{2}\mu^2}\sqrt{\frac{M_N}{\pi}}(197.327)\end{aligned} \tag{A.24}$$

Plugging numbers into Eq. (A.24) and taking into account the cutoff variation we find the range of values for I_n given below

$$\begin{aligned} I_1 &= 98.5 \ - \ 120.3\text{fm} \\ I_2 &= 33.4 \ - \ 51.9\text{fm} \\ I_4 &= -48.2 \ - \ -67.2\text{fm} \\ I_5 &= -1.85 \ - \ -10.6\text{fm} \end{aligned} \tag{A.25}$$

Now having matched our calculations to Griesshammer et al. and having matched Griesshammer et al. to Song et al. and Schiavilla et al. we can straightforwardly match our calculations to Song et al. and Schiavilla et al. using Eqs. (A.21) and (A.24) giving.

$$\begin{aligned} I_1 &= -[36.2 - 38.0]\frac{(\frac{1}{a_t} - \mu)}{4\sqrt{2}\mu^2}\frac{M_N}{N\pi}10^{26}(197.327)^{-1} \\ I_2 &= -[6.81 - 11.1]\frac{(\frac{1}{a_s} - \mu)}{4\sqrt{2}\mu^2}\frac{M_N}{N\pi}10^{26}(197.327)^{-1} \\ I_4 &= \left\{[18.7 - 19.2]\left(\frac{1}{a_t} - \mu\right) + [10.2 - 16.7]\left(\frac{1}{a_s} - \mu\right)\right\}\frac{1}{8\sqrt{2}\mu^2}\frac{M_N}{N\pi}10^{26}(197.327)^{-1} \\ I_5 &= \left\{[10.2 - 16.7]\left(\frac{1}{a_s} - \mu\right) - [18.7 - 19.2]\left(\frac{1}{a_t} - \mu\right)\right\}\frac{1}{8\sqrt{2}\mu^2}\frac{M_N}{N\pi}10^{26}(197.327)^{-1} \end{aligned} \tag{A.26}$$

where again the range of numbers is due to cutoff variation in the numerical integration. Now plugging in numbers we find the following values for I_n in units of fermis

$$I_1 = 129.3 \ - \ 135.7, I_2 \ = 35.0 \ - \ 57.1, I_4 = -59.6 \ - \ -77.2, I_5 \ = 7.16 \ - \ -8.66 \tag{A.27}$$

All the results of this appendix are summarized in Table 4.8

APPENDIX B

DIAGRAMMATIC TECHNIQUES

When projecting out the amplitudes in total angular momentum, we will inevitably run into what seems to be a mess of Clebsch-Gordan coefficients. However, this seeming mess of Clebsch-Gordan coefficients simplifies quite nicely to 6-j and 9-j symbols. This should come as no surprise since, in dealing with our Clebsch-Gordan coefficients, all magnetic quantum numbers are summed over, therefore, the physics cannot depend on these. Thus, the product of Clebsch-Gordan coefficients must reduce to 6-j symbols, 9-j symbols, and Clebsch-Gordans with 0 magnetic quantum numbers. Despite this being rather intuitive, it is difficult to show this algebraically by using the explicit definition of 6-j and 9-j symbols. Fortunately, techniques where Clebsch-Gordan coefficients are represented diagrammatically offer a more straightforward way to reduce a seeming mess of Clebsch-Gordan coefficients to its respective 3nj-symbols. There are many different diagrammatic techniques for dealing with Clebsch-Gordan coefficients [6, 20, 27, 41]. Some techniques make use of the Wigner 3-j symbols. However, the relationship between the Wigner 3j-symbols and Clebsch-Gordan coefficients is complicated by messy phase factors. Thus, we prefer to use a technique that deals with Clebsch-Gordan coefficients directly, which was developed by George Strobel [101].

The first step in this technique is the representation of the Clebsch-Gordan coefficient. Clebsch-Gordan coefficients are represented by a line with an arrow at the end as in Fig. B.1. The value in the middle of the line represents the first angular momentum of the Clebsch-Gordan coefficient, the value on the non-arrow end the

second angular momentum, and the angular momentum on the arrow end the third angular momentum.

$$C^{m_1,m_2,M}_{j_1,j_2,J} \quad = \quad \begin{array}{l} J \\ j_1 \\ j_2 \end{array}$$

Figure B.1: Diagram representing Clebsch-Gordan coefficient

One important property of the Clebsch-Gordan coefficients is the symmetry property

$$C^{m_1,m_2,M}_{j_1,j_2,J} = (-1)^{j_1+j_2-J} C^{m_2,m_1,M}_{j_2,j_1,J} \tag{B.1}$$

which is represented diagrammatically in Fig. B.2

$$\begin{array}{l} J \\ j_1 \\ j_2 \end{array} \quad = \quad (-1)^{j_1+j_2-J} \quad \begin{array}{l} J \\ j_2 \\ j_1 \end{array}$$

Figure B.2: Symmetry property of Clebsch-Gordan coefficient

This property, as we will see, is very important as it will allow us to switch the order of j_1 and j_2. In switching the ordering we obtain a phase factor that does not depend on the magnetic quantum numbers. Thus, this reordering will not affect the sum over magnetic quantum numbers, which is what we are trying to remove. In this diagrammatic approach, when a shared magnetic number between two Clebsch-Gordan coefficients is summed over, we simply cross the lines at the angular momentum corresponding to this magnetic quantum number. Several examples of how this work are given in Fig. B.3

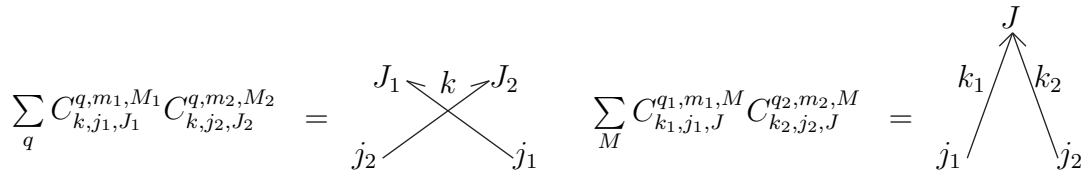

Figure B.3: Diagrammatic rules for summing over magnetic quantum numbers

When we have a single Clebsch-Gordan coefficient and we sum over its magnetic quantum numbers we represent this by a circle on the corresponding angular momentum. An example is given in Fig. B.4

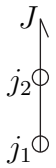

Figure B.4: More Diagrammatic rules for summing over magnetic quantum numbers

Now we wish to show how 6-j and 9-j symbols can be written in in terms of diagrams. We will first start with the 6-j symbol by making use of the identity [39]

$$(-1)^{j_1+j_2+j_3+j_6}\sqrt{\bar{j}_4\bar{j}_5}\begin{Bmatrix} j_1 & j_2 & j_4 \\ j_3 & j_6 & j_5 \end{Bmatrix} C^{m_1,m_6-m_1,m_6}_{j_1,j_5,j_6} = \tag{B.2}$$
$$= \sum_{m_2} C^{m_1,m_2,m_1+m_2}_{j_1,j_2,j_4} C^{m_1+m_2,m_6-m_1-m_2,m_6}_{j_4,j_3,j_6} C^{m_2,m_6-m_1-m_2,m_6-m_1}_{j_2,j_3,j_5}$$

(Note in the bar notation $\bar{x} = 2x+1$.) Next we use the symmetry property Eq. (B.1) on the first Clebsch-Gordan coefficient on both the left and right hand side of Eq. (B.2). Then we multiply both sides by $C^{m_6-m_1,m_1,m_7}_{j_5,j_1,j_7}$ and sum over m_1. Using the orthogonality of the Clebsch-Gordan coefficients we find

$$(-1)^{j_1+j_3+j_4+j_5}\sqrt{\bar{j}_4\bar{j}_5}\begin{Bmatrix} j_1 & j_2 & j_4 \\ j_3 & j_6 & j_5 \end{Bmatrix}\delta_{j_6 j_7}\delta_{m_6 m_7} = \tag{B.3}$$

$$= \sum_{m_1}\sum_{m_2} C^{m_6-m_1,m_1,m_7}_{j_5,j_1,j_7} C^{m_2,m_1,m_1+m_2}_{j_2,j_1,j_4} C^{m_1+m_2,m_6-m_1-m_2,m_6}_{j_4,j_3,j_6} C^{m_2,m_6-m_1-m_2,m_6-m_1}_{j_2,j_3,j_5}$$

Finally using our diagrammatic rules on Eq. (B.3) we find the following diagram for 6-j symbols given in Fig. B.5. (Note the sum over m_1 and m_2 in Eq. (B.3) can be rewritten as a sum over all magnetic quantum numbers using the fact that $C^{m_1,m_2,m_3}_{j_1,j_2,j_3} = 0$ if $m_1 + m_2 \neq m_3$.)

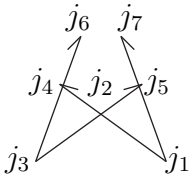

$$= (-1)^{j_1+j_3+j_4+j_5}\sqrt{\bar{j}_4\bar{j}_5}\begin{Bmatrix} j_1 & j_2 & j_4 \\ j_3 & j_6 & j_5 \end{Bmatrix}\delta_{j_6 j_7}\delta_{m_6 m_7}$$

Figure B.5: Diagram representing 6-j symbol

Now we will show how to derive such a digram for the 9-j symbols. We start from the following identity which is similar to that for the 6-j symbol [79]

$$\sum_{m_1,m_2,m_4,m_5,m_7,m_8} C^{m_7,m_8,m_9}_{j_7,j_8,j_9} C^{m_1,m_2,m_3}_{j_1,j_2,j_3} C^{m_4,m_5,m_6}_{j_4,j_5,j_6} C^{m_1,m_4,m_7}_{j_1,j_4,j_7} C^{m_2,m_5,m_8}_{j_2,j_5,j_8} = \tag{B.4}$$

$$= \sqrt{\bar{j}_3\bar{j}_6\bar{j}_7\bar{j}_8}\begin{Bmatrix} j_1 & j_2 & j_3 \\ j_4 & j_5 & j_6 \\ j_7 & j_8 & j_9 \end{Bmatrix} C^{m_3,m_6,m_9}_{j_3,j_6,j_9}$$

Next we multiply both sides by $C^{m_3,m_6,m_{10}}_{j_3,j_6,j_{10}}$ and sum over m_3 and m_6. Using the orthogonality of Clebsch-Gordan coefficients we find

$$\sum_{m_1,m_2,m_3,m_4,m_5,m_6,m_7,m_8} C^{m_3,m_6,m_{10}}_{j_3,j_6,j_{10}} C^{m_7,m_8,m_9}_{j_7,j_8,j_9} C^{m_1,m_2,m_3}_{j_1,j_2,j_3} \times \tag{B.5}$$

$$\times C^{m_4,m_5,m_6}_{j_4,j_5,j_6} C^{m_1,m_4,m_7}_{j_1,j_4,j_7} C^{m_2,m_5,m_8}_{j_2,j_5,j_8} = \sqrt{\bar{j}_3\bar{j}_6\bar{j}_7\bar{j}_8} \begin{Bmatrix} j_1 & j_2 & j_3 \\ j_4 & j_5 & j_6 \\ j_7 & j_8 & j_9 \end{Bmatrix} \delta_{j_9 j_{10}} \delta_{m_9 m_{10}}$$

Finally using our diagrammatic approach on Eq. (B.5) we find the following diagram for the 9-j symbol given in Fig. B.6

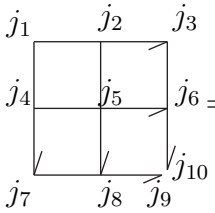

$$= \frac{(\bar{j}_3\bar{j}_6\bar{j}_9\bar{j}_7\bar{j}_8\bar{j}_{10})^{1/2}}{\bar{j}_{10}} \begin{Bmatrix} j_1 & j_2 & j_3 \\ j_4 & j_5 & j_6 \\ j_7 & j_8 & j_9 \end{Bmatrix} \delta_{j_9 j_{10}} \delta_{m_9 m_{10}}$$

Figure B.6: Diagram representing 9-j symbol

At this point we could use similar identities to derive diagrams for higher 3n-j symbols. However, for our purposes we will be content with stopping at 9-j symbols as these are the highest 3n-j symbol that will be encountered in this work. With the diagrams for the 6-j and 9-j symbol in hand it only remains to show how to use the diagrammatic technique to reduce an arbitrary product of Clebsch-Gordan coefficients summed over their magnetic quantum numbers to its respective 9-j, 6-j, and 3-j symbols. We will do this by considering the example of Clebsch-Gordan coefficients Eq. (B.6), that will appear in our angular momentum reduction for PV amplitudes

$$\sum_{m_1,m_2}\sum_{m_L,m_S}\sum_{m_1',m_2'}\sum_{m_L',m_S'}\sum_{m,m'}\sum_{k,q} \tag{B.6}$$

$$C^{m_1',m_2',m_S'}_{1,1/2,S'} C^{m_1,m_2,m_S}_{1,1/2,S} C^{m_L,m_S,M}_{L,S,J} C^{m_L',m_S',M}_{L',S',J}$$

$$C^{m,m_L',m_L}_{1,L',L} C^{m_1,m,m'}_{1,1,1} C^{m_1',q,m'}_{1,k,1} C^{m_2,q,m_2'}_{1/2,k,1/2}$$

Rewriting this product in terms of diagrams and separating certain lines by explicitly summing over magnetic quantum numbers we find the diagrams given in Fig. B.7

$$\sum_{m_S,m_{S'},m_2,m,m'}$$

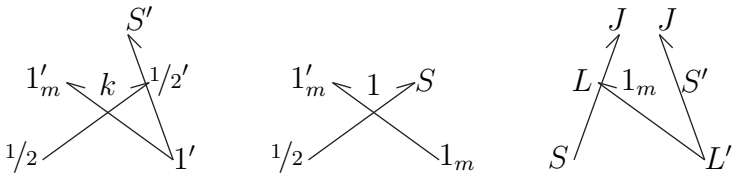

Figure B.7: (Step One) Diagrams representing Clebsch-Gordan coefficients in Eq. (B.6)

We note that by splitting up the Clebsch-Gordan coefficients in the following diagrams they are almost in the form of 6-j symbols. Thus we will now insert appropriate combinations of Clebsch-Gordan coefficients to complete each of these diagrams and have them appear in the 6-j symbol form of Fig B.5 . Then we can show that the product of Clebsch-Gordan coefficients reduces to three 6-j symbols. Clebsch-Gordan coefficients can be added to the diagram trivially by noting the identity can be rewritten as in Fig. B.8

$$\sum_{J,M}\sum_{m_1,m_2} C^{q_1,q_2,M}_{k_1,k_2,J} C^{m_1,m_2,M}_{j_1,j_2,J} \quad = \quad \sum_J$$

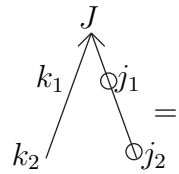

$$= \sum_{m_1,m_2} \delta_{m_1 q_1}\delta_{m_2 q_2} = 1$$

Figure B.8: Identity in terms of Clebsch-Gordan coefficients

We first add the combination of the ClebschGordan coefficients in Fig B.9 which is equivalent to the identity

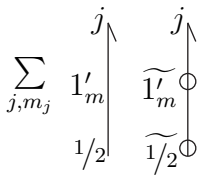

Figure B.9: Identity in terms of first combination of Clebsch-Gordan coefficients

Adding these Clebsch-Gordan coefficients to the diagrams we find the new set of diagrams given in Fig B.10

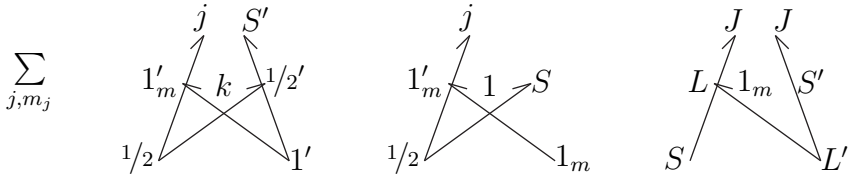

Figure B.10: (Step Two) Diagrams representing Clebsch-Gordan coefficients in Eq. (B.6)

Next we note that from from our diagrammatic rule for 6-j symbols from Fig B.5 we find $j = S'$ and $m_j = m'_S$. Thus taking this into account and inserting the identity again as defined in Fig B.11 we find our diagrams reduce to the form given in B.12

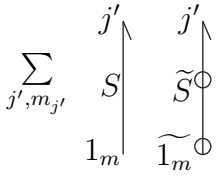

Figure B.11: Identity in terms of second combination of Clebsch-Gordan coefficients

Finally we again use the diagrammatic definition of our 6-j symbol to find that $j' = S'$ and $m_{j'} = m_{S'}$. Doing so we finally get diagrams for three 6-j symbols as seen in Fig B.13

Throughout the diagrammatic reduction of the products of Clebsch-Gordan coefficients Eq. (B.6) we have felt free to use the symmetry property Eq. (B.1) in order

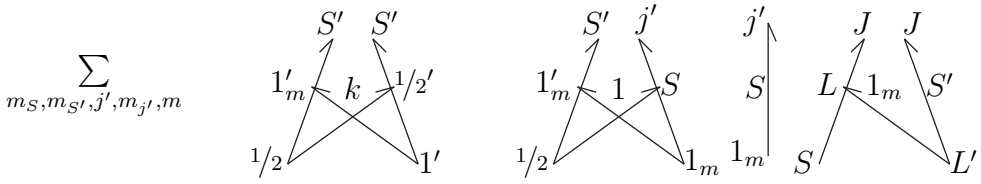

Figure B.12: (Step Three) Diagrams representing Clebsch-Gordan coefficients in Eq. (B.6)

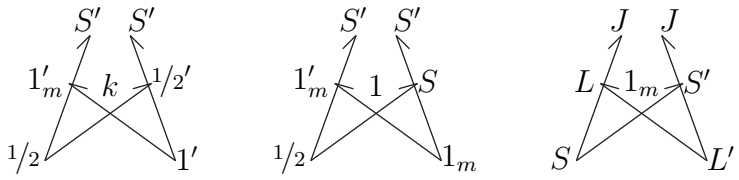

Figure B.13: (Final) Diagrams representing Clebsch-Gordan coefficients in Eq. (B.6)

to switch the first and second angular momentum. However, we have not kept close track of the phases in this reduction. Taking into account these phases and using our definition for the diagrams in Fig B.5 with Fig B.13 we find that Eq. (B.6) reduces to

$$(-1)^{L-J-S} 3\sqrt{2\bar{S}\bar{S}'\bar{L}} \left\{ \begin{array}{ccc} 1 & k & 1 \\ 1/2 & S' & 1/2 \end{array} \right\} \left\{ \begin{array}{ccc} 1 & 1 & 1 \\ 1/2 & S' & S \end{array} \right\} \left\{ \begin{array}{ccc} L' & 1 & L \\ S & J & S' \end{array} \right\} \tag{B.7}$$

APPENDIX C

ISOSPIN

The relevant isospin projections are as follows. Note the subscript $\mathbf{1} \otimes \mathbf{1/2}$ on the bras and kets simply means that the state is a product state of isospin 1 and 1/2, and τ are the usual 2×2 Pauli matrices

$$\langle 1/2, -1/2|\mathbf{1}|1/2, -1/2\rangle = 1 \tag{C.1}$$

$$\langle 1/2, -1/2|\tau_3|1/2, -1/2\rangle = -1 \tag{C.2}$$

$$\langle 1/2, -1/2|\tau^A|1/2, -1/2\rangle_{\mathbf{1}\otimes\mathbf{1/2}} = -\sqrt{3} \tag{C.3}$$

$$\epsilon^{3AB}\langle 1/2, -1/2|\tau^B|1/2, -1/2\rangle_{\mathbf{1}\otimes\mathbf{1/2}} = -i\frac{2}{\sqrt{3}} \tag{C.4}$$

$$\langle 1/2, -1/2|\tau^A\tau_3|1/2, -1/2\rangle_{\mathbf{1}\otimes\mathbf{1/2}} = -\frac{1}{\sqrt{3}} \tag{C.5}$$

$${}_{\mathbf{1}\otimes\mathbf{1/2}}\langle 1/2, -1/2|\tau^A\tau^B|1/2, -1/2\rangle_{\mathbf{1}\otimes\mathbf{1/2}} = -1 \tag{C.6}$$

$$\epsilon^{3AC}{}_{\mathbf{1}\otimes\mathbf{1/2}}\langle 1/2, -1/2|\tau^C\tau^B|1/2, -1/2\rangle_{\mathbf{1}\otimes\mathbf{1/2}} = -i\frac{2}{3} \tag{C.7}$$

APPENDIX D

ANGULAR MOMENTUM PROJECTION

The integrals that one needs to solve when projecting out the amplitudes in a partial wave basis take on the following form.

$$\int\int d\Omega_p d\Omega_k \frac{1}{a+\hat{\mathbf{k}}\cdot\hat{\mathbf{p}}} Y_\ell^m(\hat{\mathbf{k}}) Y_{\ell'}^{-m}(\hat{\mathbf{p}}) \tag{D.1}$$

In order to solve these integrals we note that integrating over all positions of $\vec{\mathbf{p}}$ and $\vec{\mathbf{k}}$ is equivalent to integrating over all angles between $\vec{\mathbf{p}}$ and $\vec{\mathbf{k}}$ where $\vec{\mathbf{k}}$ is fixed along the z-axis and then integrating over all rotations of $\vec{\mathbf{k}}$. Thus we can rewrite our integral as follows where $d\Omega$ refers to integration over the angle between $\vec{\mathbf{k}}$ and $\vec{\mathbf{p}}$

$$\int\int d\Omega d\Omega_k \frac{1}{a+\cos\theta} Y_\ell^m(\hat{\mathbf{k}}) Y_{\ell'}^{-m}(\hat{\mathbf{p}}) \tag{D.2}$$

Using rotational symmetry we can rewrite our product of spherical harmonics as follows in terms of Wigner D functions [93].

$$Y_\ell^m(\hat{\mathbf{k}}) Y_{\ell'}^{-m}(\hat{\mathbf{p}}) = \sum_{m'} \mathscr{D}_{m0}^{(\ell)}(\hat{\mathbf{k}})^* Y_\ell^0(\hat{\mathbf{z}}) \mathscr{D}_{-mm'}^{(\ell')}(\hat{\mathbf{k}})^* Y_{\ell'}^{m'}(\theta,\phi) \tag{D.3}$$

Now using the unitarity of the Wigner D functions, the Clebsch-Gordan series, and the definition of the Wigner D functions this can be rewritten as [93].

$$Y_\ell^m(\hat{\mathbf{k}})Y_{\ell'}^{-m}(\hat{\mathbf{p}}) = \sqrt{\frac{2\ell+1}{2j+1}}\sum_{m'}\sum_j C_{\ell,\ell',j}^{m,-m,0}C_{\ell,\ell,j}^{0,m',m'}Y_j^{m'*}(\hat{\mathbf{k}})Y_{\ell'}^{m'}(\theta,\phi) \tag{D.4}$$

Now plugging this expression into our integral, we find that we only get nonzero values for $j = m' = 0$. Simplifying the integral we get the simple expression

$$4\pi\sqrt{(2l+1)(2l'+1)}C_{\ell,\ell',0}^{m,-m,0}C_{\ell,\ell',0}^{0,0,0}Q_{\ell'}(a) \tag{D.5}$$

where

$$Q_\ell(a) = \frac{1}{2}\int_{-1}^{1}\frac{P_\ell(x)}{a+x}dx \tag{D.6}$$

are functions that are related to Legendre Polynomials of the second kind up to a factor of $(-1)^\ell$, and $P_\ell(x)$ are the standard Legendre polynomials. Putting this altogether and using explicit values for the Clebsch-Gordan coefficients we find our integral is

$$\int\int d\Omega_p d\Omega_k \frac{1}{a+\hat{\mathbf{k}}\cdot\hat{\mathbf{p}}}Y_\ell^m(\hat{\mathbf{k}})Y_{\ell'}^{-m}(\hat{\mathbf{p}}) = 4\pi(-1)^m\delta_{\ell\ell'}Q_{\ell'}(a) \tag{D.7}$$

Now when doing our projections we will inevitably have to solve integrals of the following kind for diagrams with a single PV vertex

$$\sqrt{\frac{4\pi}{3}}\int d\Omega_k\int d\Omega_p\frac{1}{a+\hat{\mathbf{k}}\cdot\hat{\mathbf{p}}}Y_{L'}^{m_L'\,*}(\hat{\mathbf{p}})Y_L^{m_L}(\hat{\mathbf{k}})\left(kY_1^m(\hat{\mathbf{k}}) + 2pY_1^m(\hat{\mathbf{p}})\right) \tag{D.8}$$

Using the following identity [93]

$$Y_{L_1}^{m_1}(\hat{\mathbf{r}})Y_{L_2}^{m_2}(\hat{\mathbf{r}}) = \frac{\sqrt{(2L_1+1)(2L_2+1)}}{4\pi}\sum_{L'}\sum_{m'} C_{L_1,L_2,L'}^{m_1,m_2,m'} C_{L_1,L_2,L'}^{0,0,0}\sqrt{\frac{4\pi}{2L'+1}}Y_{L'}^{m'}(\hat{\mathbf{r}}) \tag{D.9}$$

we find our integral reduces to

$$\int d\Omega_k \int d\Omega_p \frac{1}{a+\hat{\mathbf{k}}\cdot\hat{\mathbf{p}}}\left(Y_{L'}^{m'_L\,*}(\hat{\mathbf{p}})\sum_{L''}\sum_{m''}\sqrt{\frac{2L+1}{2L''+1}}C_{L,1,L''}^{0,0,0}C_{L,1,L''}^{m_L,m,m_{L''}}kY_{L''}^{m''}(\hat{\mathbf{k}})\right. \tag{D.10}$$

$$\left.+Y_L^{m_L}(\hat{\mathbf{k}})\sum_{L''}\sum_{m''}\sqrt{\frac{2L'+1}{2L''+1}}C_{L',1,L''}^{0,0,0}C_{L',1,L''}^{-m'_L,m,m''_L}(-1)^{m''+m'_L}2pY_{L''}^{-m''\,*}(\hat{\mathbf{p}})\right)$$

This integral can be performed trivially using equation (D.7) to find

$$4\pi\left(\sqrt{\frac{2L+1}{2L'+1}}C_{L,1,L'}^{0,0,0}C_{L,1,L'}^{m_L,m,m'_L}kQ_{L'}(a)+\right. \tag{D.11}$$

$$\left.+\sqrt{\frac{2L'+1}{2L+1}}(-1)^{m'_L-m_L}C_{L',1,L}^{0,0,0}C_{L',1,L}^{-m'_L,m,-m_L}2pQ_L(a)\right)$$

Using the symmetry property Eq. (D.18) of the Clebsch-Gordan coefficients we finally obtain

$$U_{JL} = \sqrt{\frac{4\pi}{3}}\int d\Omega_k\int d\Omega_p\frac{1}{a+\hat{\mathbf{k}}\cdot\hat{\mathbf{p}}}Y_{L'}^{m'_L\,*}(\hat{\mathbf{p}})Y_L^{m_L}(\hat{\mathbf{k}})\left(kY_1^m(\hat{\mathbf{k}})+2pY_1^m(\hat{\mathbf{p}})\right) = \tag{D.12}$$

$$= 4\pi\sqrt{\frac{2L+1}{2L'+1}}C_{L,1,L'}^{0,0,0}C_{L,1,L'}^{m_L,m,m'_L}(kQ_{L'}(a)+2pQ_L(a))$$

In the SD mixing case one must solve similar integrals, which are solved in an analogous manner, their results are summarized below as they will be necessary in the proceeding sections

$$\frac{4\pi}{3}k^2\int d\Omega_k\int d\Omega_p\frac{1}{a+\hat{\mathbf{k}}\cdot\hat{\mathbf{p}}}Y_{L'}^{m'_L}(\hat{\mathbf{p}})^*Y_L^{m_L}(\hat{\mathbf{k}})Y_1^{m_1}(\hat{\mathbf{k}})Y_1^{m_2}(\hat{\mathbf{k}}) = \tag{D.13}$$
$$= 4\pi k^2\sum_{L''}\sum_{m''}\sqrt{\frac{\bar{L}}{\bar{L}'}}C_{1,1,L''}^{m_1,m_2,m''}C_{L,L'',L'}^{m_L,m'',m'_L}C_{1,1,L''}^{0,0,0}C_{L,L'',L'}^{0,0,0}Q_{L'}(a)$$

$$\frac{4\pi}{3}p^2\int d\Omega_k\int d\Omega_p\frac{1}{a+\hat{\mathbf{k}}\cdot\hat{\mathbf{p}}}Y_{L'}^{m'_L}(\hat{\mathbf{p}})^*Y_L^{m_L}(\hat{\mathbf{k}})Y_1^{m_1}(\hat{\mathbf{p}})Y_1^{m_2}(\hat{\mathbf{p}}) = \tag{D.14}$$
$$= 4\pi p^2\sum_{L''}\sum_{m''}\sqrt{\frac{\bar{L}}{\bar{L}'}}C_{1,1,L''}^{m_1,m_2,m''}C_{L,L'',L'}^{m_L,m'',m'_L}C_{1,1,L''}^{0,0,0}C_{L,L'',L'}^{0,0,0}Q_L(a)$$

$$\frac{4\pi}{3}kp\int d\Omega_k\int d\Omega_p\frac{1}{a+\hat{\mathbf{k}}\cdot\hat{\mathbf{p}}}Y_{L'}^{m'_L}(\hat{\mathbf{p}})^*Y_L^{m_L}(\hat{\mathbf{k}})Y_1^{m_1}(\hat{\mathbf{k}})Y_1^{m_2}(\hat{\mathbf{p}}) = \tag{D.15}$$
$$= 4\pi kp\sum_{L''}\sum_{m''}\sqrt{\frac{\bar{L}}{\bar{L}'}}C_{L,1,L''}^{m_L,m_1,m''}C_{L'',1,L'}^{m'',m_2,m'_L}C_{L,1,L''}^{0,0,0}C_{L'',1,L'}^{0,0,0}Q_{L''}(a)$$

We also quote here various properties of the Clebsch-Gordan coefficients as they will be necessary in the proceeding.

$$\sum_m(-1)^{j-m}C_{j,j,J}^{m,-m,0} = \sqrt{2j+1}\,\delta_{J0} \tag{D.16}$$

$$\sum_{m_1}\sum_{m_2}C_{j_1,j_2,J_1}^{m_1,m_2,M_1}C_{j_1,j_2,J_2}^{m_1,m_2,M_2} = \delta_{J_1J_2}\delta M_1M_2 \tag{D.17}$$

$$C_{j_1,j_2,J}^{m_1,m_2,M} = (-1)^{j_2+m_2}\sqrt{\frac{\bar{J}}{\bar{j}_1}}C_{J,j_2,j_1}^{-M,m_2,-m_1} \tag{D.18}$$
$$= (-1)^{j_2+m_2}\sqrt{\frac{\bar{J}}{\bar{j}_1}}C_{j_2,J,j_1}^{-m_2,M,m_1} \tag{D.19}$$

D.1 Parity Violating Projection

The projection we must carry out for the PV amplitudes is of the form

$$\boldsymbol{\mathcal{K}}(k,p)^{J}_{L'S',LS} = \int d\Omega_k \int d\Omega_p \left(\mathcal{Y}^{M}_{J,L'S'}(\hat{\mathbf{p}})\right)^{*} \left(\boldsymbol{\mathcal{K}}^{ji}\right)^{\beta b}_{\alpha a}(\vec{\mathbf{k}},\vec{\mathbf{p}})\mathcal{Y}^{M}_{J,LS}(\hat{\mathbf{k}}) \tag{D.20}$$

where $\left(\boldsymbol{\mathcal{K}}^{ji}\right)^{\beta b}_{\alpha a}(\vec{\mathbf{k}},\vec{\mathbf{p}})$ is given by Eq. (4.9). (Note the polarization, spin and isospin indices are summed over corresponding indices that are not explicitly shown in the spin angle functions). Each matrix element of $\left(\boldsymbol{\mathcal{K}}^{ji}\right)^{\beta b}_{\alpha a}(\vec{\mathbf{k}},\vec{\mathbf{p}})$ has a different projection. Each of these four different projections has in turn four pieces given by Eqs. (4.7). Fortunately many of these terms can be related by time reversal simplifying the projection considerably.

D.1.1 Deuteron to Deuteron Term

We will first show how to project out the first $g^{^3S_1-{}^3P_1}$ piece of the matrix element $\left[\left(\boldsymbol{\mathcal{K}}^{ji}\right)^{\beta b}_{\alpha a}(\vec{\mathbf{k}},\vec{\mathbf{p}})\right]_{11}$ as given in (4.9) and (4.7a). In order to project this term out we use properties of spherical tensors and the Wigner-Eckart theorem to reduce the following expression to a sum over Clebsch-Gordan coefficients.

$$\begin{aligned} U_{JL} =& i\epsilon^{i\ell\kappa}\langle 1/2, m_2'|\sigma^{\kappa}\sigma^{j}|1/2, m_2\rangle(\vec{\mathbf{k}}+2\vec{\mathbf{p}})^{\ell} \\ =& \sqrt{\frac{2}{3}}\sum_{m,m'}\sum_{\kappa,q}\sqrt{\bar{\kappa}}C^{m_1,m,m'}_{1,1,1}C^{m_1',q,m'}_{1,\kappa,1}C^{m_2,q,m_2'}_{1/2,\kappa,1/2}\langle 1/2||T_{\kappa}||1/2\rangle(-1)^{m}(\vec{\mathbf{k}}+2\vec{\mathbf{p}})^{-m} \end{aligned} \tag{D.21}$$

Using the above expression with (4.9),(4.7a), and (D.20) and, for the time being ignoring the isospin, we find the expression for our projection is.

$$V_{JL} = \sqrt{\frac{4\pi}{3}}\frac{1}{kp} g^{{}^3S_1-{}^3P_1} y_t \int d\Omega_p \int d\Omega_k \frac{1}{a+\hat{\mathbf{k}}\cdot\hat{\mathbf{p}}} \sum_{m_1,m_2}\sum_{m_L,m_S}\sum_{m_1',m_2'}\sum_{m_L',m_S'} \tag{D.22}$$

$$C^{m_1',m_2',m_S'}_{1,1/2,S'} C^{m_1,m_2,m_S}_{1,1/2,S} C^{m_L,m_S,M}_{L,S,J} C^{m_L',m_S',M}_{L',S',J}$$

$$Y^{m_L'}_{L'}{}^*(\hat{\mathbf{p}}) Y^{m_L}_{L}(\hat{\mathbf{k}}) \left(kY^{-m}_1(\hat{\mathbf{k}}) + 2pY^{-m}_1(\hat{\mathbf{p}})\right)(-1)^m$$

$$\sqrt{\frac{2}{3}}\sum_{m,m'}\sum_{\kappa,q}\sqrt{\kappa} C^{m_1,m,m'}_{1,1,1} C^{m_1',q,m'}_{1,\kappa,1} C^{m_2,q,m_2'}_{1/2,\kappa,1/2} \langle 1/2||T_\kappa||1/2\rangle$$

where $a = (k^2+p^2-M_N E)/kp$ throughout the rest of the appendix. Integration over the angular variable can be carried out trivially by using (D.12) leaving a sum of products of Clebsch-Gordan coefficients .

$$V_{JL} = 4\pi g^{{}^3S_1-{}^3P_1} y_t \sqrt{\frac{2}{3}} C^{0,0,0}_{L,1,L'} \sqrt{\frac{\bar{L}}{\bar{L}'}}\frac{1}{kp} \sum_{m_1,m_2}\sum_{m_L,m_S}\sum_{m_1',m_2'}\sum_{m_L',m_S'}\sum_{m,m'}\sum_{\kappa,q} \tag{D.23}$$

$$\sqrt{\kappa}\langle 1/2||T_\kappa||1/2\rangle C^{m_1',m_2',m_S'}_{1,1/2,S'} C^{m_1,m_2,m_S}_{1,1/2,S} C^{m_L,m_S,M}_{L,S,J} C^{m_L',m_S',M}_{L',S',J}$$

$$(-1)^m C^{m_L,-m,m_L'}_{L,1,L'} C^{m_1,m,m'}_{1,1,1} C^{m_1',q,m'}_{1,\kappa,1} C^{m_2,q,m_2'}_{1/2,\kappa,1/2} \times$$

$$\times \frac{1}{kp}\left(kQ_{L'}(a) + 2pQ_L(a)\right)$$

Then using the symmetry property Eq. (D.19) of the Clebsch-Gordan coefficients we find.

$$V_{JL} = 4\pi g^{{}^3S_1-{}^3P_1} y_t \sqrt{\frac{2}{3}} C^{0,0,0}_{L,1,L'} \frac{1}{kp} \sum_{m_1,m_2}\sum_{m_L,m_S}\sum_{m_1',m_2'}\sum_{m_L',m_S'}\sum_{m,m'}\sum_{\kappa,q} \tag{D.24}$$

$$\sqrt{\kappa}\langle 1/2||T_\kappa||1/2\rangle C^{m_1',m_2',m_S'}_{1,1/2,S'} C^{m_1,m_2,m_S}_{1,1/2,S} C^{m_L,m_S,M}_{L,S,J} C^{m_L',m_S',M}_{L',S',J}$$

$$C^{m,m_L',m_L}_{1,L',L} C^{m_1,m,m'}_{1,1,1} C^{m_1',q,m'}_{1,\kappa,1} C^{m_2,q,m_2'}_{1/2,\kappa,1/2} \times$$

$$\times \frac{1}{kp}\left(kQ_{L'}(a) + 2pQ_L(a)\right)$$

Using the graphical methods one finds that the product of Clebsch-Gordan coefficients can be written as three graphs representing 6-j symbols given in Fig. D.1. (Note 1 ($1/2$), $1'$ ($1/2'$) represent m_1 (m_2) and m_1' (m_2') respectively, and also 1_m ($1'_m$) represents m (m'). This notation will be used throughout the rest of the appendices)

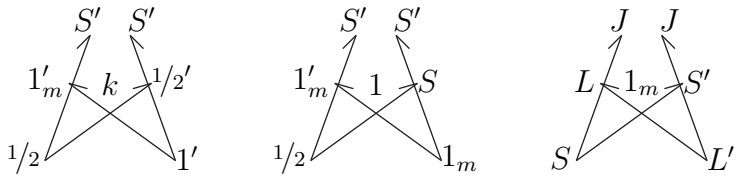

Figure D.1: Diagrams representing Clebsch-Gordan coefficients in Eq. (D.25)

Now using the definition of the diagrams and taking into account the phase factors from switching the first and second angular momenta in the Clebsch-Gordan coefficients we obtain the following expression for our projection in terms of 6-j symbols.

$$V_{JL} = 8\pi g^{{}^3S_1-{}^3P_1} y_t \sqrt{3} C^{0,0,0}_{L',1,L} (-1)^{L-S-J} \frac{1}{kp} (kQ_{L'}(a) + 2pQ_L(a)) \times \tag{D.25}$$
$$\times \sum_\kappa \sqrt{\bar{S}\bar{S}'\bar{L}'\bar{\kappa}} \langle 1/2||T_\kappa||1/2\rangle \begin{Bmatrix} 1/2 & \kappa & 1/2 \\ 1 & S' & 1 \end{Bmatrix} \begin{Bmatrix} 1 & 1 & 1 \\ 1/2 & S' & S \end{Bmatrix} \begin{Bmatrix} L' & 1 & L \\ S & J & S' \end{Bmatrix}$$

The sum over κ can be removed by use of the identity [39].

$$\sum_\kappa \bar{\kappa} \begin{Bmatrix} 1/2 & \kappa & 1/2 \\ 1 & S' & 1 \end{Bmatrix} \begin{Bmatrix} 1/2 & 1/2 & \kappa \\ 1 & 1 & j \end{Bmatrix} = \delta_{S'j} \frac{1}{\bar{S}'} \tag{D.26}$$

Knowing that $\langle 1/2||T_0||1/2\rangle = -\sqrt{3}$ and $\langle 1/2||T_1||1/2\rangle = -\sqrt{6}$ we must solve the following system of equations

$$-\sqrt{3} = A \left\{ \begin{array}{ccc} 1/2 & 1/2 & 0 \\ 1 & 1 & 1/2 \end{array} \right\} + B \left\{ \begin{array}{ccc} 1/2 & 1/2 & 0 \\ 1 & 1 & 3/2 \end{array} \right\} \tag{D.27}$$
$$-\sqrt{6} = \sqrt{3}A \left\{ \begin{array}{ccc} 1/2 & 1/2 & 1 \\ 1 & 1 & 1/2 \end{array} \right\} + \sqrt{3}B \left\{ \begin{array}{ccc} 1/2 & 1/2 & 1 \\ 1 & 1 & 3/2 \end{array} \right\}$$

whose solutions are $A = \sqrt{2}$ and $B = 4\sqrt{2}$. Combining these values with (D.26) we find the sum over κ is simplified to Eq. (D.28)

$$\sum_{\kappa} \sqrt{\bar{\kappa}} \langle 1/2 || T_\kappa || 1/2 \rangle \left\{ \begin{array}{ccc} 1/2 & \kappa & 1/2 \\ 1 & S' & 1 \end{array} \right\} = \sqrt{2} \left(\frac{1}{2} \delta_{S' 1/2} + \delta_{3/2} \right) \tag{D.28}$$

Thus the κ dependence is removed by Eq. (D.28) and our expression reduces nicely, yielding.

$$\begin{aligned} V_{JL} =& 8\pi g^{{}^3S_1 - {}^3P_1} y_t \sqrt{6} C^{0,0,0}_{L',1,L} (-1)^{L-S-J} \sqrt{\bar{S}\bar{S}'\bar{L}'} \left(\frac{1}{2} \delta_{S' 1/2} + \delta_{S' 3/2} \right) \times \\ & \times \left\{ \begin{array}{ccc} 1 & 1 & 1 \\ 1/2 & S' & S \end{array} \right\} \left\{ \begin{array}{ccc} L' & 1 & L \\ S & J & S' \end{array} \right\} \frac{1}{kp} (k Q_{L'}(a) + 2p Q_L(a)) \end{aligned} \tag{D.29}$$

We will now show how to project out the first $g^{{}^3S_1 - {}^1P_1}$ piece of the matrix element $\left[\left(\boldsymbol{\mathcal{K}}^{ji} \right)^{\beta b}_{\alpha a} (\vec{\mathbf{k}}, \vec{\mathbf{p}}) \right]_{11}$ as given in (4.9) and (4.7a). Again we use the properties of spherical tensors and the Wigner-Eckart theorem to reduce the following expression to a sum over Clebsch-Gordan coefficients.

$$U_{JL} = \langle 1/2, m_2'|\sigma^{-m_1'}|1/2, m_2\rangle = C^{m_2,-m_1',m_2'}_{1/2,1,1/2}\sqrt{3} \tag{D.30}$$

Using the above expression with (4.9),(4.7a), and (D.20) and, for the time being ignoring the isospin, we find the expression for our projection is.

$$\begin{aligned} V_{JL} =& \sqrt{4\pi} g^{{}^3S_1-{}^1P_1} y_t \frac{1}{kp}\int d\Omega_p \int d\Omega_k \frac{1}{a+\hat{\mathbf{k}}\cdot\hat{\mathbf{p}}} \sum_{m_1,m_2}\sum_{m_L,m_S}\sum_{m_1',m_2'}\sum_{m_L',m_S'} \\ & C^{m_1',m_2',m_S'}_{1,1/2,S'} C^{m_1,m_2,m_S}_{1,1/2,S} C^{m_L,m_S,M}_{L,S,J} C^{m_L',m_S',M}_{L',S',J} \\ & Y^{m_L'}_{L'}{}^*(\hat{\mathbf{p}}) Y^{m_L}_{L}(\hat{\mathbf{k}}) \left(kY^{m_1}_1(\hat{\mathbf{k}}) + 2pY^{m_1}_1(\hat{\mathbf{p}})\right) (-1)^{m_1'} C^{m_2,-m_1',m_2'}_{1/2,1,1/2} \end{aligned} \tag{D.31}$$

Now we can trivially integrate over the angular variables using Eq. (D.12) giving.

$$\begin{aligned} V_{JL} =& 4\pi g^{{}^3S_1-{}^1P_1} y_t \sqrt{3}\sqrt{\frac{\bar{L}}{\bar{L}'}} C^{0,0,0}_{L,1,L'} \sum_{m_1,m_2}\sum_{m_L,m_S}\sum_{m_1',m_2'}\sum_{m_L',m_S'} \\ & C^{m_1',m_2',m_S'}_{1,1/2,S'} C^{m_1,m_2,m_S}_{1,1/2,S} C^{m_L,m_S,M}_{L,S,J} C^{m_L',m_S',M}_{L',S',J} \\ & (-1)^{m_1'} C^{m_L,m_1,m_L'}_{L,1,L'} C^{m_2,-m_1',m_2'}_{1/2,1,1/2} \frac{1}{kp}(kQ_{L'}(a) + 2pQ_L(a)) \end{aligned} \tag{D.32}$$

Using the symmetry property for Clebsch-Gordan coefficients Eq. (D.19) and the orthogonality of Clebsch-Gordan coefficients Eq. (D.17) our projection reduces to give

$$\begin{aligned} V_{JL} =& -4\pi g^{{}^3S_1-{}^1P_1} y_t \sqrt{3}\sqrt{\frac{2L+1}{2L'+1}} C^{0,0,0}_{L,1,L'} \sum_{m_1,m_2}\sum_{m_L,m_S}\sum_{m_1',m_2'}\sum_{m_L',m_S'} \\ & C^{m_1,m_2,m_S}_{1,1/2,S} C^{m_L,m_S,M}_{L,S,J} C^{m_L',m_2,M}_{L',1/2,J} C^{m_L,m_1,m_L'}_{L,1,L'} \delta_{S'1/2} \frac{1}{kp}(kQ_{L'}(a) + 2pQ_L(a)) \end{aligned} \tag{D.33}$$

The resulting product of Clebsch-Gordan coefficients can be represented diagrammatically as a 6-j symbol giving the diagram in Fig. D.2.

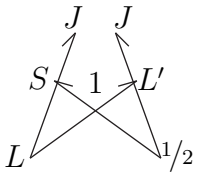

Figure D.2: Diagram representing Clebsch-Gordan coefficients in Eq. (D.33)

Writing out the diagram in terms of 6-j symbols and taking into account phase factors our projection reduces to the form.

$$V_{JL} = -4\pi g^{{}^3S_1-{}^1P_1} y_t \sqrt{3}(-1)^{3/2+2S+L-J} \delta_{S'1/2} \sqrt{\bar{S}\bar{L}} C^{0,0,0}_{L,1,L'} \begin{Bmatrix} 1/2 & 1 & S \\ L & J & L' \end{Bmatrix} \times \quad \text{(D.34)}$$
$$\times \frac{1}{kp}(kQ_{L'}(a) + 2pQ_L(a))$$

Finally using Eqs. (D.29), (D.34), and time reversal invariance, and including the isospin projections, we find the projection for the $\left[\boldsymbol{\mathcal{K}}(k,p)^J_{L'S',LS}\right]_{11}$ term is

$$
\begin{aligned}
&- g^{^3S_1-{}^1P_1} y_t 4\pi\sqrt{3}(-1)^{3/2+2S+L-J}\delta_{S'1/2}\sqrt{\bar{S}\bar{L}}C^{0,0,0}_{L,1,L'}\left\{\begin{array}{ccc} 1/2 & 1 & S \\ L & J & L' \end{array}\right\}\times \qquad \text{(D.35)}\\
&\qquad\times\frac{1}{kp}(kQ_{L'}(a)+2pQ_L(a))\\
&- g^{^3S_1-{}^1P_1} y_t 4\pi\sqrt{3}(-1)^{3/2+2S'+L'-J}\delta_{S1/2}\sqrt{\bar{S}'\bar{L}'}C^{0,0,0}_{L',1,L}\left\{\begin{array}{ccc} 1/2 & 1 & S' \\ L' & J & L \end{array}\right\}\times\\
&\qquad\times\frac{1}{kp}(2kQ_{L'}(a)+pQ_L(a))\\
&- g^{^3S_1-{}^3P_1} y_t 8\pi\sqrt{6}C^{0,0,0}_{L',1,L}(-1)^{L-S-J}\sqrt{\bar{S}\bar{S}'\bar{L}'}\left(\frac{1}{2}\delta_{S'1/2}+\delta_{S'3/2}\right)\left\{\begin{array}{ccc} 1 & 1 & 1 \\ 1/2 & S' & S \end{array}\right\}\times\\
&\qquad\times\left\{\begin{array}{ccc} L' & 1 & L \\ S & J & S' \end{array}\right\}\frac{1}{kp}(kQ_{L'}(a)+2pQ_L(a))\\
&- g^{^3S_1-{}^3P_1} y_t 8\pi\sqrt{6}C^{0,0,0}_{L,1,L'}(-1)^{L'-S'-J}\sqrt{\bar{S}\bar{S}'\bar{L}}\left(\frac{1}{2}\delta_{S1/2}+\delta_{S3/2}\right)\left\{\begin{array}{ccc} 1 & 1 & 1 \\ 1/2 & S & S' \end{array}\right\}\times\\
&\qquad\times\left\{\begin{array}{ccc} L & 1 & L' \\ S' & J & S \end{array}\right\}\frac{1}{kp}(2kQ_{L'}(a)+pQ_L(a))
\end{aligned}
$$

D.1.2 Singlet to Deuteron Term

Now for the singlet to deuteron term we have four terms to project out. However two of the terms have the same spin structure. Thus in reality we only have three terms to project. Also it is worth noting that the deuteron to singlet term is just the time reversed version of the singlet to deuteron term. We will first project out the terms corresponding to the coefficients $g^{^1S_0-{}^3P_0}_{(\Delta I=0)}$ and $g^{^1S_0-{}^3P_0}_{(\Delta I=1)}$, as these terms have the same spin structure. Projecting out the spin structure of these terms in terms of sums over Clebsch-Gordan coefficients by using properties of spherical tensors and the Wigner-Eckart gives.

$$U_{JL} = \langle 1/2, m_2'|\sigma^\ell \sigma^j |1/2, m_2\rangle (\vec{\mathbf{k}} + 2\vec{\mathbf{p}})^\ell \tag{D.36}$$
$$= -\sum_m \sum_{\kappa,q} \sqrt{\frac{\bar{\kappa}}{3}} C^{m_1',q,m}_{1,\kappa,1} (-1)^m C^{m_2,q,m_2'}_{1/2,\kappa,1/2} \langle 1/2||T_\kappa||1/2\rangle (\vec{\mathbf{k}} + 2\vec{\mathbf{p}})^{-m}$$

Using Eq. (D.36) with (4.9),(4.7b), and (D.20), and for the time being ignoring the isospin, we find the expression for our projection is. (Note we also do not include the PV coefficients as this spin structure occurs for both $g^{^1S_0-{}^3P_0}_{(\Delta I=0)}$ and $g^{^1S_0-{}^3P_0}_{(\Delta I=1)}$ but they come with different isospin structure.)

$$V_{JL} = -y_t \sqrt{\frac{4\pi}{3}} \frac{1}{kp} \int d\Omega_p \int d\Omega_k \frac{1}{a + \hat{\mathbf{k}}\cdot\hat{\mathbf{p}}} \sum_{m_2} \sum_{m_L,m_S} \sum_{m_1',m_2'} \sum_{m_L',m_S'} \tag{D.37}$$
$$C^{m_1',m_2',m_S'}_{1,1/2,S'} C^{0,m_2,m_S}_{0,1/2,S} C^{m_L,m_S,M}_{L,S,J} C^{m_L',m_S',M}_{L',S',J}$$
$$Y^{m_L'\,*}_{L'}(\hat{\mathbf{p}}) Y^{m_L}_L(\hat{\mathbf{k}}) \sum_m \sum_{\kappa,q} \sqrt{\frac{\bar{\kappa}}{3}} \left(k Y_1^{-m}(\hat{\mathbf{k}}) + 2p Y_1^{-m}(\hat{\mathbf{p}}) \right) (-1)^m$$
$$C^{m_1',q,m}_{1,\kappa,1} C^{m_2,q,m_2'}_{1/2,\kappa 1/2} \langle 1/2||T_\kappa||1/2\rangle$$

The angular integration is trivially performed by Eq. (D.12), yielding

$$V_{JL} = -4\pi y_t \sqrt{\frac{1}{3}} \sqrt{\frac{\bar{L}}{\bar{L}'}} C^{0,0,0}_{L,1,L'} \sum_{m,m_2} \sum_{m_L,m_S} \sum_{m_1',m_2'} \sum_{m_L',m_S'} \sum_{\kappa,q} \tag{D.38}$$
$$\sqrt{\bar{\kappa}} C^{m_1',m_2',m_S'}_{1,1/2,S'} C^{0,m_2,m_S}_{0,1/2,S} C^{m_L,m_S,M}_{L,S,J} C^{m_L',m_S',M}_{L',S',J}$$
$$(-1)^m C^{m_1',q,m}_{1,\kappa,1} C^{m_2,q,m_2'}_{1/2,\kappa 1/2} C^{m_L,-m,m_L'}_{L,1,L'} \langle 1/2||T_\kappa||1/2\rangle$$
$$\frac{1}{kp}(k Q_{L'}(a) + 2p Q_L(a))$$

We again use the symmetry property Eq. (D.18) of the Clebsch-Gordan coefficients and in addition note that $C^{0,m_2,m_S}_{0,1/2,S}$ implies $S = 1/2$ and $m_2 = m_S$ which give the result

$$V_{JL} = -4\pi y_t(-1)^{L+1-L'}\sqrt{\frac{1}{3}}\sqrt{\frac{\bar{L}'}{\bar{L}}}C^{0,0,0}_{L',1,L}\sum_{m,m_2}\sum_{m_L}\sum_{m'_1,m'_2}\sum_{m'_L,m'_S}\sum_{\kappa,q} \tag{D.39}$$

$$\sqrt{\bar{\kappa}}\delta_{S,1/2}C^{m'_1,m'_2,m'_S}_{1,1/2,S'}C^{m_L,m_2,M}_{L,1/2,J}C^{m'_L,m'_S,M}_{L',S',J}$$

$$C^{m'_1,q,m}_{1,\kappa,1}C^{m_2,q,m'_2}_{1/2,\kappa,1/2}C^{m'_L,m,m_L}_{L',1,L}\langle 1/2||T_\kappa||1/2\rangle$$

$$\frac{1}{kp}(kQ_{L'}(a)+2pQ_L(a))$$

Representing this product of Clebsch-Gordan coefficients diagrammatically we find the following set of diagrams in Fig. D.3

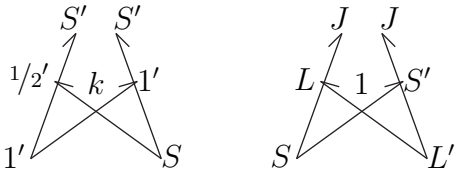

Figure D.3: Diagram representing Clebsch-Gordan coefficients in Eq. (D.39)

Writing the diagrams in terms of 6-j symbols and taking into account phase factors we obtain

$$V_{JL} = -4\pi y_t(-1)^{1+S'+L-J}\delta_{S,1/2}\sqrt{2}C^{0,0,0}_{L',1,L}\sum_{\kappa}\sqrt{\bar{L}'\bar{S}'\bar{\kappa}}\langle 1/2||T_\kappa||1/2\rangle \begin{Bmatrix} 1/2 & \kappa & 1/2 \\ 1 & S' & 1 \end{Bmatrix} \times \tag{D.40}$$

$$\times \begin{Bmatrix} L' & 1 & L \\ S & J & S' \end{Bmatrix} \frac{1}{kp}(kQ_{L'}(a)+2pQ_L(a))$$

Finally using Eq. (D.28) we remove the sum over κ and obtain the expression

$$- 8\pi y_t(-1)^{1+S'+L-J}\delta_{S,1/2}C^{0,0,0}_{L',1,L}\sqrt{\bar{L}'\bar{S}'}\left(\frac{1}{2}\delta_{S'1/2}+\delta_{S'3/2}\right)\left\{\begin{array}{ccc} L' & 1 & L \\ S & J & S' \end{array}\right\}\times \quad \text{(D.41)}$$

$$\times\frac{1}{kp}(kQ_{L'}(a)+2pQ_L(a))$$

Now we will project out the term corresponding to the $g^{^3S_1-{}^1P_1}$ coefficient. We first project out the spin piece using the properties of spherical tensors and the Wigner-Eckart theorem, yielding

$$\begin{aligned} U_{JL} &= \langle 1/2, m_2'|\mathbf{1}|1/2, m_2\rangle(2\vec{\mathbf{k}}+\vec{\mathbf{p}})^j \\ &= \delta_{m_2,m_2'}(-1)^{m_1'}(2\vec{\mathbf{k}}+\vec{\mathbf{p}})^{-m_1'} \end{aligned} \quad \text{(D.42)}$$

Ignoring isospin and using Eq. (D.42) with Eq. (4.9),Eq. (4.7b), and Eq. (D.20) we find the term we must project is

$$\begin{aligned} V_{JL} =& \sqrt{\frac{4\pi}{3}}g^{^3S_1-{}^1P_1}y_s\frac{1}{kp}\int d\Omega_p\int d\Omega_k\frac{1}{a+\hat{\mathbf{k}}\cdot\hat{\mathbf{p}}}\sum_{m_2}\sum_{m_L,m_S}\sum_{m_1',m_2'}\sum_{m_L',m_S'} \\ & C^{m_1',m_2',m_S'}_{1,1/2,S'}C^{0,m_2,m_S}_{0,1/2,S}C^{m_L,m_S,M}_{L,S,J}C^{m_L',m_S',M}_{L',S',J} \\ & Y^{m_L'\,*}_{L'}(\hat{\mathbf{p}})Y^{m_L}_{L}(\hat{\mathbf{k}})\sum_m\left(2kY_1^{-m_1'}(\hat{\mathbf{k}})+pY_1^{-m_1'}(\hat{\mathbf{p}})\right)(-1)^{m_1'}\delta_{m_2,m_2'} \end{aligned} \quad \text{(D.43)}$$

The angular integration can be trivially performed using Eq. (D.12) yielding

$$\begin{aligned} V_{JL} =& 4\pi g^{^3S_1-{}^1P_1}y_s\sqrt{\frac{\bar{L}}{\bar{L}'}}C^{0,0,0}_{L,1,L'}\sum_{m_L,m_S}\sum_{m_1'}\sum_{m_L',m_S'} \\ & C^{m_1',m_S,m_S'}_{1,S,S'}C^{m_L,m_S,M}_{L,S,J}C^{m_L',m_S',M}_{L',S',J}C^{m_L,-m_1',m_L}_{L,1,L'}(-1)^{m_1'}\delta_{S,1/2}\frac{1}{kp}\left(2kQ_{L'}(a)+pQ_L(a)\right) \end{aligned} \quad \text{(D.44)}$$

Again using the symmetry property Eq. (D.18) of the Clebsch-Gordan coefficients and the fact that $C^{0,m_2,m_S}_{0,1/2,S} = \delta_{S1/2}\delta_{m_S m_2}$ we find

$$V_{JL} = 4\pi g^{^3S_1 - {}^1P_1} y_s (-1)^{L+1-L'} \sqrt{\frac{\bar{L}'}{\bar{L}}} C^{0,0,0}_{L',1,L} \sum_{m_L,m_S} \sum_{m'_1} \sum_{m'_L,m'_S} \tag{D.45}$$
$$C^{m'_1,m_S,m'_S}_{1,S,S'} C^{m_L,m_S,M}_{L,S,J} C^{m'_L,m'_S,M}_{L',S',J} C^{m'_L,m'_1,m_L}_{L',1,L} \delta_{S,1/2} \frac{1}{kp} \left(2kQ_{L'}(a) + pQ_L(a)\right)$$

The resulting product of Clebsch-Gordan coefficients give the following diagram in Fig. D.4

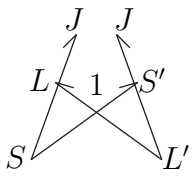

Figure D.4: Diagram representing Clebsch-Gordan coefficients in Eq. (D.45)

Finally rewriting the diagram in terms of 6-j symbols and taking into account phase factors we obtain the expression

$$V_{JL} = 4\pi g^{^3S_1 - {}^1P_1} y_s (-1)^{1/2+2S'+L-J} \delta_{S,1/2} \sqrt{\bar{L}'\bar{S}'} C^{0,0,0}_{L',1,L} \left\{ \begin{array}{ccc} L' & 1 & L \\ S & J & S' \end{array} \right\} \times \tag{D.46}$$
$$\times \frac{1}{kp} \left(2kQ_{L'}(a) + pQ_L(a)\right)$$

Now we will project out the term corresponding to the $g^{^3S_1 - {}^3P_1}$ coefficient. First the spin piece is projected out using the properties of spherical tensors and the Wigner-Eckart theorem giving

$$U_{JL} = \epsilon^{jm\ell}\langle 1/2, m_2'|\sigma^{\ell}|1/2, m_2\rangle(2\vec{\mathbf{k}}+\vec{\mathbf{p}})^m \tag{D.47}$$
$$= -i\sqrt{6}\sum_{m,m'} C^{m,m',m_1'}_{1,1,1} C^{m',m_2',m_2}_{1,1/2,1/2}(-1)^m(2\vec{\mathbf{k}}+\vec{\mathbf{p}})^{-m}$$

Combining Eq. (D.47) with (4.9),(4.7b), and (D.20) and ignoring isospin the term that must be projected is given by

$$V_{JL} = -i\sqrt{\frac{4\pi}{3}}g^{^3S_1-{}^3P_1}y_s\frac{1}{kp}\sqrt{6}\int d\Omega_p\int d\Omega_k\frac{1}{a+\hat{\mathbf{k}}\cdot\hat{\mathbf{p}}}\sum_{m_2}\sum_{m_L,m_S}\sum_{m_1',m_2'}\sum_{m_L',m_S'} \tag{D.48}$$
$$C^{m_1',m_2',m_S'}_{1,1/2,S'}C^{0,m_2,m_S}_{0,1/2,S}C^{m_L,m_S,M}_{L,S,J}C^{m_L',m_S',M}_{L',S',J}$$
$$Y^{m_L'\,*}_{L'}(\hat{\mathbf{p}})Y^{m_L}_{L}(\hat{\mathbf{k}})\sum_{m,m'}\left(2kY_1^{-m}(\hat{\mathbf{k}})+pY_1^{-m}(\hat{\mathbf{p}})\right)(-1)^m$$
$$C^{m,m',m_1'}_{1,1,1}C^{m',m_2',m_2}_{1,1/2,1/2}$$

The angular integration it trivially carried out via Eq. (D.12) yielding

$$V_{JL} = -i4\pi g^{^3S_1-{}^3P_1}y_s\sqrt{6}\sqrt{\frac{\bar{L}}{\bar{L}'}}C^{0,0,0}_{L,1,L'}\sum_{m_2}\sum_{m_L,m_S}\sum_{m_1',m_2'}\sum_{m_L',m_S'} \tag{D.49}$$
$$C^{m_1',m_2',m_S'}_{1,1/2,S'}C^{0,m_2,m_S}_{0,1/2,S}C^{m_L,m_S,M}_{L,S,J}C^{m_L',m_S',M}_{L',S',J}$$
$$(-1)^m C^{m_L,-m,m_L'}_{L,1,L'}C^{m,m',m_1'}_{1,1,1}C^{m',m_2',m_2}_{1,1/2,1/2}$$
$$\frac{1}{kp}(2kQ_{L'}(a)+pQ_L(a))$$

Again using symmetry property Eq. (D.18) of the Clebsch-Gordan coefficients and the fact that $C^{0,m_2,m_S}_{0,1/2,S} = \delta_{S1/2}\delta_{m_Sm_2}$ we find.

$$V_{JL} = -\, i4\pi g^{{}^3S_1-{}^3P_1} y_s \sqrt{6}\sqrt{\frac{\bar{L}'}{\bar{L}}}(-1)^{L'+1-L} C^{0,0,0}_{L',1,L} \sum_{m_2} \sum_{m_L,m_S} \sum_{m_1',m_2'} \sum_{m_L',m_S'} \tag{D.50}$$

$$\delta_{S1/2} C^{m_1',m_2',m_S'}_{1,1/2,S'} C^{m_L,m_S,M}_{L,S,J} C^{m_L',m_S',M}_{L',S',J} C^{m_L',m,m_L}_{L',1,L} C^{m,m',m_1'}_{1,1,1} C^{m',m_2',m_S}_{1,1/2,S}$$

$$\frac{1}{kp}(2kQ_{L'}(a) + pQ_L(a))$$

This product of Clebsch-Gordan coefficients is then represented through the following diagrams in Fig. D.5

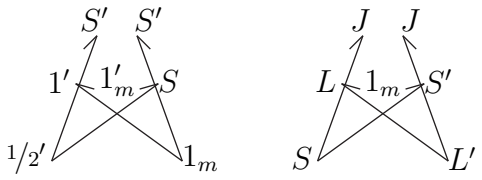

Figure D.5: Diagram representing Clebsch-Gordan coefficients in Eq. (D.50)

Replacing the diagrams with 6-j symbols and taking into account phase factors we obtain

$$V_{JL} = -\, i24\pi g^{{}^3S_1-{}^3P_1} y_s (-1)^{S'-L-J} \delta_{S1/2} \sqrt{\bar{S}'\bar{L}'} C^{0,0,0}_{L',1,L} \begin{Bmatrix} 1 & 1 & 1 \\ 1/2 & S' & 1/2 \end{Bmatrix} \times \tag{D.51}$$

$$\times \begin{Bmatrix} L' & 1 & L \\ S & J & S' \end{Bmatrix} \frac{1}{kp}(2kQ_{L'}(a) + pQ_L(a))$$

Now combining Eqs (D.41),(D.46), and (D.51) and adding the isospin projections, as well as the coefficients $g^{{}^1S_0-{}^3P_0}_{(\Delta I=0)}$ and $g^{{}^1S_0-{}^3P_0}_{(\Delta I=1)}$ we find the $\left[\boldsymbol{\mathcal{K}}(k,p)^J_{L'S',LS}\right]_{12}$ term projected out is

$$
\begin{aligned}
&- 8\pi\sqrt{3}(-1)^{1+S'+L-J}\delta_{S,1/2}y_t\left(\frac{2}{3}g^{^1S_0-{}^3P_0}_{(\Delta I=1)} - g^{^1S_0-{}^3P_0}_{(\Delta I=0)}\right)\times \qquad \text{(D.52)}\\
&\qquad \times C^{0,0,0}_{L',1,L}\sqrt{\bar{L}'\bar{S}'}\left(\frac{1}{2}\delta_{S'1/2}+\delta_{S'3/2}\right)\left\{\begin{array}{ccc} L' & 1 & L \\ S & J & S'\end{array}\right\}\frac{1}{kp}(kQ_{L'}(a)+2pQ_L(a))\\
&- y_s g^{^3S_1-{}^1P_1}4\pi\sqrt{3}(-1)^{1/2+2S'+L-J}\delta_{S,1/2}\sqrt{\bar{L}'\bar{S}'}C^{0,0,0}_{L',1,L}\left\{\begin{array}{ccc} L' & 1 & L \\ S & J & S'\end{array}\right\}\times\\
&\qquad \times\frac{1}{kp}\left(2kQ_{L'}(a)+pQ_L(a)\right)\\
&+ y_s g^{^3S_1-{}^3P_1}24\pi\frac{1}{\sqrt{3}}(-1)^{S'-L-J}\delta_{S1/2}\sqrt{\bar{S}'\bar{L}'}C^{0,0,0}_{L',1,L}\left\{\begin{array}{ccc} 1 & 1 & 1 \\ 1/2 & S' & 1/2\end{array}\right\}\times\\
&\qquad \times\left\{\begin{array}{ccc} L' & 1 & L \\ S & J & S'\end{array}\right\}\frac{1}{kp}(2kQ_{L'}(a)+pQ_L(a))
\end{aligned}
$$

D.1.3 Deuteron to Singlet Term

Now using time reversal symmetry the projection of the $\left[\boldsymbol{\mathcal{K}}(k,p)^J_{L'S',LS}\right]_{21}$ is easily obtained from the projection of the $\left[\boldsymbol{\mathcal{K}}(k,p)^J_{L'S',LS}\right]_{12}$ term, yielding

$$
\begin{aligned}
&- 8\pi\sqrt{3}(-1)^{1+S+L'-J}\delta_{S',1/2}y_t\left(\frac{2}{3}g^{^1S_0-{}^3P_0}_{(\Delta I=1)} - g^{^1S_0-{}^3P_0}_{(\Delta I=0)}\right)\times \qquad \text{(D.53)}\\
&\qquad\times C^{0,0,0}_{L,1,L'}\sqrt{\bar{L}\bar{S}}\left(\frac{1}{2}\delta_{S1/2}+\delta_{S3/2}\right)\left\{\begin{array}{ccc} L & 1 & L' \\ S' & J & S\end{array}\right\}\frac{1}{kp}(2kQ_{L'}(a)+pQ_L(a))\\
&- y_s g^{^3S_1-{}^1P_1}4\pi\sqrt{3}(-1)^{1/2+2S+L'-J}\delta_{S',1/2}\sqrt{\bar{L}\bar{S}}C^{0,0,0}_{L,1,L'}\left\{\begin{array}{ccc} L & 1 & L' \\ S' & J & S\end{array}\right\}\times\\
&\qquad\times\frac{1}{kp}\left(kQ_{L'}(a)+2pQ_L(a)\right)\\
&+ y_s g^{^3S_1-{}^3P_1}24\pi\frac{1}{\sqrt{3}}(-1)^{S-L'-J}\delta_{S'1/2}\sqrt{\bar{S}\bar{L}}C^{0,0,0}_{L,1,L'}\left\{\begin{array}{ccc} 1 & 1 & 1 \\ 1/2 & S & 1/2\end{array}\right\}\times\\
&\qquad\times\left\{\begin{array}{ccc} L & 1 & L' \\ S' & J & S\end{array}\right\}\frac{1}{kp}(kQ_{L'}(a)+2pQ_L(a))
\end{aligned}
$$

D.1.4 Singlet to Singlet Term

Now lastly we have to project out the singlet to singlet term. However, this is straightforward as there is four terms but they all have the same spin structure. Projecting out the spin structure in terms of sums of Clebsch-Gordan coefficients using the Wigner-Eckart theorem we find

$$
\begin{aligned}
U_{JL} &= \langle 1/2, m_2'|\sigma^m|1/2, m_2\rangle(\vec{\mathbf{k}}+2\vec{\mathbf{p}})^m \qquad \text{(D.54)}\\
&= \sqrt{3}C^{m_2,m,m_2'}_{1/2,1,1/2}(-1)^m(\vec{\mathbf{k}}+2\vec{\mathbf{p}})^{-m}
\end{aligned}
$$

Using Eq. (D.54) with (4.9),(4.7d), and (D.20) and ignoring isospin and the PV coefficients $g^{^1S_0-{}^3P_0}_{(\Delta I=0)}$ and $g^{^1S_0-{}^3P_0}_{(\Delta I=1)}$ for the time being we find the expression we must project is given by

$$V_{JL} = y_s\sqrt{\frac{4\pi}{3}}\frac{1}{kp}\int d\Omega_p \int d\Omega_k \frac{1}{a+\hat{\mathbf{k}}\cdot\hat{\mathbf{p}}} \sum_{m_2,m_2'}\sum_{m_L,m_S}\sum_{m_L',m_S'} \tag{D.55}$$
$$C^{0,m_2',m_S'}_{0,1/2,S'} C^{0,m_2,m_S}_{0,1/2,S} C^{m_L,m_S,M}_{L,S,J} C^{m_L',m_S',M}_{L',S',J}$$
$$Y^{m_L'\,*}_{L'}(\hat{\mathbf{p}}) Y^{m_L}_{L}(\hat{\mathbf{k}}) \sum_{m,m'}\left(2kY_1^{-m}(\hat{\mathbf{k}}) + pY_1^{-m}(\hat{\mathbf{p}})\right)$$
$$(-1)^m\sqrt{3}C^{m_2,m,m_2'}_{1/2,1,1/2}$$

The angular integration is carried out by use of Eq. (D.12) yielding

$$V_{JL} = 4\pi y_s\sqrt{3}\sqrt{\frac{\bar{L}}{\bar{L}'}}C^{0,0,0}_{L,1,L'} \sum_{m_2,m_2'}\sum_{m_L,m_S}\sum_{m_L',m_S'} \tag{D.56}$$
$$C^{0,m_2',m_S'}_{0,1/2,S'} C^{0,m_2,m_S}_{0,1/2,S} C^{m_L,m_S,M}_{L,S,J} C^{m_L',m_S',M}_{L',S',J}$$
$$(-1)^m C^{m_L,-m,m_L'}_{L,1,L'} C^{m_2,m,m_2'}_{1/2,1,1/2}$$
$$\frac{1}{kp}(kQ_{L'}(a) + 2pQ_L(a))$$

By the symmetry property Eq. (D.18) of the Clebsch-Gordan coefficients and the fact that $C^{0,m_2,m_S}_{0,1/2,S} = \delta_{S1/2}\delta_{m_S m_2}$ and $C^{0,m_2',m_S'}_{0,1/2,S'} = \delta_{S'1/2}\delta_{m_S' m_2'}$ we find

$$V_{JL} = 4\pi y_s\sqrt{3}(-1)^{L'+1-L}\sqrt{\frac{\bar{L}'}{\bar{L}}}C^{0,0,0}_{L',1,L} \sum_{m_L,m_S}\sum_{m_L',m_S'} \tag{D.57}$$
$$C^{m_L,m_S,M}_{L,S,J} C^{m_L',m_S',M}_{L',S',J} C^{m_L',m,m_L}_{L',1,L} C^{m_S,m,m_S'}_{S,1,S'}$$
$$\delta_{S',1/2}\delta_{S,1/2}\frac{1}{kp}(kQ_{L'}(a) + 2pQ_L(a))$$

The resulting product of Clebsch-Gordan coefficients can be represented diagrammatically by the diagram in Fig. D.6

Writing out the diagram as a 6-j symbol and taking into account phase factors we obtain

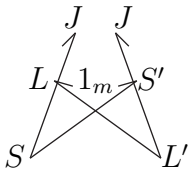

Figure D.6: Diagram representing Clebsch-Gordan coefficients in Eq. (D.57)

$$4\pi y_s\sqrt{6}(-1)^{1/2-L-J}\delta_{S',1/2}\delta_{S,1/2}\sqrt{\bar{L}'}C^{0,0,0}_{L',1,L}\left\{\begin{array}{ccc} L' & 1 & L \\ S & J & S' \end{array}\right\}\frac{1}{kp}(kQ_{L'}(a)+2pQ_L(a)) \tag{D.58}$$

Now combining Eq. (D.58) with isospin projections, the PV coefficients $g^{^1S_0-{}^3P_0}_{(\Delta I=0)}$ and $g^{^1S_0-{}^3P_0}_{(\Delta I=1)}$, and time reversal symmetry we find the projection of the $\left[\boldsymbol{\mathcal{K}}(k,p)^J_{L'S',LS}\right]_{22}$ term is

$$\begin{aligned} &-y_s g^{^1S_0-{}^3P_0}_{(\Delta I=0)}12\pi\sqrt{6}(-1)^{1/2-L-J}\delta_{S',1/2}\delta_{S,1/2}\sqrt{\bar{L}'}C^{0,0,0}_{L',1,L}\left\{\begin{array}{ccc} L' & 1 & L \\ S & J & S' \end{array}\right\}\times \\ &\times \quad \frac{1}{kp}(kQ_{L'}(a)+pQ_L(a)) \\ &+y_s g^{^1S_0-{}^3P_0}_{(\Delta I=1)}8\pi\sqrt{6}(-1)^{1/2-L-J}\delta_{S',1/2}\delta_{S,1/2}\sqrt{\bar{L}'}C^{0,0,0}_{L',1,L}\left\{\begin{array}{ccc} L' & 1 & L \\ S & J & S' \end{array}\right\}\times \\ &\times \quad \frac{1}{kp}(kQ_{L'}(a)+pQ_L(a)) \end{aligned} \tag{D.59}$$

Finally we note that for low energy parity-violation we are only concerned with S-P mixing. The appropriate projections of $(\boldsymbol{\mathcal{K}}^{xw})^{\beta b}_{\alpha a}(\vec{\mathbf{q}},\vec{\boldsymbol{\ell}})$ in total angular momentum J for S-P mixing are given below.

$$\mathcal{K}_{PV}(q,\ell)^{3/2}_{1^{3/2},0^{3/2}} = \frac{1}{q\ell}\begin{pmatrix} -8\sqrt{5}y_t^2 g_2\pi(\ell Q_0(a) + qQ_1(a)) & 0 \\ 0 & 0 \end{pmatrix} \tag{D.60}$$

$$\mathcal{K}^{11}_{PV}(q,\ell)^{3/2}_{1^{1/2},0^{3/2}} = 4\pi\frac{1}{q\ell}y_t^2(-2g_1\ell Q_0(a) - g_1 q Q_1(a) + g_2 q Q_1(a)) \tag{D.61}$$

$$\begin{aligned}\mathcal{K}^{21}_{PV}(q,\ell)^{3/2}_{1^{1/2},0^{3/2}} = y_s y_t\frac{1}{q\ell}\left(-8g_3 + \frac{16}{3}g_4 - 8g_1 - \frac{8}{3}g_2\right)\pi\ell Q_0(a) \\ y_s y_t\frac{1}{q\ell}\left(-16g_3 + \frac{32}{3}g_4 - 4g_1 - \frac{4}{3}g_2\right)\pi q Q_1(a)\end{aligned} \tag{D.62}$$

$$\mathcal{K}^{12}_{PV}(q,\ell)^{3/2}_{1^{1/2},0^{3/2}} = \mathcal{K}^{22}_{PV}(q,\ell)^{3/2}_{1^{1/2},0^{3/2}} = 0 \tag{D.63}$$

$$\mathcal{K}^{11}_{PV}(q,\ell)^{1/2}_{1^{3/2},0^{1/2}} = y_t^2\frac{1}{q\ell}\left(4\sqrt{2}g_1\ell\pi Q_0(a) - 4\sqrt{2}g_2\ell\pi Q_0(a) + 8\sqrt{2}g_1 q\pi Q_1(a)\right) \tag{D.64}$$

$$\begin{aligned}\mathcal{K}^{12}_{PV}(q,\ell)^{1/2}_{1^{3/2},0^{1/2}} = y_s y_t\frac{1}{q\ell}\left(16\sqrt{2}g_3 - \frac{32}{3}\sqrt{2}g_4 + 4\sqrt{2}g_1 + \frac{4}{3}\sqrt{2}g_2\right)\pi\ell Q_0(a) \\ + y_s y_t\frac{1}{q\ell}\left(8\sqrt{2}g_3 - \frac{16}{3}\sqrt{2}g_4 Q_1(a) + 8\sqrt{2}g_1 + \frac{8}{3}\sqrt{2}g_4\right)\pi q Q_1(a)\end{aligned} \tag{D.65}$$

$$\mathcal{K}^{21}_{PV}(q,\ell)^{1/2}_{1^{3/2},0^{1/2}} = \mathcal{K}^{22}_{PV}(q,\ell)^{1/2}_{1^{3/2},0^{1/2}} = 0 \tag{D.66}$$

$$\mathcal{K}^{11}_{PV}(q,\ell)^{1/2}_{1^1/_2,0^1/_2} = y_t^2 \frac{1}{q\ell}\left(-12 g_1 \ell\pi Q_0(a) + 8 g_2 \ell\pi Q_0(a)\right) \tag{D.67}$$
$$+ y_t^2 \frac{1}{q\ell}\left(-12 g_1 q\pi Q_1(a) + 8 g_2 q\pi Q_1(a)\right)$$

$$\mathcal{K}^{12}_{PV}(q,\ell)^{1/2}_{1^1/_2,0^1/_2} = y_s y_t \frac{1}{q\ell}\left(4g_3 - \frac{8}{3}g_4 - 8g_1 + \frac{16}{3}g_2\right)\pi\ell Q_0(a) \tag{D.68}$$
$$+ y_s y_t \frac{1}{q\ell}\left(8g_3 - \frac{16}{3}g_4 - 4g_1 + \frac{8}{3}g_2\right)\pi q Q_1(a)$$

$$\mathcal{K}^{21}_{PV}(q,\ell)^{1/2}_{1^1/_2,0^1/_2} = y_s y_t \frac{1}{q\ell}\left(8g_)3 - \frac{16}{3}g_4 - 4g_1 + \frac{8}{3}g_2\right)\pi\ell Q_0(a) \tag{D.69}$$
$$+ y_s y_t \frac{1}{q\ell}\left(4g_3 - \frac{8}{3}g_4 - 8g_1 + \frac{16}{3}g_2\right)\pi q Q_1(a)$$

$$\mathcal{K}^{22}_{PV}(q,\ell)^{1/2}_{1^1/_2,0^1/_2} = y_s^2 \frac{1}{q\ell}\left(4\ell\pi g_3 Q_0(a) - \frac{8}{3}\ell\pi g_4 Q_0(a)\right) \tag{D.70}$$
$$+ y_s^2 \frac{1}{q\ell}\left(4q\pi g_3 Q_1(a) - \frac{8}{3}q\pi g_4 Q_1(a)\right)$$

D.2 SD Mixing Projection

In this section we will show how to project out the SD mixing terms that occur at NNLO in nd scattering, and then show that they average to zero as claimed.

D.2.1 Deuteron to Deuteron Term

We will first project out the deuteron to deuteron amplitude for SD mixing for which the corresponding Feynman diagrams are given in Fig D.7. Note the circle in the diagram represents a vertex from the Lagrangian Eq. (3.7)

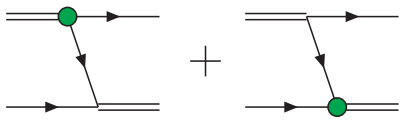

Figure D.7: Feynman diagrams of SD mixing deuteron in initial and final state

We will only project out the first diagram as the second one is related by time reversal symmetry. The part of the the diagram that must be projected out is given by Eq. (D.71) where i (j) are the initial (final) deuteron polarization, α (β) the initial (final) neutron spinor index, and a (b) the initial (final) isospinor index.

$$\frac{1}{kp}\frac{1}{a+\hat{\mathbf{k}}\cdot\hat{\mathbf{p}}}(\sigma^\ell\sigma^j)^\beta_\alpha\delta^b_a\left((2\vec{\mathbf{p}}+\vec{\mathbf{k}})^i(2\vec{\mathbf{p}}+\vec{\mathbf{k}})^\ell-\frac{1}{3}\delta_{i\ell}(2\vec{\mathbf{p}}+\vec{\mathbf{k}})^2\right) \tag{D.71}$$

We will first project out the $k^\ell k^j$ term. The spin structure is projected out using the Wigner-Eckart theorem giving Eq. (D.72)

$$\begin{aligned} U_{JL} &= \langle 1/2 m_2'|\sigma^m\sigma^{-m_1'}|1/2 m_2\rangle \\ &= -\frac{1}{\sqrt{3}}\sum_{\kappa,q}\sqrt{\bar{\kappa}}C^{m_1',q,m}_{1,\kappa,1}C^{m_2,q,m_2'}_{1/2,\kappa,1/2}\langle 1/2||T_\kappa||1/2\rangle \end{aligned} \tag{D.72}$$

Combining (D.72) with our definition for projection in total angular momentum we find our expression for the projection of the k^ik^j term is given by

$$\begin{aligned} V_{JL} = &-\frac{4\pi}{3}\frac{1}{\sqrt{3}}\frac{1}{kp}\int d\Omega_p\int d\Omega_k\frac{1}{a+\hat{\mathbf{k}}\cdot\hat{\mathbf{p}}}\sum_{m_1,m_2}\sum_{m_L,m_S}\sum_{m_1',m_2'}\sum_{m_L',m_S'}\sum_m\sum_{\kappa,q} \\ &C^{m_1,m_2m_S}_{1,1/2,S}C^{m_1',m_2'm_S'}_{1,1/2,S'}C^{m_L,m_S,M}_{L,S,J}C^{m_L',m_S',M}_{L',S',J} \\ &Y^{m_L'\,*}_{L'}(\hat{\mathbf{p}})Y^{m_L}_L(\hat{\mathbf{k}})k^2Y^{m_1}_1(\hat{\mathbf{k}})Y^{-m}_1(\hat{\mathbf{k}})(-1)^{m_1'+m}\sqrt{\bar{\kappa}}C^{m_1',q,m}_{1,\kappa,1}C^{m_2,q,m_2'}_{1/2,\kappa,1/2}\langle 1/2||T_\kappa||1/2\rangle \end{aligned} \tag{D.73}$$

Integrating over the angular variables using Eq. (D.13) we obtain

$$-\frac{4\pi}{\sqrt{3}}k^2\sqrt{\frac{\bar{L}}{\bar{L}'}}\sum_{m_1,m_2}\sum_{m_L,m_S}\sum_{m_1',m_2'}\sum_{m_L',m_S'}\sum_{L'',m''}\sum_{\kappa,q}\sum_{m} \tag{D.74}$$
$$C^{m_1,m_2m_S}_{1,1/2,S}C^{m_1',m_2'm_S'}_{1,1/2,S'}C^{m_L,m_S,M}_{L,S,J}C^{m_L',m_S',M}_{L',S',J}C^{m_1,-m,m''}_{1,1,L''}$$
$$C^{m_L,m'',m_L'}_{L,L'',L'}C^{m_1',q,m}_{1,\kappa,1}C^{m_2,q,m_2'}_{1/2,\kappa,1/2}(-1)^m\sqrt{\bar{\kappa}}\langle 1/2||T_\kappa||1/2\rangle C^{0,0,0}_{1,1,L''}C^{0,0,0}_{L,L'',L'}\frac{1}{kp}Q_{L'}(a)$$

Now using symmetry property Eq. (D.18) of the Clebsch-Gordan coefficients we find

$$\frac{4\pi}{3}k^2\sqrt{\frac{\bar{L}}{\bar{L}'}}\sum_{m_1,m_2}\sum_{m_L,m_S}\sum_{m_1',m_2'}\sum_{m_L',m_S'}\sum_{L'',m''}\sum_{\kappa,q}\sum_{m} \tag{D.75}$$
$$\sqrt{\bar{L}''}C^{m_1,m_2m_S}_{1,1/2,S}C^{m_1',m_2'm_S'}_{1,1/2,S'}C^{m_L,m_S,M}_{L,S,J}C^{m_L',m_S',M}_{L',S',J}C^{m,m'',m_1}_{1,L'',1}$$
$$C^{m_L,m'',m_L'}_{L,L'',L'}C^{m_1',q,m}_{1,\kappa,1}C^{m_2,q,m_2'}_{1/2,\kappa,1/2}\sqrt{\bar{\kappa}}\langle 1/2||T_\kappa||1/2\rangle C^{0,0,0}_{1,1,L''}C^{0,0,0}_{L,L'',L'}\frac{1}{kp}Q_{L'}(a)$$

This product of Clebsch-Gordan coefficients can be written as the following set of diagrams given in Fig. D.8

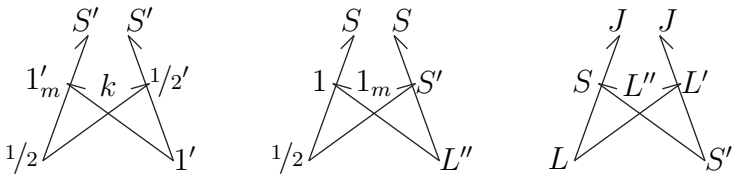

Figure D.8: Diagrams representing Clebsch-Gordan coefficients in Eq. (D.75)

Rewriting the diagrams as 6-j symbols and adding the appropriate phase factors we find our expression reduces to

$$4\pi\sqrt{2}k^2\sqrt{\bar{S}\bar{S}'\bar{L}}\sum_{\kappa,L''}C^{0,0,0}_{1,1,L''}C^{0,0,0}_{L,L'',L'}(-1)^{2S'+S+L+L''-J}\sqrt{\bar{\kappa}\bar{L}''} \tag{D.76}$$
$$\langle 1/2||T_\kappa||1/2\rangle \left\{ \begin{array}{ccc} 1 & \kappa & 1 \\ 1/2 & S' & 1/2 \end{array} \right\} \left\{ \begin{array}{ccc} L'' & 1 & 1 \\ 1/2 & S & S' \end{array} \right\} \left\{ \begin{array}{ccc} S' & L'' & S \\ L & J & L' \end{array} \right\} \frac{1}{kp} Q_{L'}(a)$$

Finally using Eq. (D.28) we find the sum over κ can be removed leaving the final expression

$$4\pi k^2\sqrt{\bar{S}\bar{S}'\bar{L}}\left(\delta_{S',1/2}+2\delta_{S',3/2}\right)\sum_{k,L''}C^{0,0,0}_{1,1,L''}C^{0,0,0}_{L,L'',L'}(-1)^{2S'+S+L+L''-J}\sqrt{\bar{L}''}\times \tag{D.77}$$
$$\times \left\{ \begin{array}{ccc} L'' & 1 & 1 \\ 1/2 & S & S' \end{array} \right\} \left\{ \begin{array}{ccc} S' & L'' & S \\ L & J & L' \end{array} \right\} \frac{1}{kp} Q_{L'}(a)$$

Next we project out the $p^\ell p^j$ term which has the same spin structure as the $k^\ell k^j$ term which is projected out by Eq. (D.72). The projection for the $p^\ell p^j$ term is given by

$$-\frac{16\pi}{3}\frac{1}{\sqrt{3}}p^2\frac{1}{kp}\int d\Omega_p\int d\Omega_k\frac{1}{a+\hat{\mathbf{k}}\cdot\hat{\mathbf{p}}}\sum_{m_1,m_2}\sum_{m_L,m_S}\sum_{m'_1,m'_2}\sum_{m'_L,m'_S}\sum_{m}\sum_{\kappa,q} \tag{D.78}$$
$$C^{m_1,m_2m_S}_{1,1/2,S}C^{m'_1,m'_2m'_S}_{1,1/2,S'}C^{m_L,m_S,M}_{L,S,J}C^{m'_L,m'_S,M}_{L',S',J}$$
$$Y^{m'_L\,*}_{L'}(\hat{\mathbf{p}})Y^{m_L}_{L}(\hat{\mathbf{k}})Y^{m_1}_{1}(\hat{\mathbf{p}})Y^{-m}_{1}(\hat{\mathbf{p}})(-1)^{m'_1+m}\sqrt{\bar{\kappa}}C^{m'_1,q,m}_{1,\kappa,1}C^{m_2,q,m'_2}_{1/2,\kappa,1/2}\langle 1/2||T_\kappa||1/2\rangle$$

Integrating over the angular variables using Eq. (D.14) we find

$$-\frac{16\pi}{\sqrt{3}}p^2\sqrt{\frac{\bar{L}}{\bar{L}'}}\sum_{m_1,m_2}\sum_{m_L,m_S}\sum_{m_1',m_2'}\sum_{m_L',m_S'}\sum_{L'',m''}\sum_{\kappa,q}\sum_{m} \tag{D.79}$$

$$C^{m_1,m_2m_S}_{1,1/2,S}C^{m_1',m_2'm_S'}_{1,1/2,S'}C^{m_L,m_S,M}_{L,S,J}C^{m_L',m_S',M}_{L',S',J}C^{m_1,-m,m''}_{1,1,L''}$$

$$C^{m_L,m'',m_L'}_{L,L'',L'}C^{m_1',q,m}_{1,\kappa,1}C^{m_2,q,m_2'}_{1/2,\kappa,1/2}(-1)^m\sqrt{\bar{\kappa}}\langle 1/2||T_\kappa||1/2\rangle C^{0,0,0}_{1,1,L''}C^{0,0,0}_{L,L'',L'}\frac{1}{kp}Q_L(a)$$

We note that this is exactly the same as the $k^\ell k^j$ term except for the factor of four, the p^2 and the $Q_L(a)$, thus the end result will be virtually the same as the $k^\ell k^j$ term except for these minor modifications. Therefore the final form of the the projected $p^\ell p^j$ term is given by

$$16\pi p^2\sqrt{\bar{S}\bar{S}'\bar{L}}\left(\delta_{S',1/2}+2\delta_{S',3/2}\right)\sum_{k,L''}C^{0,0,0}_{1,1,L''}C^{0,0,0}_{L,L'',L'}(-1)^{2S'+S+L+L''-J}\sqrt{\bar{L}''}\times \tag{D.80}$$

$$\times\left\{\begin{array}{ccc} L'' & 1 & 1 \\ 1/2 & S & S' \end{array}\right\}\left\{\begin{array}{ccc} S' & L'' & S \\ L & J & L' \end{array}\right\}\frac{1}{kp}Q_L(a)$$

We now project out the $k^\ell p^j$ term. Noting that the projected spin structure is still given by Eq. (D.72) the expression we must project for the $k^\ell p^j$ term is

$$-\frac{8\pi}{3}\frac{1}{\sqrt{3}}\frac{1}{kp}\int d\Omega_p\int d\Omega_k\frac{1}{a+\hat{\mathbf{k}}\cdot\hat{\mathbf{p}}}\sum_{m_1,m_2}\sum_{m_L,m_S}\sum_{m_1',m_2'}\sum_{m_L',m_S'}\sum_{m}\sum_{\kappa,q} \tag{D.81}$$

$$C^{m_1,m_2m_S}_{1,1/2,S}C^{m_1',m_2'm_S'}_{1,1/2,S'}C^{m_L,m_S,M}_{L,S,J}C^{m_L',m_S',M}_{L',S',J}$$

$$Y^{m_L'\,*}_{L'}(\hat{\mathbf{p}})Y^{m_L}_{L}(\hat{\mathbf{k}})kpY^{m_1}_1(\hat{\mathbf{p}})Y^{-m}_1(\hat{\mathbf{k}})(-1)^{m_1'+m}\sqrt{\bar{\kappa}}C^{m_1',q,m}_{1,\kappa,1}C^{m_2,q,m_2'}_{1/2,\kappa,1/2}\langle 1/2||T_\kappa||1/2\rangle$$

Integration over the angular variables is performed via Eq. (D.15) yielding

$$-\frac{8\pi}{\sqrt{3}}kp\sqrt{\frac{\bar{L}}{\bar{L}'}}\sum_{m_1,m_2}\sum_{m_L,m_S}\sum_{m_1',m_2'}\sum_{m_L',m_S'}\sum_{L'',m''}\sum_{\kappa,q}\sum_{m} \tag{D.82}$$

$$C^{m_1,m_2m_S}_{1,1/2,S}C^{m_1',m_2'm_S'}_{1,1/2,S'}C^{m_L,m_S,M}_{L,S,J}C^{m_L',m_S',M}_{L',S',J}C^{m_L,-m,m''}_{L,1,L''}$$

$$C^{m'',m_1,m_L'}_{L'',1,L'}C^{m_1',q,m}_{1,\kappa,1}C^{m_2,q,m_2'}_{1/2,\kappa,1/2}(-1)^m\sqrt{\bar{\kappa}}\langle 1/2||T_\kappa||1/2\rangle C^{0,0,0}_{L,1,L''}C^{0,0,0}_{L'',1,L'}\frac{1}{kp}Q_{L''}(a)$$

Now using symmetry property Eq. (D.18) of the Clebsch-Gordan coefficients we find

$$\frac{8\pi}{\sqrt{3}}kp\sqrt{\frac{1}{\bar{L}'}}\sum_{m_1,m_2}\sum_{m_L,m_S}\sum_{m_1',m_2'}\sum_{m_L',m_S'}\sum_{L'',m''}\sum_{\kappa,q}\sum_{m} \tag{D.83}$$

$$\sqrt{\bar{L}''}C^{m_1,m_2m_S}_{1,1/2,S}C^{m_1',m_2'm_S'}_{1,1/2,S'}C^{m_L,m_S,M}_{L,S,J}C^{m_L',m_S',M}_{L',S',J}C^{m,m'',m_L}_{1,L'',L}$$

$$C^{m'',m_1,m_L'}_{L'',1,L'}C^{m_1',q,m}_{1,\kappa,1}C^{m_2,q,m_2'}_{1/2,\kappa,1/2}\sqrt{\bar{\kappa}}\langle 1/2||T_\kappa||1/2\rangle C^{0,0,0}_{L,1,L''}C^{0,0,0}_{L'',1,L'}\frac{1}{kp}Q_{L''}(a)$$

This product of Clebsch-Gordan coefficients can be represented by the following set of diagrams in Fig D.9

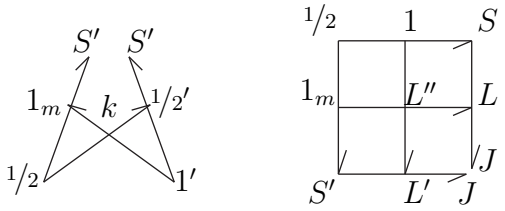

Figure D.9: Diagram representing Clebsch-Gordan coefficients in Eq. (D.83)

Using the definition of the diagrams as 6-j and 9-j symbols and taking into account phase factors our expression is reduced to

$$8\pi\sqrt{2}\sqrt{\bar{S}\bar{S}'\bar{L}}\sum_{\kappa,L''}C^{0,0,0}_{L,1,L''}C^{0,0,0}_{L'',1,L'}(-1)^{3/2-S'-L-L''}\sqrt{\bar{\kappa}\bar{L''}}\langle 1/2||T_\kappa||1/2\rangle\times \tag{D.84}$$
$$\times\left\{\begin{array}{ccc}1&\kappa&1\\1/2&S'&1/2\end{array}\right\}\left\{\begin{array}{ccc}1/2&1&S\\1&L''&L\\S'&L'&J\end{array}\right\}Q_{L''}(a)$$

Finally using Eq. (D.28) the sum over κ can be removed and our expression reduces to its final form

$$8\pi\sqrt{\bar{S}\bar{S}'\bar{L}}\left(\delta_{S',1/2}+2\delta_{S',3/2}\right)\sum_{L''}C^{0,0,0}_{L,1,L''}C^{0,0,0}_{L'',1,L'}\times \tag{D.85}$$
$$\times(-1)^{3/2-S'-L-L''}\sqrt{\bar{L''}}\left\{\begin{array}{ccc}1/2&1&S\\1&L''&L\\S'&L'&J\end{array}\right\}Q_{L''}(a)$$

We now project out the k^jp^ℓ term. Again we note the spin structure is projected out by Eq. (D.72), thus our projection is given by

$$-\frac{8\pi}{3}\frac{1}{\sqrt{3}}\frac{1}{kp}\int d\Omega_p\int d\Omega_k\frac{1}{a+\hat{\mathbf{k}}\cdot\hat{\mathbf{p}}}\sum_{m_1,m_2}\sum_{m_L,m_S}\sum_{m_1',m_2'}\sum_{m_L',m_S'}\sum_m\sum_{\kappa,q} \tag{D.86}$$
$$C^{m_1,m_2m_S}_{1,1/2,S}C^{m_1',m_2'm_S'}_{1,1/2,S'}C^{m_L,m_S,M}_{L,S,J}C^{m_L',m_S',M}_{L',S',J}$$
$$Y^{m_L'\,*}_{L'}(\hat{\mathbf{p}})Y^{m_L}_L(\hat{\mathbf{k}})kpY^{m_1}_1(\hat{\mathbf{k}})Y^{-m}_1(\hat{\mathbf{p}})(-1)^{m_1'+m}\sqrt{\bar{\kappa}}C^{m_1',q,m}_{1,\kappa,1}C^{m_2,q,m_2'}_{1/2,\kappa,1/2}\langle 1/2||T_\kappa||1/2\rangle$$

Next the angular integration can be carried out trivially using Eq. (D.15) yielding

$$-\frac{8\pi}{\sqrt{3}}kp\sqrt{\frac{\bar{\bar{L}}}{\bar{\bar{L}}'}}\sum_{m_1,m_2}\sum_{m_L,m_S}\sum_{m_1',m_2'}\sum_{m_L',m_S'}\sum_{L'',m''}\sum_{\kappa,q}\sum_{m} \tag{D.87}$$

$$C^{m_1,m_2m_S}_{1,1/2,S}C^{m_1',m_2'm_S'}_{1,1/2,S'}C^{m_L,m_S,M}_{L,S,J}C^{m_L',m_S',M}_{L',S',J}C^{m_L,m_1,m''}_{L,1,L''}$$

$$C^{m'',-m,m_L'}_{L'',1,L'}C^{m_1',q,m}_{1,\kappa,1}C^{m_2,q,m_2'}_{1/2,\kappa,1/2}(-1)^m\sqrt{\bar{\kappa}}\langle 1/2||T_\kappa||1/2\rangle C^{0,0,0}_{L,1,L''}C^{0,0,0}_{L'',1,L'}\frac{1}{kp}Q_{L''}(a)$$

Using the symmetry property Eq. (D.18) of the Clebsch-Gordan coefficients we find.

$$\frac{8\pi}{\sqrt{3}}kp\sqrt{\bar{L}}\sum_{m_1,m_2}\sum_{m_L,m_S}\sum_{m_1',m_2'}\sum_{m_L',m_S'}\sum_{L'',m''}\sum_{\kappa,q}\sum_{m} \tag{D.88}$$

$$\frac{1}{\sqrt{\bar{\bar{L}}''}}C^{m_1,m_2m_S}_{1,1/2,S}C^{m_1',m_2'm_S'}_{1,1/2,S'}C^{m_L,m_S,M}_{L,S,J}C^{m_L',m_S',M}_{L',S',J}C^{m_L,m_1,m_L}_{L,1,L''}$$

$$C^{m,m_L',m''}_{1,L',L''}C^{m_1',q,m}_{1,\kappa,1}C^{m_2,q,m_2'}_{1/2,\kappa,1/2}\sqrt{\bar{\kappa}}\langle 1/2||T_\kappa||1/2\rangle C^{0,0,0}_{L,1,L''}C^{0,0,0}_{L'',1,L'}\frac{1}{kp}Q_{L''}(a)$$

The resulting product of Clebsch-Gordan coefficients is represented by the following series of diagrams given in Fig. D.10

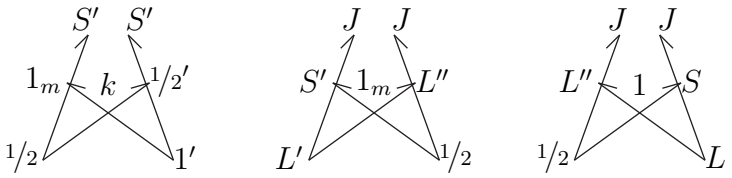

Figure D.10: Diagrams representing Clebsch-Gordan coefficients in Eq. (D.88)

Turning the diagrams into the appropriate 6-j symbols and taking into account phase factors we find

$$8\pi\sqrt{2}\sqrt{\bar{S}\bar{S}'\bar{L}}\sum_{\kappa,L''}C^{0,0,0}_{L,1,L''}C^{0,0,0}_{L'',1,L'}(-1)^{1/2+S'+L+L''}\sqrt{\bar{\kappa}\bar{L}''} \tag{D.89}$$
$$\langle 1/2||T_\kappa||1/2\rangle \begin{Bmatrix} 1 & \kappa & 1 \\ 1/2 & S' & 1/2 \end{Bmatrix} \begin{Bmatrix} 1/2 & 1 & S' \\ L' & J & L'' \end{Bmatrix} \begin{Bmatrix} L & 1 & L'' \\ 1/2 & J & S \end{Bmatrix} Q_{L''}(a)$$

Finally using Eq. (D.28) we obtain the final form

$$8\pi\sqrt{\bar{S}\bar{S}'\bar{L}}\left(\delta_{S',1/2}+2\delta_{S',3/2}\right)\sum_{L''}C^{0,0,0}_{L,1,L''}C^{0,0,0}_{L'',1,L'}(-1)^{1/2+S'+L+L''}\times \tag{D.90}$$
$$\times\sqrt{\bar{L}''}\begin{Bmatrix} 1/2 & 1 & S' \\ L' & J & L'' \end{Bmatrix} \begin{Bmatrix} L & 1 & L'' \\ 1/2 & J & S \end{Bmatrix} Q_{L''}(a)$$

We now project out the $\vec{\mathbf{k}}^2$ term. The spin structure for the $\vec{\mathbf{k}}^2$ term is projected out by the Wigner-Eckart theorem and is given by

$$\begin{aligned} U_{JL} &= \langle 1/2 m_2'|\sigma^{m_1}\sigma^{-m_1'}|1/2 m_2\rangle \\ &= -\frac{1}{\sqrt{3}}\sum_{\kappa,q}\sqrt{\bar{\kappa}}C^{m_1',q,m_1}_{1,\kappa,1}C^{m_2,q,m_2'}_{1/2,\kappa,1/2}\langle 1/2||T_\kappa||1/2\rangle \end{aligned} \tag{D.91}$$

Now using Eq. (D.91) with our definition for projecting into total angular momentum we find the following projection

$$\frac{4\pi}{9}\frac{1}{\sqrt{3}}\frac{1}{kp}\int d\Omega_p\int d\Omega_k\frac{1}{a+\hat{\mathbf{k}}\cdot\hat{\mathbf{p}}}\sum_{m_1,m_2}\sum_{m_L,m_S}\sum_{m_1',m_2'}\sum_{m_L',m_S'}\sum_{m}\sum_{\kappa,q} \tag{D.92}$$
$$C^{m_1,m_2m_S}_{1,1/2,S}C^{m_1',m_2'm_S'}_{1,1/2,S'}C^{m_L,m_S,M}_{L,S,J}C^{m_L',m_S',M}_{L',S',J}$$
$$Y^{m_L'\,*}_{L'}(\hat{\mathbf{p}})Y^{m_L}_{L}(\hat{\mathbf{k}})k^2Y^{m}_{1}(\hat{\mathbf{k}})Y^{-m}_{1}(\hat{\mathbf{k}})(-1)^m\sqrt{\bar{\kappa}}C^{m_1',q,m_1}_{1,\kappa,1}C^{m_2,q,m_2'}_{1/2,\kappa,1/2}\langle 1/2||T_\kappa||1/2\rangle$$

Integrating over the angular variables via Eq. (D.13) we find

$$\frac{4\pi}{3\sqrt{3}}k^2\sqrt{\frac{\bar{L}}{\bar{L}'}}\sum_{m_1,m_2}\sum_{m_L,m_S}\sum_{m_1',m_2'}\sum_{m_L',m_S'}\sum_{L'',m''}\sum_{\kappa,q}\sum_{m} \tag{D.93}$$
$$C^{m_1,m_2m_S}_{1,1/2,S}C^{m_1',m_2'm_S'}_{1,1/2,S'}C^{m_L,m_S,M}_{L,S,J}C^{m_L',m_S',M}_{L',S',J}C^{m,-m,m''}_{1,1,L''}$$
$$C^{m_L,m'',m_L'}_{L,L'',L'}C^{m_1',q,m_1}_{1,\kappa,1}C^{m_2,q,m_2'}_{1/2,\kappa,1/2}(-1)^m\sqrt{\bar{\kappa}}\langle 1/2||T_\kappa||1/2\rangle C^{0,0,0}_{1,1,L''}C^{0,0,0}_{L,L'',L'}\frac{1}{kp}Q_{L'}(a)$$

Next using Eq. (D.16) we can sum over m and find that $L''=0$ and our expression reduces to.

$$-\frac{4\pi}{3}k^2\sqrt{\frac{\bar{L}}{\bar{L}'}}\sum_{m_1,m_2}\sum_{m_L,m_S}\sum_{m_1',m_2'}\sum_{m_L',m_S'}\sum_{\kappa,q} \tag{D.94}$$
$$C^{m_1,m_2m_S}_{1,1/2,S}C^{m_1',m_2'm_S'}_{1,1/2,S'}C^{m_L,m_S,M}_{L,S,J}C^{m_L',m_S',M}_{L',S',J}$$
$$C^{m_L,0,m_L'}_{L,0,L'}C^{m_1',q,m_1}_{1,\kappa,1}C^{m_2,q,m_2'}_{1/2,\kappa,1/2}\sqrt{\bar{\kappa}}\langle 1/2||T_\kappa||1/2\rangle C^{0,0,0}_{1,1,0}C^{0,0,0}_{L,0,L'}\frac{1}{kp}Q_{L'}(a)$$

Noting that $C^{0,0,0}_{1,1,0}=-1/\sqrt{3}$ and $C^{0,0,0}_{L,0,L'}=\delta_{L'L}$ we find

$$\frac{4\pi}{3\sqrt{3}}k^2\sum_{m_1,m_2}\sum_{m_L,m_S}\sum_{m_1',m_2'}\sum_{m_S'}\sum_{\kappa,q} \tag{D.95}$$
$$C^{m_1,m_2m_S}_{1,1/2,S}C^{m_1',m_2'm_S'}_{1,1/2,S'}C^{m_L,m_S,M}_{L,S,J}C^{m_L,m_S',M}_{L,S',J}$$
$$C^{m_1',q,m_1}_{1,\kappa,1}C^{m_2,q,m_2'}_{1/2,\kappa,1/2}\sqrt{\bar{\kappa}}\langle 1/2||T_\kappa||1/2\rangle\delta_{L,L'}\frac{1}{kp}Q_{L'}(a)$$

Just using some of the resulting Clebsch-Gordan coefficients we find the following diagrams given in Fig. D.11

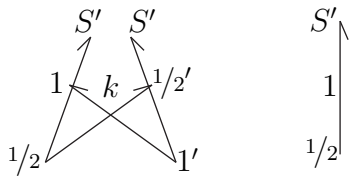

Figure D.11: Diagrams representing Clebsch-Gordan coefficients in Eq. (D.95)

The first diagram is simply gives an appropriate 6-j symbol with additional factors. The remaining single line diagram represents the Clebsch-Gordan coefficient $C^{m_1,m_2,m'_S}_{1,1/2,S'}$. This Clebsch-Gordan coefficient can be used with the remaining Clebsch-Gordan coefficient $C^{m_1,m_2,m_S}_{1,1/2,S}$ by using the orthogonality of Clebsch-Gordan coefficients given in Eq. (D.17). Using these two Clebsch-Gordan coefficients and orthogonality we get a Kronecker delta $\delta_{S'S}$. Finally we are left with two Clebsch-Gordan coefficients that are exactly the same and are $C^{m_L,m_S,M}_{L,S,J}$. Again using orthogonality of the Clebsch-Gordan coefficients it can be shown that these two Clebsch-Gordan coefficients after summing over the magnetic quantum numbers give one. Hence our expression reduces to

$$\frac{4\pi}{3}\sqrt{2}k^2\delta_{L,L'}\delta_{S,S'}\sum_{\kappa}(-1)^{1/2-S'}\sqrt{\bar{\kappa}}\langle 1/2||T_\kappa||1/2\rangle \begin{Bmatrix} 1 & \kappa & 1 \\ 1/2 & S' & 1/2 \end{Bmatrix} \frac{1}{kp}Q_{L'}(a) \quad \text{(D.96)}$$

Finally using Eq. (D.28) we find the final form for our expression

$$\frac{4\pi}{3}k^2\delta_{L,L'}\delta_{S,S'}(-1)^{1/2-S'}\left(\delta_{S',1/2}+2\delta_{S',3/2}\right)\frac{1}{kp}Q_{L'}(a) \quad \text{(D.97)}$$

We now project out the $\vec{\mathbf{p}}^2$ term and noting that the spin projection is again given by Eq. (D.91) we find our term to be projected is

$$\frac{16\pi}{9}\frac{1}{\sqrt{3}}\frac{1}{kp}\int d\Omega_p \int d\Omega_k \frac{1}{a+\hat{\mathbf{k}}\cdot\hat{\mathbf{p}}} \sum_{m_1,m_2}\sum_{m_L,m_S}\sum_{m_1',m_2'}\sum_{m_L',m_S'}\sum_{m}\sum_{\kappa,q} \tag{D.98}$$
$$C^{m_1,m_2m_S}_{1,1/2,S} C^{m_1',m_2'm_S'}_{1,1/2,S'} C^{m_L,m_S,M}_{L,S,J} C^{m_L',m_S',M}_{L',S',J}$$
$$Y^{m_L'\,*}_{L'}(\hat{\mathbf{p}}) Y^{m_L}_{L}(\hat{\mathbf{k}}) p^2 Y^{m}_{1}(\hat{\mathbf{p}}) Y^{-m}_{1}(\hat{\mathbf{p}}) (-1)^m \sqrt{\kappa} C^{m_1',q,m_1}_{1,\kappa,1} C^{m_2,q,m_2'}_{1/2,\kappa,1/2} \langle 1/2||T_\kappa||1/2\rangle$$

The angular integration is performed trivially using Eq. (D.14) yielding

$$\frac{16\pi}{3\sqrt{3}} p^2 \sqrt{\frac{\bar{L}}{\bar{L}'}} \sum_{m_1,m_2}\sum_{m_L,m_S}\sum_{m_1',m_2'}\sum_{m_L',m_S'}\sum_{L'',m''}\sum_{\kappa,q}\sum_{m} \tag{D.99}$$
$$C^{m_1,m_2m_S}_{1,1/2,S} C^{m_1',m_2'm_S'}_{1,1/2,S'} C^{m_L,m_S,M}_{L,S,J} C^{m_L',m_S',M}_{L',S',J} C^{m,-m,m''}_{1,1,L''}$$
$$C^{m_L,m'',m_L'}_{L,L'',L'} C^{m_1',q,m_1}_{1,\kappa,1} C^{m_2,q,m_2'}_{1/2,\kappa,1/2} (-1)^m \sqrt{\kappa} \langle 1/2||T_\kappa||1/2\rangle C^{0,0,0}_{1,1,L''} C^{0,0,0}_{L,L'',L'} \frac{1}{kp} Q_L(a)$$

We note this has the same form as the $\vec{\mathbf{k}}^2$ term except for the factor of four, the p^2, and the $Q_L(a)$, therefore we can use the answer we obtained for the $\vec{\mathbf{k}}^2$ term with slight modifications. The projected $\vec{\mathbf{p}}^2$ term is given by

$$\frac{16\pi}{3} p^2 \delta_{L,L'}\delta_{S,S'} (-1)^{1/2-S'} \left(\delta_{S',1/2} + 2\delta_{S',3/2}\right) \frac{1}{kp} Q_L(a) \tag{D.100}$$

Finally we project out the $\vec{\mathbf{k}}\cdot\vec{\mathbf{p}}$ term noting again that the spin structure projected out is given by Eq. (D.91) we find the term we must project is given by

$$\frac{16\pi}{9}\frac{1}{\sqrt{3}}\frac{1}{kp}\int d\Omega_p \int d\Omega_k \frac{1}{a+\hat{\mathbf{k}}\cdot\hat{\mathbf{p}}} \sum_{m_1,m_2}\sum_{m_L,m_S}\sum_{m_1',m_2'}\sum_{m_L',m_S'}\sum_{m}\sum_{\kappa,q} \tag{D.101}$$

$$C^{m_1,m_2m_S}_{1,1/2,S} C^{m_1',m_2'm_S'}_{1,1/2,S'} C^{m_L,m_S,M}_{L,S,J} C^{m_L',m_S',M}_{L',S',J}$$

$$Y^{m_L'\,*}_{L'}(\hat{\mathbf{p}}) Y^{m_L}_{L}(\hat{\mathbf{k}}) kp Y^{m}_{1}(\hat{\mathbf{k}}) Y^{-m}_{1}(\hat{\mathbf{p}}) (-1)^{m_1'+m}\sqrt{\bar{\kappa}} C^{m_1',q,m_1}_{1,\kappa,1} C^{m_2,q,m_2'}_{1/2,\kappa,1/2} \langle 1/2||T_\kappa||1/2\rangle$$

We now carry out the angular integration using Eq. (D.15) which gives

$$\frac{16\pi}{3\sqrt{3}} kp \sqrt{\frac{\bar{L}}{\bar{L}'}} \sum_{m_1,m_2}\sum_{m_L,m_S}\sum_{m_1',m_2'}\sum_{m_L',m_S'}\sum_{L'',m''}\sum_{\kappa,q}\sum_{m} \tag{D.102}$$

$$C^{m_1,m_2m_S}_{1,1/2,S} C^{m_1',m_2'm_S'}_{1,1/2,S'} C^{m_L,m_S,M}_{L,S,J} C^{m_L',m_S',M}_{L',S',J} C^{m_L,-m,m''}_{L,1,L''}$$

$$C^{m'',m,m_L'}_{L'',1,L'} C^{m_1',q,m_1}_{1,\kappa,1} C^{m_2,q,m_2'}_{1/2,\kappa,1/2} (-1)^m \sqrt{\bar{\kappa}} \langle 1/2||T_\kappa||1/2\rangle C^{0,0,0}_{L,1,L''} C^{0,0,0}_{L'',1,L'} \frac{1}{kp} Q_{L''}(a)$$

Now using the symmetry properties Eq. (D.18) of the Clebsch-Gordan coefficients we find

$$-\frac{16\pi}{3\sqrt{3}} kp \sqrt{\frac{1}{\bar{L}'}} \sum_{m_1,m_2}\sum_{m_L,m_S}\sum_{m_1',m_2'}\sum_{m_L',m_S'}\sum_{L'',m''}\sum_{\kappa,q}\sum_{m} \tag{D.103}$$

$$\sqrt{\bar{L}''} C^{m_1,m_2m_S}_{1,1/2,S} C^{m_1',m_2'm_S'}_{1,1/2,S'} C^{m_L,m_S,M}_{L,S,J} C^{m_L',m_S',M}_{L',S',J} C^{m,m'',m_L}_{1,L'',L}$$

$$C^{m'',m,m_L'}_{L'',1,L'} C^{m_1',q,m_1}_{1,\kappa,1} C^{m_2,q,m_2'}_{1/2,\kappa,1/2} \sqrt{\bar{\kappa}} \langle 1/2||T_\kappa||1/2\rangle C^{0,0,0}_{L,1,L''} C^{0,0,0}_{L'',1,L'} \frac{1}{kp} Q_{L''}(a)$$

Noting that $C^{m'',m,m_L'}_{L'',1,L'} = (-1)^{1+L''-L'} C^{m,m'',m_L'}_{1,L'',L'}$ we can then use the orthogonality of Clebsch-Gordan coefficients Eq. (D.17) to reduce our expression to

$$
\begin{aligned}
&-\frac{16\pi}{3\sqrt{3}}kp\sqrt{\frac{1}{\bar{L}}}\delta_{L,L'}\sum_{m_1,m_2}\sum_{m_L,m_S}\sum_{m_1',m_2'}\sum_{,m_S'}\sum_{L''}\sum_{\kappa,q} \\
&\sqrt{\bar{L}''}C^{m_1,m_2m_S}_{1,1/2,S}C^{m_1',m_2'm_S'}_{1,1/2,S'}C^{m_L,m_S,M}_{L,S,J}C^{m_L,m_S',M}_{L,S',J} \\
&C^{m_1',q,m_1}_{1,\kappa,1}C^{m_2,q,m_2'}_{1/2,\kappa,1/2}\sqrt{\bar{\kappa}}\langle 1/2||T_\kappa||1/2\rangle C^{0,0,0}_{L,1,L''}C^{0,0,0}_{1,L'',L}\frac{1}{kp}Q_{L''}(a)
\end{aligned}
\tag{D.104}
$$

The resulting diagrams for the Clebsch-Gordan coefficients are the same in the $\vec{\mathbf{k}}^2$ case and are given in Fig. D.11. Then carrying out the same procedures as in the $\vec{\mathbf{k}}^2$ case we find the following expression

$$
-\frac{16\pi}{3}\sqrt{2}\frac{1}{\sqrt{\bar{L}}}(-1)^{1/2-S'}\delta_{L,L'}\delta_{S,S'}\sum_{\kappa,L''}C^{0,0,0}_{L,1,L''}C^{0,0,0}_{1,L'',L}\sqrt{\bar{\kappa}\bar{L}''}\begin{Bmatrix} 1/2 & \kappa & 1/2 \\ 1 & S' & 1 \end{Bmatrix}Q_{L''}(a)
\tag{D.105}
$$

Finally using Eq. (D.28) we remove the sum over κ and are left with

$$
-\frac{16\pi}{3}\frac{1}{\sqrt{\bar{L}}}\left(\delta_{S',1/2}+2\delta_{S',3/2}\right)(-1)^{1/2-S'}\delta_{L,L'}\delta_{S,S'}\sum_{L''}C^{0,0,0}_{L,1,L''}C^{0,0,0}_{1,L'',L}\sqrt{\bar{L}''}Q_{L''}(a)
\tag{D.106}
$$

Combining all the k^2 and p^2 terms we find

$$4\pi\sqrt{\bar{S}\bar{S}'\bar{L}}\left(\delta_{S',1/2}+2\delta_{S',3/2}\right)\sum_{L''}C^{0,0,0}_{1,1,L''}C^{0,0,0}_{L,L'',L'}(-1)^{2S'+S+L+L''-J}\sqrt{\bar{L}''} \tag{D.107}$$
$$\left\{\begin{array}{ccc} L'' & 1 & 1 \\ 1/2 & S & S' \end{array}\right\}\left\{\begin{array}{ccc} S' & L'' & S \\ L & J & L' \end{array}\right\}(k^2Q_{L'}(a)+4p^2Q_L(a))$$
$$+\frac{4\pi}{3}\delta_{L,L'}\delta_{S,S'}(-1)^{1/2-S'}\left(\delta_{S',1/2}+2\delta_{S',3/2}\right)\frac{1}{kp}(k^2Q_{L'}(a)+4p^2Q_L(a))$$

Now the sum over L'' can be simplified by noting that for $L''=1$ the term with L'' dependence is zero since $C^{0,0,0}_{1,1,1}=0$. For the case of $L''=0$ we use the following identity for 6-j symbols

$$\left\{\begin{array}{ccc} j_1 & j_2 & 0 \\ j_3 & j_4 & j_5 \end{array}\right\}=\delta_{j_1,j_2}\delta_{j_3,j_4}\frac{(-1)^{j_1+j_3+j_5}}{\sqrt{\bar{j}_1\bar{j}_3}} \tag{D.108}$$

Upon using this identity on can show that both terms cancel for $L''=0$. Thus the only nonzero value comes from setting $L''=2$. Setting $L''=2$ for the k^2 and p^2 terms, collecting all the remaining terms, and using time reversal symmetry to find the contribution from the second diagram in Fig. D.7 we finally find Eq. (D.109) for the projected diagrams.

$$4\pi\sqrt{\bar{S}\bar{S}'\bar{L}}\sqrt{\frac{10}{3}}\left(\delta_{S',1/2}+2\delta_{S',3/2}\right)C^{0,0,0}_{L,2,L'}(-1)^{2S'+S+L-J} \tag{D.109}$$

$$\left\{\begin{array}{ccc} 2 & 1 & 1 \\ 1/2 & S & S' \end{array}\right\}\left\{\begin{array}{ccc} S' & 2 & S \\ L & J & L' \end{array}\right\}]\frac{1}{kp}(k^2Q_{L'}(a)+4p^2Q_L(a))$$

$$+8\pi\sqrt{\bar{S}\bar{S}'\bar{L}}\left(\delta_{S',1/2}+2\delta_{S',3/2}\right)\sum_{L''}C^{0,0,0}_{L,1,L''}C^{0,0,0}_{L'',1,L'}\times$$

$$\times(-1)^{3/2-S'-L-L''}\sqrt{\bar{L''}}\left\{\begin{array}{ccc} 1/2 & 1 & S \\ 1 & L'' & L \\ S' & L' & J \end{array}\right\}Q_{L''}(a)$$

$$+8\pi\sqrt{\bar{S}\bar{S}'\bar{L}}\left(\delta_{S',1/2}+2\delta_{S',3/2}\right)\sum_{L''}C^{0,0,0}_{L,1,L''}C^{0,0,0}_{L'',1,L'}(-1)^{1/2+S'+L+L''}\times$$

$$\times\sqrt{\bar{L''}}\left\{\begin{array}{ccc} 1/2 & 1 & S' \\ L' & J & L'' \end{array}\right\}\left\{\begin{array}{ccc} L & 1 & L'' \\ 1/2 & J & S \end{array}\right\}Q_{L''}(a)$$

$$-\frac{16\pi}{3}\frac{1}{\sqrt{\bar{L}}}\left(\delta_{S',1/2}+2\delta_{S',3/2}\right)(-1)^{1/2-S'}\delta_{L,L'}\delta_{S,S'}\sum_{L''}C^{0,0,0}_{L,1,L''}C^{0,0,0}_{1,L'',L}\sqrt{\bar{L''}}Q_{L''}(a)$$

$$+(S\longleftrightarrow S')(L\longleftrightarrow L')(k\longleftrightarrow p)$$

Now we are at the point where we can show that the projected amplitudes averaged over J give zero. In order to average over J we multiply Eq. (D.109) by $\bar{J}$ and then sum over all J values. First we will show how the $Q_{L''}(a)$ terms cancel. For the $Q_{L''}(a)$ term with no 6-j or 9-j symbols the sum over $\bar{J}$ simply gives a factor of $\bar{S}\bar{L}$ since this term has no explicit J dependence. The 9-j symbol averaged over J can be obtained using Eq. (D.110) which is derived in the final appendix. The two 6-j symbols averaged over J can be reduced by using the orthogonality of 6-j symbols Eq. (D.111) [39]. Finally using the symmetry property Eq. (B.1) on the Clebsch-Gordan coefficient $C^{0,0,0}_{L'',1,L'}$ we find that all the $Q_{L''}(a)$ terms cancel.

$$\sum_{j_{33}} \bar{j}_{33} \begin{Bmatrix} j_{11} & j_{12} & j_{13} \\ j_{21} & j_{22} & j_{23} \\ j_{31} & j_{32} & j_{33} \end{Bmatrix} = \frac{1}{\bar{j}_{12}} \delta_{j_{21}j_{12}} \delta_{j_{13}j_{31}} \delta_{j_{32}j_{23}} \tag{D.110}$$

$$\sum_{j_3} \bar{j}_3 \begin{Bmatrix} j_1 & j_2 & j_3 \\ j_4 & j_5 & j_6 \end{Bmatrix} \begin{Bmatrix} j_1' & j_2' & j_3 \\ j_4' & j_5 & j_6' \end{Bmatrix} = \frac{1}{\bar{j}_6} \delta_{j_1 j_1'} \delta_{j_2 j_2'} \delta_{j_4 j_4'} \delta_{j_6 j_6'} \delta(j_1 j_5 j_6) \delta(j_4 j_2 j_6) \tag{D.111}$$

Next we must show how the k^2 and p^2 terms cancel. The only terms that contain J are the one 6-j symbol and the phase factor. Using the definition of the 6-j symbol the averaging of these terms over J is given by Eq. (D.112) [39]

$$\begin{aligned} \sum_J \bar{J}(-1)^{S-J} \begin{Bmatrix} S' & 2 & S \\ L & J & L' \end{Bmatrix} = & \sum_J \sum_{\text{all m}} \bar{J}(-1)^{\phi} \times \\ & \times \begin{pmatrix} S' & 2 & S \\ m_S' & m_2 & m_S \end{pmatrix} \begin{pmatrix} S' & J & L' \\ -m_S' & M & -m_L' \end{pmatrix} \times \\ & \times \begin{pmatrix} L & 2 & L' \\ -m_L & -m_2 & m_L' \end{pmatrix} \begin{pmatrix} L & J & S \\ m_L & -M & -m_S \end{pmatrix} \end{aligned} \tag{D.112}$$

where $\phi = 2S + S' + m_2 + m_S + m_L$. Now using the symmetry properties of the Wigner-3j symbols Eq. (D.151) and (D.113)

$$\begin{pmatrix} j_1 & j_2 & j_3 \\ m_1 & m_2 & m_3 \end{pmatrix} = (-1)^{j_1+j_2+j_3} \begin{pmatrix} j_1 & j_2 & j_3 \\ -m_1 & -m_2 & -m_3 \end{pmatrix} \tag{D.113}$$

and the orthogonality of the Wigner-3j symbols Eq. (D.152) we find our expression reduces to

$$\sum_J \bar{J}(-1)^{S-J} \begin{Bmatrix} S' & 2 & S \\ L & J & L' \end{Bmatrix} = \sum_{m_2,m_S,m_L} (-1)^{3S+m_2+m_S+m_L} \begin{pmatrix} S & 2 & S \\ -m_S & m_2 & m_S \end{pmatrix} \times \tag{D.114}$$

$$\times \begin{pmatrix} L & 2 & L \\ m_L & m_2 & m_L \end{pmatrix} \delta_{SS'}\delta_{LL'}\bar{S}\bar{L}$$

Now again using Eq. (D.113) on the first Wigner-3j symbol and noting the identity Eq. (D.115)

$$\sum_m (-1)^{j-m} \begin{pmatrix} j & j & J \\ m & -m & 0 \end{pmatrix} = \sqrt{\bar{j}}\delta_{J0} \tag{D.115}$$

we find our average over J reduces to

$$\sum_J \bar{J}(-1)^{S-J} \begin{Bmatrix} S' & 2 & S \\ L & J & L' \end{Bmatrix} = \begin{pmatrix} L & 2 & L \\ 0 & 0 & 0 \end{pmatrix} \delta_{SS'}\delta_{LL'}\bar{S}\bar{L}\sqrt{\bar{S}}\delta_{20} \tag{D.116}$$

Finally it is trivial to see that this average gives zero since $\delta_{20} = 0$. Therefore the k^2 and p^2 terms averaged over J give zero and the whole projected amplitude averaged over J gives zero as claimed

D.2.2 Deuteron to Singlet Term

We will now project out the SD mixing term where a deuteron goes to singlet dibaryon field. The corresponding diagram of interest is given in Fig. D.12.

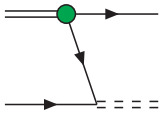

Figure D.12: Feynman diagram for deuteron initial state and singlet dibaryon final state

The resulting spin and isospin dependent structure that one must project out from this diagram is given by

$$\frac{1}{kp}\frac{1}{a+\hat{\mathbf{k}}\cdot\hat{\mathbf{p}}}(\sigma^{\ell})^{\beta}_{\alpha}(\tau^{B})^{b}_{a}\left((2\vec{\mathbf{p}}+\vec{\mathbf{k}})^{i}(2\vec{\mathbf{p}}+\vec{\mathbf{k}})^{\ell}-\frac{1}{3}\delta_{i\ell}(2\vec{\mathbf{p}}+\vec{\mathbf{k}})^{2}\right) \tag{D.117}$$

We will first project out the $k^i k^\ell$ term using the Wigner-Eckart theorem we find the spin structure reduces to Eq. (D.118)

$$\langle 1/2 m_2' | \sigma^m | 1/2 m_2 \rangle = \sqrt{3} C^{m_2,m,m_2'}_{1/2,1,1/2} \tag{D.118}$$

Combining Eq. (D.118) with the definition for projection out in total angular momentum, and for the time being ignoring isospin we find the following for the projection of the $k^i k^\ell$ term

$$\begin{aligned}&\frac{4\pi}{3}\sqrt{3}\frac{1}{kp}\int d\Omega_p \int d\Omega_k \frac{1}{a+\hat{\mathbf{k}}\cdot\hat{\mathbf{p}}} \sum_{m_1,m_2}\sum_{m_L,m_S}\sum_{m_2'}\sum_{m_L',m_S'}\sum_{m} \\ &C^{m_1,m_2 m_S}_{1,1/2,S} C^{0,m_2' m_S'}_{0,1/2,S'} C^{m_L,m_S,M}_{L,S,J} C^{m_L',m_S',M}_{L',S',J} \\ &{Y^{m_L'}_{L'}}^{*}(\hat{\mathbf{p}}) Y^{m_L}_{L}(\hat{\mathbf{k}}) k^2 Y^{m_1}_{1}(\hat{\mathbf{k}}) Y^{-m}_{1}(\hat{\mathbf{k}}) (-1)^m C^{m_2,m,m_2'}_{1/2,1,1/2}\end{aligned} \tag{D.119}$$

The angular integration is then carried out via Eq. (D.13) yielding

$$4\pi\sqrt{3}k^2\sqrt{\frac{\bar{L}}{\bar{L}'}}\sum_{m_1,m_2}\sum_{m_L,m_S}\sum_{m_2'}\sum_{m_L',m_S'}\sum_{L'',m''}\sum_{m} \tag{D.120}$$
$$C^{m_1,m_2m_S}_{1,1/2,S}C^{0,m_2',m_S'}_{0,1/2,S'}C^{m_L,m_S,M}_{L,S,J}C^{m_L',m_S',M}_{L',S',J}C^{m_1,-m,m''}_{1,1,L''}$$
$$C^{m_L,m'',m_L'}_{L,L'',L'}(-1)^m C^{m_2,m,m_2'}_{1/2,1,1/2}C^{0,0,0}_{1,1,L''}C^{0,0,0}_{L,L'',L'}\frac{1}{kp}Q_{L'}(a)$$

Now using symmetry property (D.18) of the Clebsch-Gordan coefficients and the fact that $C^{0,m_2',m_S'}_{0,1/2,S'} = \delta_{1/2,S'}\delta_{m_2',m_S'}$ we find

$$-4\pi k^2\sqrt{\frac{\bar{L}}{\bar{L}'}}\sum_{m_1,m_2}\sum_{m_L,m_S}\sum_{m_2'}\sum_{m_L',m_S'}\sum_{L'',m''}\sum_{m} \tag{D.121}$$
$$\sqrt{\bar{L}''}C^{m_1,m_2m_S}_{1,1/2,S}C^{m_L,m_S,M}_{L,S,J}C^{m_L',m_S',M}_{L',S',J}C^{m,m'',m_1}_{1,L'',1}$$
$$C^{m_L,m'',m_L'}_{L,L'',L'}C^{m_2,m,m_S'}_{1/2,1,S'}C^{0,0,0}_{1,1,L''}C^{0,0,0}_{L,L'',L'}\delta_{S'1/2}\frac{1}{kp}Q_{L'}(a)$$

The resulting product of the Clebsch-Gordan coefficients is represented diagrammatically in Fig. D.13

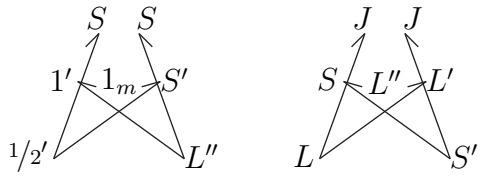

Figure D.13: Diagram representing Clebsch-Gordan coefficients in Eq. (D.121)

Using the definition of the diagrams as 6-j symbols and taking into account phase factors we find the following solution

$$4\pi\sqrt{6}k^2\sqrt{\bar{S}\bar{L}}\delta_{S'1/2}\sum_{L''}\sqrt{\bar{L''}}C^{0,0,0}_{1,1,L''}C^{0,0,0}_{L,L'',L'}(-1)^{1+S+L+L''-J}\times \tag{D.122}$$
$$\times\left\{\begin{array}{ccc} L'' & 1 & 1 \\ 1/2 & S & S' \end{array}\right\}\left\{\begin{array}{ccc} S' & L'' & S \\ L & J & L' \end{array}\right\}\frac{1}{kp}Q_{L'}(a)$$

We now calculate the p^ip^j term, noting that the spin structure is projected out by Eq. (D.118) we find the term we must project out is given by

$$\frac{16\pi}{3}\sqrt{3}\frac{1}{kp}\int d\Omega_p\int d\Omega_k\frac{1}{a+\hat{\mathbf{k}}\cdot\hat{\mathbf{p}}}\sum_{m_1,m_2}\sum_{m_L,m_S}\sum_{m_2'}\sum_{m_L',m_S'}\sum_{m} \tag{D.123}$$
$$C^{m_1,m_2m_S}_{1,1/2,S}C^{0,m_2'm_S'}_{0,1/2,S'}C^{m_L,m_S,M}_{L,S,J}C^{m_L',m_S',M}_{L',S',J}$$
$$Y^{m_L'\,*}_{L'}(\hat{\mathbf{p}})Y^{m_L}_{L}(\hat{\mathbf{k}})p^2Y^{m_1}_1(\hat{\mathbf{p}})Y^{-m}_1(\hat{\mathbf{p}})(-1)^mC^{m_2,m,m_2'}_{1/2,1,1/2}$$

Carrying out the angular integration by using Eq. (D.14) we find

$$16\pi\sqrt{3}p^2\sqrt{\frac{\bar{L}}{\bar{L}'}}\sum_{m_1,m_2}\sum_{m_L,m_S}\sum_{m_2'}\sum_{m_L',m_S'}\sum_{L'',m''}\sum_{m} \tag{D.124}$$
$$C^{m_1,m_2m_S}_{1,1/2,S}C^{0,m_2'm_S'}_{0,1/2,S'}C^{m_L,m_S,M}_{L,S,J}C^{m_L',m_S',M}_{L',S',J}C^{m_1,-m,m''}_{1,1,L''}$$
$$C^{m_L,m'',m_L'}_{L,L'',L'}(-1)^mC^{m_2,m,m_2'}_{1/2,1,1/2}C^{0,0,0}_{1,1,L''}C^{0,0,0}_{L,L'',L'}\frac{1}{kp}Q_L(a)$$

At this point we note that the p^ip^ℓ term is identical to the k^ik^ℓ term except for the p^2, the factor of four, and the $Q_L(a)$, thus the answer for p^ip^ℓ term is identical to the k^ik^ℓ term except for a few minor modifications. So we simply write down the answer

$$16\pi\sqrt{6}p^2\sqrt{\bar{S}\bar{L}}\delta_{S'1/2}\sum_{L''}\sqrt{\bar{L}''}C^{0,0,0}_{1,1,L''}C^{0,0,0}_{L,L'',L'}(-1)^{1+S+L+L''-J}\times \tag{D.125}$$
$$\times\left\{\begin{array}{ccc} L'' & 1 & 1 \\ 1/2 & S & S' \end{array}\right\}\left\{\begin{array}{ccc} S' & L'' & S \\ L & J & L' \end{array}\right\}\frac{1}{kp}Q_L(a)$$

Next we calculate the $k^i p^\ell$ term, and again the spin structure projected out is given by Eq. (D.118) and we find the term we must project is given by

$$\frac{8\pi}{3}\sqrt{3}\frac{1}{kp}\int d\Omega_p\int d\Omega_k\frac{1}{a+\hat{\mathbf{k}}\cdot\hat{\mathbf{p}}}\sum_{m_1,m_2}\sum_{m_L,m_S}\sum_{m'_2}\sum_{m'_L,m'_S}\sum_{m} \tag{D.126}$$
$$C^{m_1,m_2m_S}_{1,1/2,S}C^{0,m'_2m'_S}_{0,1/2,S'}C^{m_L,m_S,M}_{L,S,J}C^{m'_L,m'_S,M}_{L',S',J}$$
$$Y^{m'_L\,*}_{L'}(\hat{\mathbf{p}})Y^{m_L}_{L}(\hat{\mathbf{k}})kpY^{m_1}_1(\hat{\mathbf{k}})Y^{-m}_1(\hat{\mathbf{p}})(-1)^mC^{m_2,m,m'_2}_{1/2,1,1/2}$$

The angular integration is trivially carried out by using Eq. (D.15) which gives

$$8\pi\sqrt{3}kp\sqrt{\frac{\bar{L}}{\bar{L}'}}\sum_{m_1,m_2}\sum_{m_L,m_S}\sum_{m'_2}\sum_{m'_L,m'_S}\sum_{m}\sum_{L''}\sum_{m''} \tag{D.127}$$
$$C^{m_1,m_2m_S}_{1,1/2,S}C^{0,m'_2m'_S}_{0,1/2,S'}C^{m_L,m_S,M}_{L,S,J}C^{m'_L,m'_S,M}_{L',S',J}C^{m_L,-m,m''}_{L,1,L''}C^{m'',m_1,m'_L}_{L'',1,L'}$$
$$(-1)^mC^{m_2,m,m'_2}_{1/2,1,1/2}C^{0,0,0}_{L,1,L''}C^{0,0,0}_{L'',1,L'}\frac{1}{kp}Q_{L''}(a)$$

Using symmetry property Eq. (D.18) of the Clebsch-Gordan coefficients and the fact that $C^{0,m'_2,m'_S}_{0,1/2,S'}=\delta_{1/2,S'}\delta_{m'_2,m'_S}$ we find

$$
\begin{aligned}
&-8\pi\sqrt{3}kp\sqrt{\frac{1}{\bar{L}'}}\sum_{m_1,m_2}\sum_{m_L,m_S}\sum_{m'_L,m'_S}\sum_{m}\sum_{L''}\sum_{m''} \qquad \text{(D.128)}\\
&\sqrt{\bar{L}''}C^{m_1,m_2m_S}_{1,1/2,S}C^{m_L,m_S,M}_{L,S,J}C^{m'_L,m'_S,M}_{L',S',J}C^{m,m'',m_L}_{1,L'',L}C^{m'',m_1,m'_L}_{L'',1,L'}\\
&C^{m_2,m,m'_S}_{1/2,1,S'}C^{0,0,0}_{L,1,L''}C^{0,0,0}_{L'',1,L'}\delta_{S'1/2}\frac{1}{kp}Q_{L''}(a)
\end{aligned}
$$

The resulting diagrams for the this product of Clebsch-Gordan coefficients is given in Fig. (D.14)

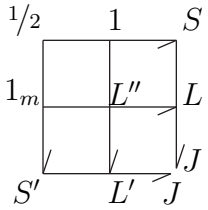

Figure D.14: Diagram representing Clebsch-Gordan coefficients in Eq. (D.128)

Converting the diagram into its corresponding 9-j symbol and taking into account phase factors we obtain

$$
8\pi\sqrt{6}\sqrt{\bar{L}\bar{S}}\delta_{S'1/2}\sum_{L''}\sqrt{\bar{L}''}C^{0,0,0}_{L,1,L''}C^{0,0,0}_{L'',1,L'}\begin{Bmatrix} 1/2 & 1 & S \\ 1 & L'' & L \\ S' & L' & J \end{Bmatrix}Q_{L''}(a) \qquad \text{(D.129)}
$$

We now calculate the $k^\ell p^i$ term, where the spin structure as before is projected out in Eq. (D.118) and the projection for our term is given by

$$\frac{8\pi}{3}\frac{1}{kp}\sqrt{3}\int d\Omega_p \int d\Omega_k \frac{1}{a+\hat{\mathbf{k}}\cdot\hat{\mathbf{p}}} \sum_{m_1,m_2}\sum_{m_L,m_S}\sum_{m_2'}\sum_{m_L',m_S'}\sum_{m} \tag{D.130}$$

$$C^{m_1,m_2m_S}_{1,1/2,S} C^{0,m_2'm_S'}_{0,1/2,S'} C^{m_L,m_S,M}_{L,S,J} C^{m_L',m_S',M}_{L',S',J}$$

$$Y^{m_L'\,*}_{L'}(\hat{\mathbf{p}}) Y^{m_L}_{L}(\hat{\mathbf{k}}) kp Y^{m_1}_1(\hat{\mathbf{p}}) Y^{-m}_1(\hat{\mathbf{k}}) (-1)^m C^{m_2,m,m_2'}_{1/2,1,1/2}$$

The angular integration is then carried out by use of Eq. (D.15) which gives

$$8\pi\sqrt{3}kp\sqrt{\frac{\bar{L}}{\bar{L}'}} \sum_{m_1,m_2}\sum_{m_L,m_S}\sum_{m_2'}\sum_{m_L',m_S'}\sum_{m}\sum_{L''}\sum_{m''} \tag{D.131}$$

$$C^{m_1,m_2m_S}_{1,1/2,S} C^{0,m_2'm_S'}_{0,1/2,S'} C^{m_L,m_S,M}_{L,S,J} C^{m_L',m_S',M}_{L',S',J} C^{m_L,m_1,m''}_{L,1,L''} C^{m'',-m,m_L'}_{L'',1,L'}$$

$$(-1)^m C^{m_2,m,m_2'}_{1/2,1,1/2} C^{0,0,0}_{L,1,L''} C^{0,0,0}_{L'',1,L'} \frac{1}{kp} Q_{L''}(a)$$

Using the symmetry property Eq. (D.18) of the Clebsch-Gordan coefficients and the fact that $C^{0,m_2',m_S'}_{0,1/2,S'} = \delta_{1/2,S'}\delta_{m_2',m_S'}$ we find

$$-8\pi\sqrt{3}kp\sqrt{\bar{L}} \sum_{m_1,m_2}\sum_{m_L,m_S}\sum_{m_L',m_S'}\sum_{m}\sum_{L''}\sum_{m''} \tag{D.132}$$

$$\sqrt{\frac{1}{\bar{L}''}} C^{m_1,m_2m_S}_{1,1/2,S} C^{m_L,m_S,M}_{L,S,J} C^{m_L',m_S',M}_{L',S',J} C^{m_L,m_1,m''}_{L,1,L''} C^{m,m_L',m''}_{1,L',L''}$$

$$C^{m_2,m,m_S'}_{1/2,1,S'} C^{0,0,0}_{L,1,L''} C^{0,0,0}_{L'',1,L'} \delta_{S'1/2} \frac{1}{kp} Q_{L''}(a)$$

The resulting diagrams for this product of Clebsch-Gordan coefficients is given in Fig. D.15

Then plugging in the definition of the diagrams and taking into account the various phase factors we obtain

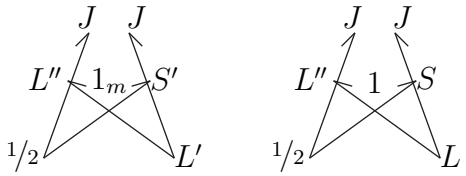

Figure D.15: Diagram representing Clebsch-Gordan coefficients in Eq. (D.132)

$$8\pi\sqrt{6}\sqrt{\bar{L}\bar{S}}\delta_{S'1/2}\sum_{L''}(-1)^{1+L+L''}\sqrt{\bar{L}''}C^{0,0,0}_{L,1,L''}C^{0,0,0}_{L'',1,L'}\times \tag{D.133}$$
$$\times\begin{Bmatrix} L' & 1 & L'' \\ 1/2 & J & S' \end{Bmatrix}\begin{Bmatrix} L & 1 & L'' \\ 1/2 & J & S \end{Bmatrix}Q_{L''}(a)$$

We now project out the $\vec{\mathbf{k}}^2$ term we fist note the Wigner-Eckart theorem tells us the the projected spin component is given by Eq. (D.134)

$$\langle 1/2 m_2'|\sigma^{m_1}|1/2 m_2\rangle = \sqrt{3}C^{m_2,m_1,m_2'}_{1/2,1,1/2} \tag{D.134}$$

Combining Eq. (D.134) with the definition for projection in total angular momentum we find the term we must project is given by

$$-\frac{4\pi}{9}\sqrt{3}\frac{1}{kp}\int d\Omega_p\int d\Omega_k\frac{1}{a+\hat{\mathbf{k}}\cdot\hat{\mathbf{p}}}\sum_{m_1,m_2}\sum_{m_L,m_S}\sum_{m_2'}\sum_{m_L',m_S'}\sum_{m} \tag{D.135}$$
$$C^{m_1,m_2m_S}_{1,1/2,S}C^{0,m_2'm_S'}_{0,1/2,S'}C^{m_L,m_S,M}_{L,S,J}C^{m_L',m_S',M}_{L',S',J}$$
$$Y^{m_L'\,*}_{L'}(\hat{\mathbf{p}})Y^{m_L}_{L}(\hat{\mathbf{k}})k^2Y^{m}_{1}(\hat{\mathbf{k}})Y^{-m}_{1}(\hat{\mathbf{k}})(-1)^mC^{m_2,m_1,m_2'}_{1/2,1,1/2}$$

The angular integration is then done using Eq. (D.13) yielding

$$\frac{4\pi}{\sqrt{3}}k^2\sqrt{\frac{\bar{L}}{\bar{L}'}}\sum_{m_1,m_2}\sum_{m_L,m_S}\sum_{m_2'}\sum_{m_L',m_S'}\sum_{L'',m''}\sum_{m} \tag{D.136}$$
$$C^{m_1,m_2m_S}_{1,1/2,S}C^{0,m_2'm_S'}_{0,1/2,S'}C^{m_L,m_S,M}_{L,S,J}C^{m_L',m_S',M}_{L',S',J}C^{m,-m,m''}_{1,1,L''}$$
$$C^{m_L,m'',m_L'}_{L,L'',L'}(-1)^mC^{m_2,m_1,m_2'}_{1/2,1,1/2}C^{0,0,0}_{1,1,L''}C^{0,0,0}_{L,L'',L'}\frac{1}{kp}Q_{L'}(a)$$

Using Eq. (D.16) on the Clebsch-Gordan coefficient $C^{m,-m,m''}_{1,1,L''}$ we can remove the sum over m and show that $L''=0$. Also using the fact that $C^{0,m_2',m_S'}_{0,1/2,S'}=\delta_{1/2,S'}\delta_{m_2',m_S'}$ we find our solution simplifies to

$$-4\pi k^2\sqrt{\frac{\bar{L}}{\bar{L}'}}\sum_{m_1,m_2}\sum_{m_L,m_S}\sum_{m_2'}\sum_{m_L',m_S'} \tag{D.137}$$
$$C^{m_1,m_2m_S}_{1,1/2,S}C^{0,m_2'm_S'}_{0,1/2,S'}C^{m_L,m_S,M}_{L,S,J}C^{m_L',m_S',M}_{L',S',J}$$
$$C^{m_L,0,m_L'}_{L,0,L'}C^{m_2,m_1,m_2'}_{1/2,1,1/2}C^{0,0,0}_{1,1,0}C^{0,0,0}_{L,0,L'}\delta_{S'1/2}\frac{1}{kp}Q_{L'}(a)$$

Next we note that $C^{m_L,0,m_L'}_{L,0,L'}=\delta_{LL'}\delta_{m_Lm_L'}$, $C^{0,0,0}_{1,1,0}=-1/\sqrt{3}$, and $C^{0,m_2',m_S'}_{0,1/2,S'}=\delta_{S'1/2}\delta_{m_2'm_S'}$ reducing our expression to

$$-\frac{4\pi}{\sqrt{3}}k^2\sum_{m_1,m_2}\sum_{m_L,m_S}\sum_{m_S'}C^{m_1,m_2m_S}_{1,1/2,S}C^{m_L,m_S,M}_{L,S,J}C^{m_L,m_S',M}_{L,S',J}C^{m_2,m_1,m_S'}_{1/2,1,S'}\delta_{L'L}\delta_{S'1/2}\frac{1}{kp}Q_{L'}(a) \tag{D.138}$$

Finally using the orthogonality of Clebsch-Gordan coefficients Eq. (D.17) we find expression reduces nicely to

$$\frac{4\pi}{\sqrt{3}}k^2\delta_{S'1/2}\delta_{S'S}\delta_{L'L}\frac{1}{kp}Q_{L'}(a) \tag{D.139}$$

We now project out the p^2 term, noting that the spin projection is again given by Eq. (D.134) we find the projection for the p^2 term is given by

$$-\frac{16\pi}{9}\sqrt{3}\frac{1}{kp}\int d\Omega_p\int d\Omega_k\frac{1}{a+\hat{\mathbf{k}}\cdot\hat{\mathbf{p}}}\sum_{m_1,m_2}\sum_{m_L,m_S}\sum_{m_2'}\sum_{m_L',m_S'}\sum_{m} \tag{D.140}$$
$$C^{m_1,m_2m_S}_{1,1/2,S}C^{0,m_2'm_S'}_{0,1/2,S'}C^{m_L,m_S,M}_{L,S,J}C^{m_L',m_S',M}_{L',S',J}$$
$$Y_{L'}^{m_L'}{}^*(\hat{\mathbf{p}})Y_L^{m_L}(\hat{\mathbf{k}})p^2Y_1^m(\hat{\mathbf{p}})Y_1^{-m}(\hat{\mathbf{p}})(-1)^mC^{m_2,m_1,m_2'}_{1/2,1,1/2}$$

The angular integration then performed by Eq. (D.14) which gives

$$\frac{16\pi}{\sqrt{3}}p^2\sqrt{\frac{\bar{L}}{\bar{L}'}}\sum_{m_1,m_2}\sum_{m_L,m_S}\sum_{m_2'}\sum_{m_L',m_S'}\sum_{L'',m''}\sum_{m} \tag{D.141}$$
$$C^{m_1,m_2m_S}_{1,1/2,S}C^{0,m_2'm_S'}_{0,1/2,S'}C^{m_L,m_S,M}_{L,S,J}C^{m_L',m_S',M}_{L',S',J}C^{m,-m,m''}_{1,1,L''}$$
$$C^{m_L,m'',m_L'}_{L,L'',L'}(-1)^mC^{m_2,m_1,m_2'}_{1/2,1,1/2}C^{0,0,0}_{1,1,L''}C^{0,0,0}_{L,L'',L'}\frac{1}{kp}Q_L(a)$$

This again is identical to the $\vec{\mathbf{k}}^2$ term except for p^2, the factor of 4, and $Q_L(a)$, thus the solution for p^2 is the same as that for k^2 except for these few minor modifications. Hence the solution for the p^2 term is

$$\frac{16\pi}{\sqrt{3}} p^2 \delta_{S'1/2} \delta_{S'S} \delta_{L'L} \frac{1}{kp} Q_L(a) \tag{D.142}$$

Finally we project out the $\vec{\mathbf{k}} \cdot \vec{\mathbf{p}}$ term. Again the projected spin structure is given by Eq. (D.134) and therefore the projection for the $\vec{\mathbf{k}} \cdot \vec{\mathbf{p}}$ term is given by

$$-\frac{16\pi}{9}\sqrt{3}\frac{1}{kp}\int d\Omega_p \int d\Omega_k \frac{1}{a+\hat{\mathbf{k}}\cdot\hat{\mathbf{p}}} \sum_{m_1,m_2}\sum_{m_L,m_S}\sum_{m_2'}\sum_{m_L',m_S'}\sum_{m} \tag{D.143}$$
$$C^{m_1,m_2 m_S}_{1,1/2,S} C^{0,m_2' m_S'}_{0,1/2,S'} C^{m_L,m_S,M}_{L,S,J} C^{m_L',m_S',M}_{L',S',J}$$
$$Y^{m_L'}_{L'}{}^{*}(\hat{\mathbf{p}}) Y^{m_L}_{L}(\hat{\mathbf{k}}) kp Y^{m}_{1}(\hat{\mathbf{k}}) Y^{-m}_{1}(\hat{\mathbf{p}}) (-1)^m C^{m_2,m_1,m_2'}_{1/2,1,1/2}$$

Carrying out the angular integration via Eq. (D.15) we find

$$\frac{16\pi}{\sqrt{3}} kp \sqrt{\frac{\bar{L}}{\bar{L}'}} \sum_{m_1,m_2}\sum_{m_L,m_S}\sum_{m_2'}\sum_{m_L',m_S'}\sum_{L'',m''}\sum_{m} \tag{D.144}$$
$$C^{m_1,m_2 m_S}_{1,1/2,S} C^{0,m_2' m_S'}_{0,1/2,S'} C^{m_L,m_S,M}_{L,S,J} C^{m_L',m_S',M}_{L',S',J} C^{m_L,m,m''}_{L,1,L''}$$
$$C^{m'',-m,m_L'}_{L'',1,L'} (-1)^m C^{m_2,m_1,m_2'}_{1/2,1,1/2} C^{0,0,0}_{L,1,L''} C^{0,0,0}_{L'',1,L'} \frac{1}{kp} Q_{L''}(a)$$

Now using Eq. (D.18) of the Clebsch-Gordan coefficients we have $C^{m_L,m,m''}_{L,1,L''} = (-1)^{1-m}\sqrt{L''/L} C^{-m,m'',m_L}_{1,L'',L}$. Then we can use the orthogonality of the Clebsch-Gordan coefficients Eq. (D.17) to sum over m and m'' and obtain a Kronecker delta of $\delta_{L'L}$. Also noting that $C^{0,m_2',m_S'}_{0,1/2,S'} = \delta_{S'1/2}\delta_{m_2' m_S'}$ we find

$$\frac{16\pi}{\sqrt{3}}kp(-1)^{L''-L}\sqrt{\frac{1}{\bar{L}'}}\sum_{m_1,m_2}\sum_{m_L,m_S}\sum_{m'_S}\sum_{L''} \tag{D.145}$$
$$\sqrt{\bar{L}''}C^{m_1,m_2m_S}_{1,1/2,S}C^{m_L,m_S,M}_{L,S,J}C^{m_L,m'_S,M}_{L,S',J}$$
$$C^{m_2,m_1,m'_S}_{1/2,1,S'}C^{0,0,0}_{L,1,L''}C^{0,0,0}_{L'',1,L'}\delta_{L'L}\delta_{S'1/2}\frac{1}{kp}Q_{L''}(a)$$

Next we use orthogonality of the Clebsch-Gordan coefficients Eq. (D.17) to obtain

$$\frac{16\pi}{\sqrt{3}}(-1)^{L''-L}\sqrt{\frac{1}{\bar{L}'}}\sum_{L''}\sqrt{\bar{L}''}C^{0,0,0}_{L,1,L''}C^{0,0,0}_{L'',1,L'}\delta_{S'1/2}\delta_{S'S}\delta_{L'L}Q_{L''}(a) \tag{D.146}$$

As before the sum over L'' can be simplified by noting that for $L''=1$ the term with L'' dependence is zero since $C^{0,0,0}_{1,1,1}=0$. For the case of $L''=0$ we use identity Eq (D.108) for 6-j symbols. Upon using this identity one can show that both terms cancel for $L''=0$. Thus the only nonzero value comes from setting $L''=2$. Setting $L''=2$ for the k^2 and p^2, collecting all the $Q_{L''}(a)$ terms we finally find the following expression for the projected diagrams.

$$8\pi\sqrt{5}\sqrt{\bar{S}\bar{L}}\delta_{S'1/2}C^{0,0,0}_{L,2,L'}(-1)^{1+S+L-J} \tag{D.147}$$
$$\left\{\begin{array}{ccc} 2 & 1 & 1 \\ 1/2 & S & S' \end{array}\right\}\left\{\begin{array}{ccc} S' & 2 & S \\ L & J & L' \end{array}\right\}\frac{1}{kp}(k^2Q_{L'}(a)+4p^2Q_L(a))$$
$$+8\pi\sqrt{6}\sqrt{\bar{L}\bar{S}}\delta_{S'1/2}\sum_{L''}\sqrt{\bar{L}''}C^{0,0,0}_{L,1,L''}C^{0,0,0}_{L'',1,L'}\left\{\begin{array}{ccc} 1/2 & 1 & S \\ 1 & L'' & L \\ S' & L' & J \end{array}\right\}Q_{L''}(a)$$
$$+8\pi\sqrt{6}\sqrt{\bar{L}\bar{S}}\delta_{S'1/2}\sum_{L''}(-1)^{1+L+L''}\sqrt{\bar{L}''}C^{0,0,0}_{L,1,L''}C^{0,0,0}_{L'',1,L'}\times$$
$$\times\left\{\begin{array}{ccc} L' & 1 & L'' \\ 1/2 & J & S' \end{array}\right\}\left\{\begin{array}{ccc} L & 1 & L'' \\ 1/2 & J & S \end{array}\right\}Q_{L''}(a)$$
$$+\frac{16\pi}{\sqrt{3}}(-1)^{L''-L}\sqrt{\frac{1}{\bar{L}'}}\sum_{L''}\sqrt{\bar{L}''}C^{0,0,0}_{L,1,L''}C^{0,0,0}_{L'',1,L'}\delta_{S'1/2}\delta_{S'S}\delta_{L'L}Q_{L''}(a)$$

This can again be shown to give zero when averaged over J. The average over J for the k^2 and p^2 terms is zero by the exact same reasoning as in the deuteron to deuteron case. The $Q_{L''}(a)$ terms again vanish by the same reasoning as in the deuteron to deuteron case. However, here we do not need to change the Clebsch-Gordan coefficients, as they are all the same for each $Q_{L''}(a)$ term.

D.3 9-j Identity

In this last section we will derive (D.110). We do this by first noting the following definition for 9-j symbols in terms of Wigner-3j symbols [39]

$$\left\{ \begin{array}{ccc} j_{11} & j_{12} & j_{13} \\ j_{21} & j_{22} & j_{23} \\ j_{31} & j_{32} & j_{33} \end{array} \right\} = \sum_{\text{all m's}} \left(\begin{array}{ccc} j_{11} & j_{12} & j_{13} \\ m_{11} & m_{12} & m_{13} \end{array} \right) \left(\begin{array}{ccc} j_{21} & j_{22} & j_{23} \\ m_{21} & m_{22} & m_{23} \end{array} \right) \times \quad \text{(D.148)}$$
$$\times \left(\begin{array}{ccc} j_{31} & j_{32} & j_{33} \\ m_{31} & m_{32} & m_{33} \end{array} \right) \left(\begin{array}{ccc} j_{11} & j_{21} & j_{31} \\ m_{11} & m_{21} & m_{31} \end{array} \right) \times$$
$$\times \left(\begin{array}{ccc} j_{12} & j_{22} & j_{32} \\ m_{12} & m_{22} & m_{32} \end{array} \right) \left(\begin{array}{ccc} j_{13} & j_{23} & j_{33} \\ m_{13} & m_{23} & m_{33} \end{array} \right)$$

Next we use the orthogonality property of the Wigner-3j symbols given in Eq. (D.149)

$$\sum_{j_3 m_3} \bar{j}_3 \left(\begin{array}{ccc} j_1' & j_2' & j_3 \\ m_1' & m_2' & m_3 \end{array} \right) \left(\begin{array}{ccc} j_1 & j_2 & j_3 \\ m_1 & m_2 & m_3 \end{array} \right) = \delta_{j_1 j_1'} \delta_{j_2 j_2'} \delta m_1 m_1' \delta_{m_2 m_2'} \quad \text{(D.149)}$$

to sum over j_{33} giving

$$\left\{ \begin{array}{ccc} j_{11} & j_{12} & j_{13} \\ j_{21} & j_{22} & j_{23} \\ j_{31} & j_{32} & j_{33} \end{array} \right\} = \sum_{\text{all m's}} \left(\begin{array}{ccc} j_{11} & j_{12} & j_{13} \\ m_{11} & m_{12} & m_{13} \end{array} \right) \left(\begin{array}{ccc} j_{21} & j_{22} & j_{23} \\ m_{21} & m_{22} & m_{23} \end{array} \right) \times \quad \text{(D.150)}$$
$$\times \left(\begin{array}{ccc} j_{11} & j_{12} & j_{13} \\ m_{11} & m_{12} & m_{13} \end{array} \right) \left(\begin{array}{ccc} j_{12} & j_{22} & j_{23} \\ m_{12} & m_{22} & m_{23} \end{array} \right) \delta_{j_{13} j_{31}} \delta_{j_{32} j_{23}}$$

Now using the symmetry property Eq. (D.151)

$$\left(\begin{array}{ccc} j_1 & j_2 & j_3 \\ m_1 & m_2 & m_3 \end{array} \right) = (-1)^{P(j_1+j_2+j_3)} \left(\begin{array}{ccc} j_{\sigma(1)} & j_{\sigma(2)} & j_{\sigma(3)} \\ m_{\sigma(1)} & m_{\sigma(2)} & m_{\sigma(3)} \end{array} \right) \quad \text{(D.151)}$$

(where $\{\sigma(1)\sigma(2)\sigma(3)\} \in S_3$ and $P = 0$ if $\{\sigma(1)\sigma(2)\sigma(3)\}$ is an even permutation and $P = 1$ otherwise) we will reorder the second and fourth Wigner-3j symbol such that j_{21} and j_{12} are at the end. Then we can use the orthogonality of the Wigner-3j symbols Eq. (D.152)

$$\sum_{m_1 m_2} \begin{pmatrix} j_1 & j_2 & j_3 \\ m_1 & m_2 & m_3 \end{pmatrix} \begin{pmatrix} j_1 & j_2 & j_3' \\ m_1 & m_2 & m_3' \end{pmatrix} = \frac{1}{\bar{j}_3} \delta_{j_3 j_3'} \delta_{m_3 m_3'} \delta(j_1 j_2 j_3) \tag{D.152}$$

to reduce our expression down to

$$\begin{Bmatrix} j_{11} & j_{12} & j_{13} \\ j_{21} & j_{22} & j_{23} \\ j_{31} & j_{32} & j_{33} \end{Bmatrix} = \sum_{\text{all m's}} \begin{pmatrix} j_{11} & j_{12} & j_{13} \\ m_{11} & m_{12} & m_{13} \end{pmatrix} \times \tag{D.153}$$
$$\times \begin{pmatrix} j_{11} & j_{12} & j_{13} \\ m_{11} & m_{12} & m_{13} \end{pmatrix} \frac{1}{\bar{j}_{12}} \delta_{j_{12} j_{12}} \delta_{j_{13} j_{31}} \delta_{j_{32} j_{23}}$$

Finally using Eq. (D.152) again we find our desired expression

$$\begin{Bmatrix} j_{11} & j_{12} & j_{13} \\ j_{21} & j_{22} & j_{23} \\ j_{31} & j_{32} & j_{33} \end{Bmatrix} = \frac{1}{\bar{j}_{12}} \delta_{j_{12} j_{12}} \delta_{j_{13} j_{31}} \delta_{j_{32} j_{23}} \tag{D.154}$$

BIBLIOGRAPHY

[1] Aaron, R., and Amado, R. D. Theory of the Reaction n+d → n+n+p. *Phys. Rev. 150* (1966), 857–866.

[2] Adelberger, E. G., Hindi, M. M., Hoyle, C. D., Swanson, H. E., Von Lintig, R. D., and Haxton, W. C. Beta decays of ^{18}Ne and ^{19}Ne and their relation to parity mixing in ^{18}F and ^{19}F. *Phys. Rev. C 27* (Jun 1983), 2833–2856.

[3] Altarelli, Guido, Ellis, R. Keith, Maiani, L., and Petronzio, R. The Structure of Parity Violating Strangeness Conserving Weak Nonleptonic Amplitudes in an Asymptotically Free Theory. *Nucl.Phys. B88* (1975), 215.

[4] Altarelli, Guido, and Maiani, L. Octet Enhancement of Nonleptonic Weak Interactions in Asymptotically Free Gauge Theories. *Phys.Lett. B52* (1974), 351–354.

[5] Ando, Shung-ichi, and Birse, Michael C. Effective field theory of 3He. *J. Phys. G37* (2010), 105108.

[6] A.P. Yutsis, I.B. Levinson, V.V. Vanagas. *Mathematical Apparatus of the Theory of Angular Momentum.* Academy of Sciences of the Lithuanian SSR, 1960. translated into English by the Israel Program for Scientific Translations, Jerusalem, 1962.

[7] Barnes, C.A., Lowry, M.M, Davidson, J.M., Marrs, R.E., Morinigo, F.B., et al. Search for Neutral Weak Current Effects in the Nucleus F-18. *Phys.Rev.Lett. 40* (1978), 840–843.

[8] Barton, G. Notes on the static parity non-conserving internucleon potential. *Nuovo Cim. 19* (1961), 512–527.

[9] Beane, Silas R., Bedaque, Paulo F., Haxton, Wick C., Phillips, Daniel R., and Savage, Martin J. From hadrons to nuclei: Crossing the border.

[10] Beane, Silas R., and Savage, Martin J. Hadronic parity violation on the lattice. *Nucl.Phys. B636* (2002), 291–304.

[11] Bedaque, Paulo F., and Griesshammer, Harald W. Quartet S Wave Neutron Deuteron Scattering in Effective Field Theory. *Nucl. Phys. A671* (2000), 357–379.

[12] Bedaque, Paulo F., Hammer, H.W., and van Kolck, U. Renormalization of the three-body system with short range interactions. *Phys.Rev.Lett. 82* (1999), 463–467.

[13] Bedaque, Paulo F., Hammer, H.W., and van Kolck, U. The Three boson system with short range interactions. *Nucl.Phys. A646* (1999), 444–466.

[14] Bedaque, Paulo F., Hammer, H.W., and van Kolck, U. Effective theory of the triton. *Nucl.Phys. A676* (2000), 357–370.

[15] Bedaque, Paulo F., Rupak, Gautam, Griesshammer, Harald W., and Hammer, Hans-Werner. Low Energy Expansion in the Three Body System to All Orders and the Triton Channel. *Nucl. Phys. A714* (2003), 589–610.

[16] Bini, M., Bizzeti, P.G., and Sona, P. Calculation of the parity mixing between the lowest 0-, 0 and 0+, 1 levels in F-18. *Phys.Rev. C23* (1981), 1265–1268.

[17] Bini, M., Fazzini, T.F., Poggi, G., and Taccetti, N. Search for the Circular Polarization of the 1081-keV Gamma Ray in F-18. *Phys.Rev.Lett. 55* (1985), 795–798.

[18] Bizzeti, P.G., Fazzini, T.F., Maurenzig, P.R., Perego, A., Poggi, G., et al. SEARCH FOR PARITY MIXING IN F-18. *Lett.Nuovo Cim. 29* (1980), 167–172.

[19] Brayshaw, D. D. Off- and on-shell analyticity of three-particle scattering amplitudes. *Phys. Rev. 176* (1968), 1855–1870.

[20] Brink, D.M., and Satchler, G.R. *Angular Momentum*. Clarendon Press, Oxford, 1979.

[21] Cahill, R.T., and Sloan, I.H.

[22] Carlson, J., Schiavilla, R., Brown, V.R., and Gibson, B.F. Parity violating interaction effects 1: The Longitudinal asymmetry in pp elastic scattering. *Phys.Rev. C65* (2002), 035502.

[23] Chen, Jiunn-Wei, Rupak, Gautam, and Savage, Martin J. Nucleon nucleon effective field theory without pions. *Nucl. Phys. A653* (1999), 386–412.

[24] Chodos, A., Jaffe, R.L., Johnson, K., and Thorn, Charles B. Baryon Structure in the Bag Theory. *Phys.Rev. D10* (1974), 2599.

[25] Chodos, A., Jaffe, R.L., Johnson, K., Thorn, Charles B., and Weisskopf, V.F. A New Extended Model of Hadrons. *Phys.Rev. D9* (1974), 3471–3495.

[26] C.S. Wu, E. Ambler, R.W. Hayward D.D. Hoppes, and Hudson, R.P. Experimental test of parity conservation in beta decay. *Phys. Rev. 105*, 1413.

[27] D.A. Varshalovich, A.N. Moskalev, and Khersonskii, V.K. *Quantum Theory of Angular Momentum*. Nauka, Leningrad, 1975.

[28] Danilov, G.S. *Phys. Lett. 18* (1965), 40.

[29] Delves, L. M., and Walsh, J. *Numerical Solution of Integral Equations*. Clarendon, Oxford.

[30] Desplanques, B. Parity-non-conservation in nuclear forces at low energy: Phenomenology and questions. *Phys.Rept. 297* (1998), 1–61.

[31] Desplanques, Bertrand, Donoghue, John F., and Holstein, Barry R. Unified Treatment of the Parity Violating Nuclear Force. *Ann. Phys. 124* (1980), 449.

[32] Desplanques, Bertrand, and Missimer, John H. An Analysis of Parity Violating Nuclear Effects at Low-Energy. *Nucl.Phys. A300* (1978), 286–312.

[33] Donoghue, John F., Golowich, Eugene, and Holstein, Barry R. Kaon decays and a determination of the scale of chiral symmetry. *Phys. Rev. D 30* (Aug 1984), 587–593.

[34] Driscoll, D.E., and Meissner, Ulf G. Topological soliton model calculation of the proton proton parity violating interaction. *Phys.Rev. C41* (1990), 1303–1305.

[35] Driscoll, D.E., and Miller, G.A. POTENTIAL MODEL CALCULATIONS OF PARITY VIOLATION IN PROTON PROTON SCATTERING. *Phys.Rev. C39* (1989), 1951–1962.

[36] Driscoll, D.E., and Miller, G.A. Relativistic and strong distortion effects in proton proton parity violation. *Phys.Rev. C40* (1989), 2159–2167.

[37] Dubovik, V. M., and Zenkin, S. V. FORMATION OF PARITY NONCONSERVING NUCLEAR FORCES IN THE STANDARD MODEL SU(2)(L) X U(1) X SU(3)(C). *Annals Phys. 172* (1986), 100–135.

[38] Earle, E.D., Mcdonald, A.B., Adelberger, E.G., Snover, K.A., Swanson, H.E., et al. PARITY MIXING IN NE-21: EVIDENCE FOR WEAK NEUTRAL CURRENTS IN NUCLEI. (TALK). *Nucl.Phys. A396* (1983), 221C–230C.

[39] Edmonds, A.R. *Angular Momentum In Qauntum Mechanics*. Princeton University Press, 1960.

[40] Edwards, N.H., Phipp, S.J., Baird, P.E.G., and Nakayama, S. Precise Measurement of Parity Nonconserving Optical Rotation in Atomic Thallium. *Phys.Rev.Lett. 74* (1995), 2654–2657.

[41] El-Baz, E., and Castel, B. *Graphical Methods of Spin Algebras*. Marcel Dekker, New York, 1972.

[42] Elsener, K., Grubler, W., Konig, V., Schmelzbach, P.A., Ulbricht, J., et al. CONSTRAINTS ON WEAK MESON NUCLEON COUPLING FROM PARITY NONCONSERVATION IN F-19. *Phys.Rev.Lett. 52* (1984), 1476–1479.

[43] Elsener, K., Grubler, W., Konig, V., Schmelzbach, P.A., Ulbricht, J., et al. PARITY NONCONSERVATION IN F-19 NUCLEI. *Nucl.Phys. A461* (1987), 579–602.

[44] Endt, P.M., and vaderLeun, C.

[45] Endt, P.M., and vaderLeun, C.

[46] et al., P.D. Evershiem. . *Phys.Lett. B256* (1991), 11.

[47] Evans, H.C., Ewan, G.T., Kwan, S.-P., Leslie, J.R., MacArthur, J.D., et al. Parity Mixing of 0+ and 0- Levels in F-18. *Phys.Rev.Lett. 55* (1985), 791–794.

[48] Feldman, G. B., Crawford, Gregory A., Dubach, J., and Holstein, Barry R. Delta contributions to the parity violating nuclear interaction. *Phys. Rev. C43* (1991), 863–874.

[49] G. Ahrens, W. Harfst, J.R. Kass E.V. Mason-H. Schober G. Steffens H. Waeffler. Search for parity violation in the 1081 keV gamma transition of F-18. *Nucl. Phys. A390* (1982), 486–508.

[50] Gabbiani, Fabrizio, Bedaque, Paulo F., and Griesshammer, Harald W. Higher partial waves in an effective field theory approach to n d scattering. *Nucl. Phys. A675* (2000), 601–620.

[51] Gaillard, M.K., and Lee, Benjamin W. Delta I = 1/2 Rule for Nonleptonic Decays in Asymptotically Free Field Theories. *Phys.Rev.Lett. 33* (1974), 108.

[52] Gericke, M.T., Alarcon, R., Balascuta, S., Barron-Palos, L., Blessinger, C., et al. Measurement of parity-violating gamma-ray asymmetry in the capture of polarized cold neutrons on protons. *Phys.Rev. C83* (2011), 015505.

[53] Girlanda, Luca. On a redundancy in the parity-violating 2-nucleon contact Lagrangian. *Phys.Rev. C77* (2008), 067001.

[54] Grach, I., and Shmatikov, M. Parity violation in p p scattering and quark degrees of freedom. *Phys.Lett. B316* (1993), 467–471.

[55] Griesshammer, Harald W. Improved Convergence in the Three-Nucleon System at Very Low Energies. *Nucl. Phys. A744* (2004), 192–226.

[56] Griesshammer, Harald W., and Schindler, Matthias R. On Parity-Violating Three-Nucleon Interactions and the Predictive Power of Few-Nucleon EFT at Very Low Energies. *Eur. Phys. J. A46* (2010), 73–83.

[57] Griesshammer, Harald W., Schindler, Matthias R., and Springer, Roxanne P. Parity-violating neutron spin rotation in hydrogen and deuterium. *Eur.Phys.J. A48* (2012), 7. 44 pages, 17 figures/ minor corrections/ to be published in EPJA.

[58] Gudkov, Vladimir. Parity violation in $n +^3 He \rightarrow^3 H + p$ reaction: resonance approach. *Phys. Rev. C82* (2010), 065502.

[59] Gudkov, Vladimir, and Song, Young-Ho. Faddeev-type equations for three-body symmetry violating scattering amplitudes. *Phys.Rev. C82* (2010), 028502.

[60] G.V.Skornyakov, and K.A.Ter-Martirosian. *Sov. Phys.JETP 4*.

[61] Haxton, W.C., Gibson, B.F., and Henley, E.M. PARITY NONCONSERVATION IN F-18, F-19, AND NE-21. *Phys.Rev.Lett. 45* (1980), 1677–1681.

[62] Haxton, W.C., Liu, C.P., and Ramsey-Musolf, M.J. Nuclear anapole moments. *Phys.Rev. C65* (2002), 045502.

[63] Haxton, W.C., and Wieman, Carl E. Atomic parity nonconservation and nuclear anapole moments. *Ann.Rev.Nucl.Part.Sci. 51* (2001), 261–293.

[64] Hetherington, J. H., and Schick, L. H. Exact Multiple-Scattering Analysis of Low-Energy Elastic K–d Scattering with Separable Potentials. *Phys. Rev. 137* (1965), B935–B948.

[65] Holstein, Barry R. Topics in advanced quantum mechanics. Redwood City, USA: Addison-Wesley (1992) 436 p. (The advanced book program).

[66] Holstein, Barry R. NUCLEAR PARITY VIOLATION PARAMETER H (RHO) (1)'. *Phys.Rev. D23* (1981), 1618–1623.

[67] Holstein, Barry R. Hadronic parity violation. *Nucl. Phys. A844* (2010), 160c–164c.

[68] Iqbal, M.J., and Niskanen, J.A. Isobar excitation in parity nonconserving proton proton scattering. *Phys.Rev. C49* (1994), 355–359.

[69] J. Lang, Th. Maier, R. Muller F. Nessi-Tedaldi Th. Roser M. Simonius, and Sromicki, J.

[70] Kaplan, D. B. Effective field theory expansions for nonrelativistic scattering. Prepared for INT Workshop on Nuclear Physics with Effective Field Theory, Seattle, Washington, 25-26 Feb 1999.

[71] Kaplan, David B., Savage, Martin J., and Wise, Mark B. A new expansion for nucleon nucleon interactions. *Phys. Lett. B424* (1998), 390–396.

[72] Kaplan, David B., Savage, Martin J., and Wise, Mark B. Two-nucleon systems from effective field theory. *Nucl. Phys. B534* (1998), 329–355.

[73] Keinonen, J., Mak, H.B., Alexander, T.K., Ball, G.C., Davies, W.G., et al. Lifetime of the 1.04 MeV state in F-18, measured through the inverse reaction He-3 (O-16, p) F-18. *Phys.Rev. C23* (1981), 2073–2077.

[74] Keinonen, J., Mak, H.B., Skensved, P., Leslie, J.R., and McLatchie, W. Lifetime of the 1.04 MeV state in F-18. *Phys.Rev. C22* (1980), 351–355.

[75] Kok, Lambrecht P., and van Haeringen, H. Off-shell Coulomb T matrix in connection with the exact solution of three-particle equations with Coulomb interaction. *Phys. Rev. C21* (1980), 512–517.

[76] Konig, Sebastian, and Hammer, H. W. Low-energy p-d scattering and He-3 in pionless EFT. *Phys. Rev. C83* (2011), 064001.

[77] Krane, K. S., Olsen, C. E., Sites, James R., and Steyert, W. A. Observation of 1.5 *Phys. Rev. Lett. 26* (1971), 1579–1581.

[78] Krane, K. S., Olsen, C. E., Sites, James R., and Steyert, W. A. Parity-Violating Asymmetry of the 501-keV Gamma Ray Emitted in the Decay of Hf-180m. *Phys. Rev. C4* (1971), 1906–1913.

[79] L.C. Biedenharn, J.D. Louck. *Angular Momentum In Qauntum Physics.* Addison-Wesley Publishing Company, 1981.

[80] Lee, T.D., and Yang, C.N. Question of parity conservation in weak interactions. *Phys. Rev. 104*, 254.

[81] Liu, C.-P. Parity-Violating Observables of Two-Nucleon Systems in Effective Field Theory. *Phys.Rev. C75* (2007), 065501.

[82] Manohar, Aneesh, and Georgi, Howard. Chiral Quarks and the Nonrelativistic Quark Model. *Nucl.Phys. B234* (1984), 189.

[83] McDonald, A. B., Earle, E. D., Simpson, J. J., Robertson, R. G. H., and Mak, H. B. Measurement of pair emission from the 2.8-mev parity-mixed doublet of ^{21}Ne. *Phys. Rev. Lett. 47* (Dec 1981), 1720–1723.

[84] Mckellar, B.H.J., and Pick, P. Pion-pole dominance of the divergence of the weak parity-nonconserving n n rho amplitude. *Phys.Rev. D6* (1972), 2184–2188.

[85] Mckellar, B.H.J., and Pick, P. Su(6)w model of delta-s=0 and delta-s=1 non-leptonic parity-violating weak interactions. *Phys.Rev. D7* (1973), 260–266.

[86] Michel, F. Curtis. Parity Nonconservation in Nuclei. *Phys.Rev. 133* (1964), B329–B349.

[87] Phillips, Daniel R., Rupak, Gautam, and Savage, Martin J. Improving the convergence of N N effective field theory. *Phys. Lett. B473* (2000), 209–218.

[88] Phillips, Daniel R., Schindler, Matthias R., and Springer, Roxanne P. An effective-field-theory analysis of low-energy parity- violation in nucleon-nucleon scattering. *Nucl. Phys. A822* (2009), 1–19.

[89] R. Balzer, R. Henneck, Ch. Jacquemart J. Lang-M. Simonius W. Haeberli Ch. Weddigen, Reichart, W., and Jaccard, S. Measurement of parity non-conservation in pp scattering at 45 mev. *Phys.Rev.Lett. 44* (1980), 699.

[90] Rupak, Gautam. Precision calculation of n+p-¿d+gamma cross section for Big-Bang Nucleosyntesis. *Nucl. Phys. A678* (2000), 405–423.

[91] Rupak, Gautam, and Kong, Xin-wei. Quartet S-wave p d scattering in EFT. *Nucl. Phys. A717* (2003), 73–90.

[92] S. Kistryn, J. Lang, J. Liechti Th. Maier-R. Müller F. Nessi-Tedaldi M. Simonius J. Smyrski S. Jaccard W. Haeberli, and Sromicki, J. Precision measurement of parity nonconservation in proton-proton scattering at 45 mev. *Phys.Rev.Lett. 58* (1987), 1616.

[93] Sakurai, J.J. *Modern Quantum Mechanics*. Addison-Wesley, 1994.

[94] Schiavilla, R., Carlson, J., and Paris, M. W. Parity-Violating Interaction Effects in the np System. *Phys. Rev. C70* (2004), 044007.

[95] Schiavilla, R., Viviani, M., Girlanda, L., Kievsky, A., and Marcucci, L. E. Erratum: Neutron spin rotation in $\vec{n}$-d scattering [phys. rev. c 78, 014002 (2008)]. *Phys. Rev. C 83* (Feb 2011), 029902.

[96] Schiavilla, R., Viviani, M., Girlanda, L., Kievsky, A., and Marcucci, L.E. Neutron spin rotation in n-polarized - d scattering. *Phys.Rev. C78* (2008), 014002.

[97] Schindler, Matthias R., and Springer, Roxanne P. Two parity violating asymmetries from $np \to d\gamma$ in pionless effective field theories. *Nucl. Phys. A846* (2010), 51–62.

[98] Schmid, E.W., and Ziegelmann, H. *The Qauntum Mechanical Three-Body Problem, Vieweg Tract in Pure and Applied Physics Vol. 2*. Pergamon Press, 1974.

[99] Snover, K.A., von Lintig, R., Adelberger, E.G., Swanson, H.E., Trainor, T.A., et al. Upper Limit on Parity Mixing in Ne-21. *Phys.Rev.Lett. 41* (1978), 145–148.

[100] Song, Young-Ho, Lazauskas, Rimantas, and Gudkov, Vladimir. Parity violation in low energy neutron deuteron scattering. *Phys.Rev. C83* (2011), 015501.

[101] Strobel, George. *Nucl.Phys. A96* (1967), 229–237.

[102] Tanner, N. Parity in nuclear reactions. *Phys. Rev. 107*, 1203.

[103] Vetter, P.A., Meekhof, D.M., Majumder, P.K., Lamoreaux, S.K., and Fortson, E.N. Precise test of electroweak theory from a new measurement of parity nonconservation in atomic thallium. *Phys.Rev.Lett. 74* (1995), 2658–2661.

[104] Viviani, M., Schiavilla, R., Girlanda, L., Kievsky, A., and Marcucci, L. E. The parity-violating asymmetry in the 3He(n,p)3H reaction. *Phys. Rev. C82* (2010), 044001.

[105] Warburton, E. K., Olness, J. W., and Lister, C. J. Erratum: Lifetimes of the ^{21}Ne 2796-, 1747-, and 2867-kev levels. *Phys. Rev. C 23* (Feb 1981), 941–941.

[106] Warburton, E.K., Olness, J.W., and Lister, C.J. Lifetimes of the Ne-21 2796-, 1747-, and 2867-keV levels. *Phys.Rev. C20* (1979), 619–640.

[107] W.N. Catford, L.K. Fifield, E.G. Garman, and Pringle, D.M.

[108] Wood, C.S., Bennett, S.C., Cho, D., Masterson, B.P., Roberts, J.L., et al. Measurement of parity nonconservation and an anapole moment in cesium. *Science 275* (1997), 1759–1763.

[109] YaB., Zeldovich.

[110] Zhu, Shi-Lin, Maekawa, C. M., Holstein, B. R., Ramsey-Musolf, M. J., and van Kolck, U. Nuclear parity-violation in effective field theory. *Nucl. Phys. A748* (2005), 435–498.